Universiteit Utrecht
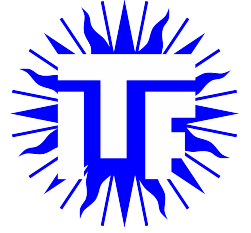
Time Crystals in Open Quantum Systems

Dynamical Localisation of Particles Coupled to a Two-Level System Reservoir

Faculty of Science

MASTER THESIS

Wies Uijttewaal

Theoretical Physics

Supervisors:

Prof. CRISTIANE DE MORAIS SMITH
Institute for Theoretical Physics, Utrecht University

Dr. RODRIGO AROUCA DE ALBUQUERQUE
Institute for Theoretical Physics, Utrecht University
Materials Theory Division, Uppsala University

May 25, 2022

Abstract

Ever since the existence of a time crystal was theorised by Frank Wilczek in 2012, physicists have proposed several possible realisations. Some of these have been experimentally realised, such as excited state time crystals and Floquet (or driven) time crystals. Yet another possible realisation is offered in Ref. [1]. It shows that the coupling of a particle to a reservoir of two-level systems can lead under certain conditions to a long term oscillation of the particle. This thesis revisits this research from a time crystal perspective and aims to understand the parameters controlling the time crystalline phase. The particle-bath system is essentially a modified Caldeira-Leggett model and can be solved analytically. By examining the position of the particle and the pole structure of its Laplace transform, we can conclude that a time crystal phase is indeed present. The parameters that govern this phase are the damping constant, the temperature, and the long term properties of the bath. Depending on these parameters, we observe either persistent or decaying oscillations. Investigating the pole structure, we find properties that describe a phase transition between these two phases.

Contents

1   Time Crystals

When atoms form an ordered pattern in space we call that a crystal. Crystals are fairly common in our everyday life, we find them for example in our kitchen as sugar and salt, but they are also abundant in nature in the form of diamonds and other gems and minerals. The formation of a crystal relies on the self-organising properties of the atoms it is made of. The attractive or repulsive interactions between these atoms causes them to arrange themselves in a regular pattern (see Figure 1.1). This process occurs on the quantum mechanical level and is related to the spontaneous breaking of translation symmetry in space. Spontaneous symmetry breaking is a process that happens when nature makes a choice. Suppose you want to study a system that is described by symmetrical equations. Then, there would exist multiple solutions, or states, of that system, each equally likely to occur. However, by performing the measurement, the system gets an infinitesimally small nudge that causes it to randomly choose one of these solutions, which then spontaneously breaks the symmetry. Noether's theorem tells us that each symmetry of a system corresponds to a conserved quantity. When this symmetry is broken, spontaneously or otherwise, the quantity is no longer conserved. For 'normal' crystals, or space crystals, the spatial translation symmetry is (partially) broken. The conserved quantity that is associated with this type of symmetry is linear momentum. Full spatial translation symmetry would mean that any translation in space would not change the system. However, in an ordered pattern, only translations along certain axes or distances leave the crystal unchanged. Therefore, we can say that in a space crystal, the linear momentum of the particles is not conserved.
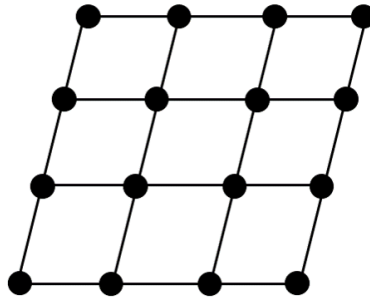
Figure 1.1: A two-dimensional representation of a crystal in space.

American physicist Frank Wilczek considered this description of space crystals and wondered whether a similar breaking of translation symmetry could not also happen in time. He asked the question whether atoms could self-organise in time and then undergo a periodic motion, or in other words, could form a 'time crystal' [2]. When he put forth this claim in 2012, it was met with some scepticism by the community. In Wilczek's description of time crystals, the time translation symmetry of an isolated system is spontaneously broken, which according to Noether's theorem would imply that the energy of such a system would not be conserved. Some physicists proved that Wilczek's formulation of the problem would be impossible to realise experimentally, such as Bruno et al.[3], whereas others proposed different ways in which time crystals might be realised.

Before we go into detail about Wilczek's idea, we must ask ourselves how we can 'detect' a time crystal. In other words, what is the relevant quantity that we can measure? To detect a crystal in space, we look at the probability density of particles, which gives us information on where and when particles are located. If this probability density changes periodically in space at a certain point in time (i.e. the time of measuring), there is a space crystal. Now, when we reverse the roles of space and time, we find that a time crystal is formed when the probability density changes periodically in time at a given position in space. We can also write down a more mathematical formulation of this. A system is described by a Hamiltonian H. Its evolution in time is given by the time translation operator, which operates on the eigenstates ψ of the system: $\mathcal{T}\psi = e^{-iEt}\psi$. For general time-independent systems, this operator commutes with the Hamiltonian and therefore the probability density does not change in time: $|\psi(t)|^2 = |\psi(0)|^2$. However, if a system breaks time translation symmetry, we will see that this no longer holds and the probability density does depend on time.

Wilczek's original idea

Frank Wilczek considered a system of N bosonic particles on a superconducting ring of unit length, through which a magnetic flux is threaded [2]. Such a system is also known as an Aharanov-Bohm ring. The mass of the particles and $\hbar$ are set equal to unity and the bosons interact according to the attractive local potential $V(x) = g_0\delta(x)$, such that the Hamiltonian of this system is given by [4]

$$H = \sum_{i=1}^{N} \frac{(p_i - \alpha)^2}{2} + g_0 \sum_{i<j}^{N} \delta(x_i - x_j),\tag{1.1}$$

where x_i and p_i are the particle positions and momenta, and $g_0 < 0$ is the strength of the attractive potential between the particles. α is a parameter that is connected to the magnetic flux through the ring.

Let us first consider what happens when there is only one particle with charge q on the ring in the presence of a flux $2\pi\alpha/q$. The Hamiltonian of this simple system is given by

$$H = \frac{1}{2}(p - \alpha)^2,\tag{1.2}$$

where $p = \dot{\phi} + \alpha$ is the angular momentum and ϕ is the angular coordinate of the particle. When we apply periodic boundary conditions, the momentum is quantised and we find that the probability current

$$\frac{\partial E_n}{\partial p_n} = 2\pi n - \alpha,\tag{1.3}$$

where $E_n = (p_n - \alpha)^2/2$ are the energy eigenvalues and n is an integer eigenvalue of the quantised momentum operator p_n. For certain (non-integer) values of α, we can find a state that minimises the energy and yet still leaves a non-zero probability current. In other words, we can get a moving particle along a ring in the ground state of the system. However, the single-particle probability density is still time-independent and does not exhibit a periodicity.

What we need is to expand our system and take a large number of interacting particles such that the ground state becomes more robust for a possible experimental realisation. Thus, switching to the many-body system, we arrive at the Hamiltonian given in Equation (1.1).

This system is invariant under continuous time and space translations, which means that the probability density of the eigenstates is also invariant under these translations. For a time crystal however, this probability would have to exhibit discrete periodic behaviour in time. Wilczek claimed that there exists a possibility that both symmetries are spontaneously broken and a time crystal can be formed in the ground state.

That the spatial translation symmetry breaks is a well-known phenomenon and can easily be explained. If we assume the magnetic flux to be zero and perform a mean field approximation, reducing the many-body system to a single particle with an effective interaction potential, we find that all bosons occupy the same single-particle state ϕ. In other words, they form a Bose-Einstein condensate. The many-body ground state, although initially spatially symmetrical, is strongly vulnerable to any perturbation and its symmetry can be broken by the measurement of even a single particle. The 'lump of charge', as Wilczek calls it [2], that is then formed can also be described by the bright soliton solution.

Wilczek predicted that for a non-zero α, a type of magnetic flux through the ring would be created and therefore the bright soliton would feel a torque, analogous to Faraday's law of induction, causing it to move along the ring similar to the single particle case. Then, for certain values of α, the localised particle density will also move periodically around the ring, breaking time translation symmetry and forming a time crystal in the ground state of the system.

No-go theorem

However, this claim was quickly disputed by other physicists, such as Bruno [3]. He argued that the solution offered by Wilczek in Ref. [2] is in fact not the ground state of the system, and effectively showed that another state existed with a lower energy than Wilczek's solution [3]. This can easily be seen by considering the Hamiltonian in its center of mass coordinate frame [4]

$$H = \frac{(P - N\alpha)^2}{2N} + \text{relative degrees of freedom,} \tag{1.4}$$

where P is the total momentum, which in an eigenstate of the system is given by $P_n = 2\pi n$, with n an integer value. The ground state is obtained by minimising the kinetic energy of the center of mass degree of freedom. However, in the limit $N \to \infty$, its probability flux, given by

$$\frac{\partial H}{\partial P_n} = 2\pi \frac{n}{N} - \alpha, \tag{1.5}$$

vanishes, because it is always possible to choose n such that $2\pi n/N$ is arbitrarily close to α. Therefore, even for $\alpha \neq 0$, the probability current vanishes and the state exhibits no motion. Other versions of Wilczek's original idea were also proven to be impossible to realise and indicate that a many-body system prepared in the ground state does not exhibit spontaneous breaking of time translation symmetry.

Other realisations of time crystals

Nevertheless, Wilczek's idea brought forth inspiration for many other physicists. Perhaps a time crystal could be realised, but based on different underlying principles. Wilczek's original idea mentions several prerequisites for what would constitute a time crystal. It must be a many-body system that exhibits spontaneous breaking of continuous time translation symmetry in the ground state. In addition to this, it must be experimentally realisable.

Although his original model proved not to be experimentally realisable, it did inspire other physicists to propose modified versions. We will discuss several of them below, including excited state time crystals, Floquet time crystals and dissipative time crystals.

Excited State Time Crystals

After it was established that the spontaneous symmetry breaking of the continuous time translation symmetry into a discrete time translation symmetry of a system prepared in the ground state could not be observed, the question was put forth whether this could happen when the system is prepared in an *excited* state. After all, eigenstates of a time-independent Hamiltonian H are also eigenstates of the time translation operator $\mathcal{T} = e^{-iHt}$. It turns out that the answer to this question is yes.

We can consider once again the Hamiltonian for Wilczek's system in Equation (1.1). The probability current $\partial H / \partial P_n$ vanishes for any value of α for a system prepared in the ground state, as we saw above. However, for a system prepared in an excited state, with total momentum $P_N = 2\pi N$, we find that the current is given by

$$\frac{\partial H}{\partial P_N} = 2\pi - \alpha. \tag{1.6}$$

Then, for $\alpha \neq 2\pi$, the probability current does not vanish and the state exhibits periodic motion around the ring with a period $T = (2\pi - \alpha)^{-1}$.

Thus, if it is possible to prepare a system in the excited state corresponding to $P_N = 2\pi N$, an experimentally stable time crystal can be realised. To do this, one must take a ground state prepared with $P_N = 2\pi N$ and $\alpha = 2\pi$. Then, once the flux is switched off ($\alpha = 0$), this state will automatically become an excited state of the system. This theory is described by Syrwid et al. and the simulations they performed indeed shows a periodic behaviour in time of the probability density that remains stable in the limit $N \to \infty$ [5]. However, these types of time crystals have not yet been experimentally realised. It seems that ultra-cold atom gasses may be an ideal basis for experimental realisation, as they allow for the creation and control of many-body systems prepared in an excited state [4].

Floquet Time Crystals

Another type of time crystal that was proposed are so-called Floquet time crystals. The idea behind these is that the Hamiltonian of the system is dependent on time, i.e. $H = H(t)$. Such systems break continuous time translation symmetry and their energy is not conserved. However, it is possible to realise time periodic systems $H(t + T) = H(t)$, which are driven

by an external periodic force. Their stationary states are known as Floquet eigenstates $|u_n(t+T)\rangle = |u_n(t)\rangle$ and exhibit properties analogous to the Bloch states that are often used to describe periodic systems in space. Analogous to the Bloch theorem, these eigenstates can be used to write down the Schrödinger equation for the Floquet Hamiltonian H_F

$$H_F|u_n(t)\rangle = [H(t) - i\partial_t]|u_n(t)\rangle = E_n|u_n(t)\rangle, \tag{1.7}$$

where $|u_n(t)\rangle$ must fulfill periodic boundary conditions in time. The time evolution of a Floquet state contains a time-dependent phase $e^{-iE_nt}|u_n(t)\rangle$, which can be shown to be an eigenstate of the time translation operator $\mathcal{T}$

$$\mathcal{T}|u_n(0)\rangle = e^{-iE_nT}|u_n(T)\rangle = e^{-iE_nT}|u_n(0)\rangle. \tag{1.8}$$

Therefore, the probability density for detecting a particle or many particles at a fixed point in space, is periodic in time when the system is prepared in a Floquet eigenstate. It has also been shown that this process can occur spontaneously and that a periodically driven system can start to evolve with a period that differs from the original drive periodicity. This is known as a Floquet time crystal. Because they break the discrete time translation symmetry, they are also known as discrete time crystals.

There are several ways in which Floquet time crystals can be realised. In Ref. [6], it is shown that a system of ultra-cold atoms bouncing on an oscillating atom mirror will produce a time crystal. Their simulations show that the time evolution of the system has a period that is twice as long as the period of the many-body Floquet Hamiltonian. Although the experimental set-up which recreates this model has been outlined and researched [7], [8], it has not yet been done.

Another possible set-up which produces a Floquet time crystal that has been experimentally verified is a system of periodically driven spin systems. These one-dimensional spin chains are driven to flip periodically. However, the time evolution of these systems show that they not only localise in space, but also start to oscillate with a period that is twice as long as the driving period. The theory for these systems was first described in Refs. [9] and [10] and eventually realised experimentally in Refs. [11] and [12].

Dissipative Time Crystals

Statistical physics is usually a powerful tool in studying the behaviour of many-body systems from their microscopic principles. If a system has relaxed to a steady state, statistical physics can be used to derive its classical thermodynamic properties, such as temperature and pressure. However, not all systems reach this statistical equilibrium. Time crystals in particular are characterised by their non-stationary dynamics and therefore require an alternative physical approach.

Relaxation to a stationary state occurs in isolated systems according to the eigenstate thermalization process (ETH) [13]. In a generic many-body system, there is enough destructive interference to quickly destroy any coherent motion and relax the system [13]. In open quantum systems, similar relaxation processes can occur, but on a longer time scale due to the interactions with the environment [13]. However, some open quantum systems do not relax

and instead exhibit non-stationary dynamics in the long-time limit. These open systems, which under closed conditions would normally thermalise according to the ETH, are known as dissipative time crystals. Specifically, they are defined as a quantum system coupled to a noise inducing environment, which exhibits periodic motion in some observable at late time for generic initial conditions [13]. This periodic motion is usually a form of persistent oscillations. In this choice of environment, they differ from discrete, or Floquet, time crystals, which require an external time-dependent driving. It also makes them more appealing for experimental realisation, since quantum systems in practical settings are always subject to some external environment. Whereas this external noise is usually a destructive force for quantum behaviour, in the case of dissipative time crystals it is a necessary condition to induce the persistent oscillations.

Generally, the study of dissipative time crystals requires a quantum system that is weakly coupled to a noisy environment with Markovian interactions [13]. The resulting behaviour is captured by the Lindblad master equation which describes the evolution of the system with Hamiltonian H,

$$\dot{\rho}(t) = \mathcal{L}\rho = -i[H, \rho] + \sum_{\mu}(2L_{\mu}\rho L_{\mu}^{\dagger} - L_{\mu}^{\dagger}L_{\mu}\rho - \rho L_{\mu}^{\dagger}L_{\mu}), \qquad (1.9)$$

where $\mathcal{L}$ is the Liouville superoperator. The coupling to the environment is described by the set of Lindblad jump operators $\{L_{\mu}\}$. These operators are for example particle creation/annihilation operators and number operators. Carefully selecting which operators to include allows for a model that describes the interactions between the system and the environment without knowledge of the underlying mechanics. In the long-time regime, the study of dissipative time crystals focuses mainly on the study of the (purely imaginary) eigenvalues of $\mathcal{L}$ [13]. We can easily show this when we consider a time-independent Hamiltonian of our system. In this case, the Liouville superoperator is also time-independent, resulting in the following expression for the dynamics of the system

$$\rho(t) = \exp\{[\mathcal{L}(t - t_0)]\rho(t_0)\}. \qquad (1.10)$$

From this, we can easily see that persistent oscillations will only occur when the eigenvalues of $\mathcal{L}$ are purely imaginary. However, finding the full eigenvalue spectrum for many-body systems is currently both analytically and computationally very complex. Nevertheless, it has been shown [13] that purely imaginary eigenvalues arise from the presence of dark states and strong dynamical symmetries, which can lead to time crystalline behaviour. Dark states are eigenstates of the closed system Hamiltonian which cannot be accessed by the external noise of the environment.

Dynamical localisation of dissipative systems

Although the Lindblad formalism outlined in the previous section is useful in the study of dissipative time crystals, it does come with limitations. The Caldeira-Leggett formalism, developed in 1983 by Amir Caldeira and Sir Anthony James Leggett, describes a (quantum) particle that is coupled to a bath [14]. It is more generic than the Lindblad formalism, as it also accounts for memory (non-Markovian) effects. In this thesis, we will look at such a

dissipative system using the Caldeira-Leggett model. The motivation for this choice stems from a study in 2007 [1], which shows the behaviour of a particle coupled to a thermal reservoir of two-level systems (TLSs). Surprisingly, deep in the sub-ohmic regime ($s \ll 1$), the particle position q exhibits a behaviour close to what nowadays we would call a time crystal (see Figure 1.2). Under certain conditions, the particle exhibits long-term oscillations in time. Naturally, as the concept had not yet been established at the time, the article does not argue that a time crystal is formed. Instead, it concludes that the oscillatory behaviour arises from "the non-Markovian character of the dissipative process, which [...] is provided by inelastic scattering of the particle of interest by the TLSs" [1]. However, in light of the new research on time crystals, it is interesting to revisit the system and analyse it from this new perspective. Can we determine whether the dynamical behaviour is due to the breaking of time translation invariance and how robust is it to the change of parameters?
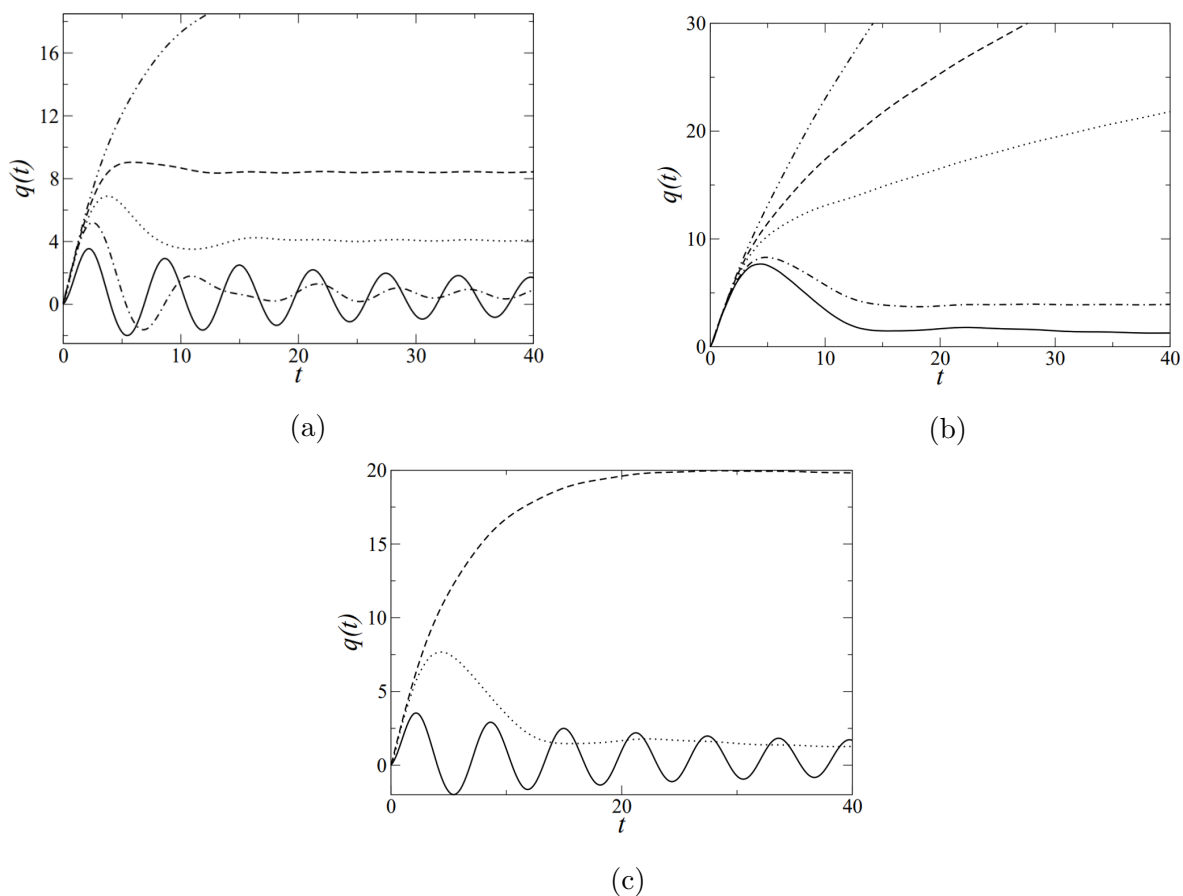

(a)

(b)

(c)

Figure 1.2: Time dependence of the particle center of mass in dimensionless units for (a) $s = 0$, and (b) $s = 0.5$, and different values T of temperature. The continuous line corresponds to $T = 0.0001$, while the dash-dotted, dotted, dashed and double-dotted lines are for $T = 0.01$, $T = 0.1$, $T = 0.2$ and $T = 0.5$, respectively. (c) Time dependence of the particle center of mass for $T = 0.001$ and different values of s. The continuous line corresponds to $s = 0$, while the dotted and dashed lines are for $s = 0.5$ and $s = 1$, respectively. In all cases $\Omega = 1$, $\gamma = 0.3$ and the initial velocity was taken equal to 1. Figures taken from Ref. [1].

Relevance

Obviously, one might wonder whether the theory and subsequent realisation of time crystals is a useful concept. Once time crystals can be formed, will they become as useful and ubiquitous as the ordinary space crystals that abound the world around us?

For a relatively new field in physics, these questions are difficult to answer. Much research needs to be done to reveal the various realisations of time crystals and their properties, whether they are designed experimentally or discovered to exist in nature. However, according to Wilczek [15], it seems that one of the possible applications for time crystals is in high-precision clocks. Currently, the most accurate clocks are based on the resonance frequency of atoms. Although they are accurate, they are also vulnerable to instability in the long term. A clock based on the principle of time crystals could prove to be more stable and rigid and therefore lend itself to be an excellent replacement for GPS [15].

Another area in which time crystals could become quite useful is quantum simulators [10], [4]. These are devices that use quantum effects to answer questions about systems that cannot be solved efficiently by classical computers. Current quantum simulators are used to better understand low-temperature physics and many-body systems, which are difficult to efficiently solve due to the complex quantum mechanical effects that are at play. By tuning several parameters, the simulated systems can be completely controlled. Time crystals could offer an additional degree of freedom, time, to control the simulation, which could make them more versatile than the current quantum simulators [4].

Structure of thesis

In this thesis we will focus mainly on a specific type of dissipative time crystal, one where we couple a quantum system to a bath consisting of two-level systems. We start in Chapter 2 with classical dissipative systems, introducing the Langevin equation and Brownian dynamics. We then transition from the classical case to a quantum mechanical description, motivated by a short overview of Josephson Junctions and SQUIDs. Chapter 3 introduces the Caldeira-Leggett model that describes quantum dissipative systems. In Chapter 4, we replace the generic bath of the Caldeira-Leggett model with a bath consisting of two-level systems. Using this bath will result in time-crystalline behaviour, which we then model and analyse in Chapters 5 and 6.

PART I

THEORETICAL MODEL

2   Quantum Brownian Motion

The goal of this thesis is to understand and analyse the dynamics of a dissipative quantum system coupled to a thermal bath of two-level systems. However, before we get to that point, we will first lay some groundwork. In this chapter, we aim to provide a short introduction to dissipative systems and some tools we will later require. Starting from perhaps the most well-known example of classical dissipation, Brownian motion, we then provide a link through Josephson Junctions and SQUIDs, to its quantum mechanical equivalent.

2.1   Classical Brownian Motion and the Langevin Equation

A dissipative, or open, system is connected to its environment such that energy and matter can be exchanged freely between the two. As a result, the system does not reach an equilibrium, or steady state. The dynamics of such systems require the use of non-equilibrium physics. Perhaps the simplest example of an open system is Brownian motion. It was first described in 1827 by botanist Robert Brown, who studied the motion of pollen immersed in water. These particles seemed to perform a random walk, moved by the influence of the water molecules. More precisely, the theory of Brownian motion describes the random motion that small particles in a viscous fluid exhibit due to collisions with the fluid molecules, which are caused by thermal fluctuations of the fluid.

A Langevin equation can be used to describe the time evolution of a Brownian particle. For a classical system, Newton's equation of motion for a particle with mass M and position q is

$$M\ddot{q}(t) = F_{tot}(t), \tag{2.1}$$

where $F_{tot}(t)$ is the total force on the particle at time t. The exact expression of this force is usually difficult to derive. Instead, it can be separated into two parts, a friction term proportional to the velocity of the particle, and a random force field that represents the thermal fluctuations of the fluid. The result is a stochastic differential equation, known as the Langevin equation

$$M\ddot{q} + \eta\dot{q} + V'(q) = f(t) \tag{2.2}$$

where η is the dissipation constant, or friction coefficient, $V(q)$ is an external potential, and $f(t)$ is the random force field. The fluctuating force obeys a Gaussian probability distribution with correlation function

$$\langle f(t) \rangle = 0, \quad \langle f(t)f(t') \rangle = 2\eta k_B T \delta(t - t'), \tag{2.3}$$

where k_B is Boltzmann's constant and T is temperature.

2.2   SQUIDs

So far, we have only talked about the classical example of Brownian motion, historically and physically. There are, however, also systems whose dynamics obey a similar equation, but which exist in the quantum mechanical regime. An example of this is the magnetic flux in the interior of superconducting micro-circuits observed at $T_0 \lesssim 1K$ [16], [17]. These

types of systems are called Superconducting QUantum Interference Devices, or SQUIDs. They generally consist of a superconducting ring closed by a weak contact, the Josephson junction. In this low temperature regime, it should be possible to observe quantum effects on a macroscopic scale. To illustrate the workings of a SQUID, we will give a brief overview here. For a more detailed explanation of SQUIDs and Josephson junctions, see Appendix A.
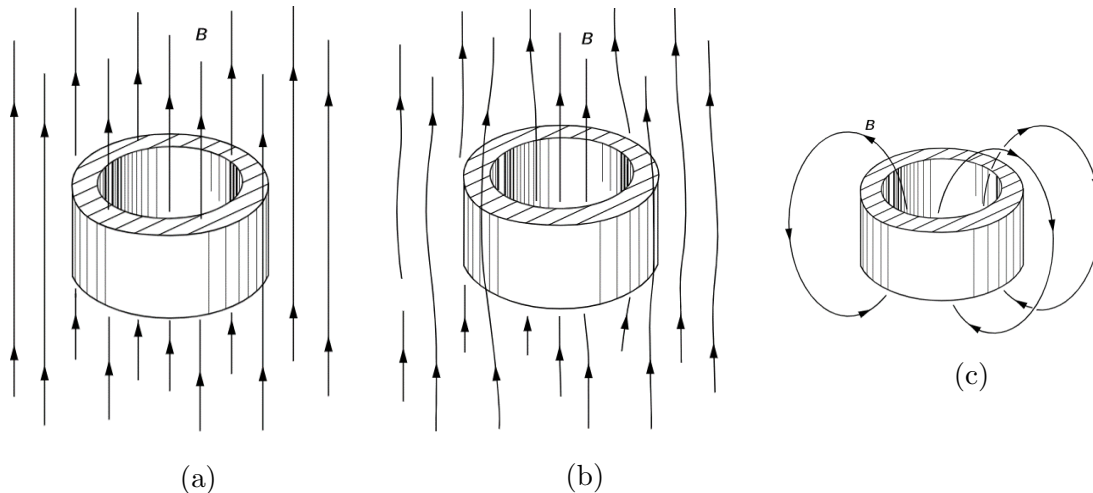

Figure 2.1: A ring in a magnetic field: (a) in the normal state; (b) in the superconducting state; (c) after the external magnetic field has been turned off. Figures extracted from Ref. [18].

The first step to creating a SQUID is by placing a closed, superconducting ring inside a magnetic field, see Figure 2.1. At high temperatures, the ring is in a normal state and inside, around and through this ring runs the magnetic flux, ϕ (Figure 2.1(a)). When the temperature of the ring is brought down with liquid helium, e.g. $T \rightarrow 0K$, the material becomes superconducting and expels the flux through the ring (Figure 2.1(b)). In addition, the flux trapped inside the superconducting ring is quantized, i.e. an integer number of the flux quantum $\phi_0 = hc/2e$. If we then turn off the magnetic field outside the ring, the flux inside the ring is trapped (Figure (c)). We can create a "little door" using a small point of non-superconducting material, also known as a Josephson junction. Through this door, the flux can escape through a process known as quantum tunnelling. Each time that a flux quantum escapes the ring, a current can be measured. Combining the results derived in Appendix A, we can write down the full flux quantization for SQUID rings

$$\phi + \frac{\phi_0}{2\pi}\bar{\varphi} = n\phi_0, \tag{2.4}$$

where n is an integer and $\bar{\varphi} = \varphi_1 - \varphi_2$ is the phase difference from both sides of the junction.

The total flux ϕ can also be calculated using the current

$$\phi = \phi_x + L \cdot i, \tag{2.5}$$

where ϕ_x is the flux created by the external magnetic field, L is the self-inductance and i the total current. In the resistively shunted junction (RSJ) model, additional resistive effects due

to an alternating current are included. The current is composed of three parts: the Josephson current i_S, the normal current i_N, and the polarization current i_C. The Josephson current is created by the Cooper pairs that tunnel through the junction. Therefore, it is dependent on the phase difference across the junction, $\bar{\varphi}$, and the critical current i_0:

$$i_S = i_0 \sin \bar{\varphi}.$$

The normal current originates from the two-fluid model and obeys Ohm's law

$$i_N = \frac{V}{R},$$

where V and R are the voltage across the junction and the normal resistance, respectively. Lastly, there is the polarization current, which appears due to the finite capacitance (C) of the junction

$$i_C = C\dot{V}.$$

Bringing these elements together, we can write down the full expression for the current

$$i = i_S + i_N + i_C$$
$$= i_0 \sin \bar{\varphi} + \frac{V}{R} + C\dot{V}, \tag{2.6}$$

where i_0 is the critical current, $\bar{\varphi}$ the phase difference across the junction, V the voltage across the junction, R the normal resistance, and C the capacitance. Substituting Eq. (2.6) into Eq. (2.5) and using $V = -\dot{\phi}$ and $\bar{\varphi} = 2\pi(n - \phi/\phi_0)$, gives the following relation

$$\frac{\phi_x - \phi}{L} = i_0 \sin\left(\frac{2\pi\phi}{\phi_0}\right) + \frac{\dot{\phi}}{R} + C\ddot{\phi}, \tag{2.7}$$

which we can rewrite into an equation of motion for a particle with coordinate ϕ.

$$C\ddot{\phi} + \frac{\dot{\phi}}{R} + U'(\phi) = 0, \quad \text{with} \tag{2.8}$$

$$U(\phi) = \frac{(\phi_x - \phi)^2}{2L} - \frac{\phi_0 i_0}{2\pi} \cos\left(\frac{2\pi\phi}{\phi_0}\right). \tag{2.9}$$

In order to properly take the thermodynamical properties of the system into account, we must include a fluctuating current $I_f(t)$ on the right-hand side of Eq.(2.8), with the following correlation functions

$$\langle I_f(t) \rangle = 0 \qquad \langle I_f(t) I_f(t') \rangle = 2\frac{k_B T}{R} \delta(t - t'). \tag{2.10}$$

Comparing Eq.(2.8) to Eq.(2.2), we find that in the case of a SQUID, the capacitance C of the ring has the same function as the mass M of a Brownian particle, and the resistance R is inversely related to the dissipation constant η.

In conclusion, we have seen in the example of the SQUID, a device that behaves according to the same principles as the classical Brownian motion, but instead operates at such low

temperatures that quantum effects should and do appear. The current that is created in the ring is the result of a quantum of flux escaping, or tunnelling, through the Josephson junction. This is a quantum mechanical process. However, the Langevin equation describing the behaviour of the flux does not allow for a direct quantum mechanical description. Due to the presence of a dissipative term in the Langevin equation, it is impossible to create a Lagrangian or Hamiltonian for this system. Therefore, it cannot be quantized using the procedure of second quantisation that is commonly used for closed systems.

The solution to this problem is to couple the system of interest to a heat reservoir, and then quantize the composite system. The difficulty that arises from this method is that we need to know how the reservoir behaves and interacts with our system of interest. This method is explained in Chapter 3 and calculated for a well-known bath of harmonic oscillators.

3   Caldeira-Leggett Model

As physicists measured the flux flow ϕ through the Josephson junction in the SQUIDs, they observed quantum mechanics at work on a macroscopic scale. Microscopic (or quantum) tunnelling describes the process of electrons crossing a potential barrier that has a higher energy than the kinetic energy of the particle. Classically, a particle would not be able to go from one side of the barrier to the other, but due to the Heisenberg uncertainty principle, quantum effects allow the electron to 'tunnel' through. With the development of Josephson junctions, this phenomenon could be observed on a macroscopic scale: a current of particles flowing through a ring without generating a voltage. For SQUIDs, the macroscopic variable tunnelling through the junction is the magnetic flux. This flux behaved according to the Langevin equation for Brownian motion, as we have seen in Section 2.2. However, in order to describe the quantum mechanical effects of this dissipative system, a new theoretical framework was needed.

The Caldeira-Leggett model, developed by Amir Caldeira and Sir Anthony James Leggett in 1983, offers a solution to this quantisation problem. In the simplest case, a dissipative system is coupled to a reservoir. This composite system can then be considered closed, without any dissipation occurring. In the semi-classical limit, the system obeys the Langevin equation for Brownian motion. However, the coupling of the system of interest to the bath causes each particle in the reservoir to be slightly perturbed. This perturbation contains the quantum mechanical information that we are interested in. We can represent this perturbation using a set of independent harmonic oscillators. This choice is especially useful, because harmonic oscillators are one of the few systems that can be solved analytically. This forms the basis for the Caldeira-Leggett model [14].

3.1   Model

The Caldeira-Leggett model is described by

$$L = L_S + L_I + L_R + L_{CT}, \tag{3.1}$$

where

$$L_S = \frac{1}{2}M\dot{q}^2 - V(q) \tag{3.2}$$

$$L_I = -\sum_k C_k q_k q \tag{3.3}$$

$$L_R = \sum_k \frac{1}{2}m_k\dot{q}_k^2 - \sum_k \frac{1}{2}m_k\omega_k^2 q_k \tag{3.4}$$

$$L_{CT} = -\sum_k \frac{1}{2}\frac{C_k^2}{m_k\omega_k^2}q^2, \tag{3.5}$$

are the Lagrangians of the system of interest, interactions, reservoir and counter-term, respectively. M and q are the mass and coordinate of the particle, and $V(q)$ is an external potential. The reservoir consists of a set of non-interacting harmonic oscillators with mass

m_k, coordinate q_k and natural frequency ω_k. C_k is the coupling constant between the system and the reservoir.

In order to check that this system reduces to the Langevin equation in the classical limit, we can calculate the Euler-Lagrange equations of motion for $q(t)$ and $q_k(t)$, the variables for our system of interest and the heat bath, respectively. It turns out that the Euler-Lagrange equations are coupled to each other. In order to 'decouple' them, we perform a Laplace transformation to express $\tilde{q}_k$ in terms of $\dot{q}_k(0)$, $q_k(0)$ and $\tilde{q}$. This both 'cancels' the counter-term from the Lagrangian and provides us with a force $f(t)$ that depends on $\dot{q}_k(0)$ and $q_k(0)$. Using the convolution theorem and a spectral function, we can rewrite the $\tilde{q}$ term into a dissipative term $\eta\dot{q}$. This results in the Langevin equation for classical Brownian motion.

Calculating the Euler-Lagrange Equations

The action for the Caldeira Leggett model is given by

$$S[q, q_k] = \int L \, \mathrm{d}q \, \mathrm{d}q_k, \tag{3.6}$$

with L given in Equation (3.1). Varying the action with respect to the parameters of the system, q, and the environment, q_k, we can calculate their respective Euler-Lagrange equations. We find

$$M\ddot{q} = -V'(q) - \sum_k C_k q_k - \sum_k \frac{C_k^2}{m_k \omega_k^2} q, \tag{3.7}$$

and

$$m_k \ddot{q}_k = -m_k \omega_k^2 q_k - C_k q. \tag{3.8}$$

We see that the equation for the system of interest, i.e. Equation (3.7), still depends on the parameters of the environment, q_k, and vice versa. In order to decouple these equations, we perform a Laplace transformation. The Laplace transformation is defined as

$$\mathscr{L}\{f(t)\} = F(s) = \int_0^\infty f(t)e^{-st} \, \mathrm{d}t, \tag{3.9}$$

where $s = \sigma + i\omega$. Its inverse is defined as

$$f(t) = \mathscr{L}^{-1}\{F(s)\}(t) = -\frac{1}{2\pi i} \lim_{T \to \infty} \int_{\gamma-iT}^{\gamma+iT} e^{st} F(s) \, \mathrm{d}s. \tag{3.10}$$

From partial integration of Equation (3.9), it follows that

$$\mathscr{L}\{f'(t)\} = sF(s) - f(0^-) \tag{3.11}$$

$$\mathscr{L}\{f'(t)\} = s^2 F(s) - sf(0^-) - f'(0). \tag{3.12}$$

Using these relations, we can now rewrite Equation (3.8) so that it reads

$$\tilde{q}_k(s) = \frac{\dot{q}_k(0)}{s^2 + \omega_k^2} + \frac{sq_k(0)}{s^2 + \omega_k^2} - \frac{C_k \tilde{q}(s)}{m_k(s^2 + \omega_k^2)}. \tag{3.13}$$

Taking the inverse Laplace transformation of this expression, we can then replace the second term on the right hand side of Equation (3.7)

$$M\ddot{q} + V'(q) + \sum_k \frac{C_k^2}{m_k \omega_k^2} q = -\frac{1}{2\pi i} \lim_{T \to \infty} \int_{\gamma-iT}^{\gamma+iT} \sum_k C_k \left(\frac{\dot{q}_k(0)}{s^2 + \omega_k^2} + \frac{s q_k(0)}{s^2 + \omega_k^2} \right) e^{st} \, \mathrm{d}s$$

$$+ \frac{1}{2\pi i} \lim_{T \to \infty} \int_{\gamma-iT}^{\gamma+iT} \sum_k \frac{C_k^2}{m_k} \frac{\tilde{q}(s)}{(s^2 + \omega_k^2)} e^{st} \, \mathrm{d}s. \quad (3.14)$$

Using that $1/(s^2 + \omega_k^2) = (1/\omega_k^2)[1 - s^2/(s^2 + \omega_k^2)]$, we can rewrite the last term on the RHS so that it partly cancels out the counter-term on the LHS. We are left with

$$M\ddot{q} + V'(q) + \sum_k \frac{C_k^2}{m_k \omega_k^2} \frac{1}{2\pi i} \lim_{T \to \infty} \int_{\gamma-iT}^{\gamma+iT} \frac{s^2 \tilde{q}(s)}{(s^2 + \omega_k^2)} e^{st} \, \mathrm{d}s =$$

$$- \frac{1}{2\pi i} \lim_{T \to \infty} \int_{\gamma-iT}^{\gamma+iT} \sum_k C_k \left(\frac{\dot{q}_k(0)}{s^2 + \omega_k^2} + \frac{s q_k(0)}{s^2 + \omega_k^2} \right) e^{st} \, \mathrm{d}s. \quad (3.15)$$

We have now almost arrived at an expression for the dynamics of the system, which only depends on the system variable q. We will make use of the convolution theorem in order to rewrite the term containing the Laplace function $\tilde{q}(s)$. The convolution theorem for inverse Laplace functions is given by

$$\mathscr{L}^{-1}\{F(s)G(s)\} = f(t) * g(t) = \int_0^t f(t')g(t-t') \, \mathrm{d}t'. \quad (3.16)$$

Applying this to the $\tilde{q}(s)$-term, we find that

$$\frac{1}{2\pi i} \sum_k \frac{C_k^2}{m_k \omega_k^2} \lim_{T \to \infty} \int_{\gamma-iT}^{\gamma+iT} \frac{s^2 \tilde{q}(s)}{(s^2 + \omega_k^2)} e^{st} \, \mathrm{d}s = \frac{\mathrm{d}}{\mathrm{d}t} \frac{1}{2\pi i} \sum_k \frac{C_k^2}{m_k \omega_k^2} \lim_{T \to \infty} \int_{\gamma-iT}^{\gamma+iT} \frac{s}{(s^2 + \omega_k^2)} \tilde{q}(s) e^{st} \, \mathrm{d}s$$

$$= \frac{\mathrm{d}}{\mathrm{d}t} \sum_k \frac{C_k^2}{m_k \omega_k^2} \int_0^t \cos \omega_k(t - t') q(t') \, \mathrm{d}t'$$

$$= \frac{\mathrm{d}}{\mathrm{d}t} \frac{2}{\pi} \int_0^t \int_0^\infty \frac{J(\omega)}{\omega} \cos \omega(t - t') q(t') \, \mathrm{d}\omega \, \mathrm{d}t',$$

$$(3.17)$$

where in the last line we have introduced the spectral function

$$J(\omega) = \frac{\pi}{2} \sum_k \frac{C_k^2}{m_k \omega_k} \delta(\omega - \omega_k) = \begin{cases} \eta\omega & \omega < \Omega \\ 0 & \omega > \Omega \end{cases}, \quad (3.18)$$

where Ω is a high-frequency cutoff value.

The spectral density function describes the bath in a well-known limit. It is officially defined as the imaginary part of the Fourier transformation of the retarded dynamical susceptibility of the bath of oscillators

$$J(\omega) = \mathrm{Im} \left\{ \mathfrak{F} \langle -i\theta(t - t')[F(t), F(t')] \rangle \right\}, \quad (3.19)$$

where $F(t)$ is the force of the particle on the thermal bath, $\theta(t)$ is the Heaviside step function, and $\mathfrak{F}$ denotes the Fourier transformation.

Using the assumption in Equation(3.18) for the spectral function, and taking the limit $\Omega \to \infty$, we can write

$$\frac{\mathrm{d}}{\mathrm{d}t}\frac{2}{\pi}\int_0^t \lim_{\Omega \to \infty}\int_0^\Omega \eta \cos\omega(t-t')q(t')\,\mathrm{d}\omega\,\mathrm{d}t' = \frac{\mathrm{d}}{\mathrm{d}t}2\int_0^t \eta\delta(t-t')q(t')\,\mathrm{d}t'$$

$$= \eta\dot{q}. \tag{3.20}$$

Substituting this expression back into Equation (3.15), we find

$$M\ddot{q} + \eta\dot{q} + V'(q) = f(t), \tag{3.21}$$

i.e. we have arrived at the Langevin equation for classical Brownian motion Equation (2.2), where we have interpreted the RHS of Equation (3.15) as a fluctuating force $f(t)$. Assuming the bath is in thermodynamic equilibrium, we can use the equipartition theorem to check that this force obeys the same correlation function for white noise. Starting from

$$\langle q_k(0)\rangle = \langle \dot{q}_k(0)\rangle = \langle \dot{q}_k(0)q_{k'}(0)\rangle = 0$$

$$\langle \dot{q}_k(0)\dot{q}_{k'}(0)\rangle = \frac{k_BT}{m_k}\delta_{k,k'}$$

$$\langle q_k(0)q_{k'}(0)\rangle = \frac{k_bT}{m_k\omega_k^2}\delta_{k,k'}, \tag{3.22}$$

we indeed find

$$\langle f(t)\rangle = 0, \quad \langle f(t)f(t')\rangle = 2\eta k_BT\delta(t-t'). \tag{3.23}$$

3.2   Dynamical Reduced Density Operator

Now that we know that the Caldeira-Leggett model produces the classical Brownian motion, we can use it to extract the quantum mechanics of our system of interest from the composite system. This can be done by taking the partial trace of the density operator with respect to the variables of the system of interest, giving the dynamical reduced density operator. The function that describes its time evolution is called the influence functional.

We will start by giving a general approach to calculating the dynamical reduced density operator, before applying it to our model.

General Approach

Suppose we have a generic Hamiltonian of a system with coordinates (q,p) in contact with a heat reservoir consisting of oscillators with coordinates (q_k, p_k)

$$H = H_S(q,p) + H_I(q,q_k) + H_R(q_k,p_k) + H_{CT}, \tag{3.24}$$

where H_S is the Hamiltonian of our system of interest, H_I of the interactions, H_R of the reservoir, and H_{CT} of the counter-term. The total density operator $\hat{\rho}(t)$ can be expressed in

terms of the system coordinates (x, y) and the reservoir coordinates $(\mathbf{R}, \mathbf{Q})$, which correspond to a forward and backward in time travelling path. Also, the reservoir coordinates are vectors $\mathbf{R} = (R_1, \ldots, R_N)$, where R_k is the value of q_k. The total density operator is given by

$$\hat{\rho}(x, \mathbf{R}, y, \mathbf{Q}, t) = \iiiint \mathrm{d}x' \, \mathrm{d}y' \, \mathrm{d}\mathbf{R}' \, \mathrm{d}\mathbf{Q}' K(x, \mathbf{R}, t; x', \mathbf{R}', 0) K^*(y, \mathbf{Q}, t; y', \mathbf{Q}', 0) \times \hat{\rho}(x', \mathbf{R}', y', \mathbf{Q}', 0),$$
(3.25)

where

$$K(x, \mathbf{R}, t; x', \mathbf{R}', 0) = \langle x, \mathbf{R} | e^{-\frac{i}{\hbar} H t} | x', \mathbf{R}' \rangle \tag{3.26}$$

is the quantum mechanical propagator of the composite system, and $K^*(y, \mathbf{Q}, t; y', \mathbf{Q}', 0)$ its time reversed counterpart. The density

$$\hat{\rho}(x', \mathbf{R}', y', \mathbf{Q}', 0) = \langle x', \mathbf{R}' | \hat{\rho}_0 | y', \mathbf{Q}' \rangle \tag{3.27}$$

is the coordinate representation of the initial state.

In order to extract the dynamics of the system, we must take a partial trace of Equation (3.25) with respect to the variables of the reservoir: $\hat{\rho}_S(t) = \mathrm{Tr}_R \, \hat{\rho}(t)$. This means that we must set $\mathbf{R} = \mathbf{Q}$ and integrate over it. If the density of the initial state can be separated into a part belonging to the system and a part belonging to the reservoir, i.e.

$$\hat{\rho}(x', \mathbf{R}', y', \mathbf{Q}', 0) = \hat{\rho}(x', y', 0) \times \hat{\rho}(\mathbf{R}', \mathbf{Q}', 0), \tag{3.28}$$

we can write down the dynamical reduced density operator of the system

$$\tilde{\rho}(x, y, t) = \iint \mathrm{d}x' \, \mathrm{d}y' J(x, y, t; x', y', 0) \hat{\rho}(x', y', 0), \tag{3.29}$$

where J is its so-called "superpropagator" and is given by

$$J(x, y, t; x', y', 0) = \iiint \mathrm{d}\mathbf{R} \, \mathrm{d}\mathbf{R}' \, \mathrm{d}\mathbf{Q}' K(x, \mathbf{R}, t; x', \mathbf{R}', 0) K^*(y, \mathbf{Q}, t; y', \mathbf{Q}', 0) \times \hat{\rho}(\mathbf{R}', \mathbf{Q}', 0). \tag{3.30}$$

Because the reservoir consists of N oscillators, the most efficient method for calculating the propagator K is by writing them in the Feynman representation of functional integrals. The propagator then reads

$$K(x, \mathbf{R}, t; x', \mathbf{R}', 0) = \int_{x'}^{x} \int_{\mathbf{R}'}^{\mathbf{R}} \mathcal{D}x(t') \, \mathcal{D}\mathbf{R}(t') \exp\left\{\frac{i}{\hbar} S[x(t'), \mathbf{R}(t')]\right\}, \tag{3.31}$$

where $x(0) = x'$, $x(t) = x$, $\mathbf{R}(0) = \mathbf{R}'$, $\mathbf{R}(t) = \mathbf{R}$, and

$$S[x(t'), \mathbf{R}(t')] = \int_0^t \mathrm{d}t' L\left[x(t'), \mathbf{R}(t'), \dot{x}(t'), \dot{\mathbf{R}}(t')\right] \tag{3.32}$$

is the action of the system plus the reservoir. Plugging this expression and its time reversed counterpart into Equation (3.30), we find

$$J(x, y, t; x', y', 0) = \int_{x'}^{x} \int_{y'}^{y} \mathcal{D}x(t') \, \mathcal{D}y(t') \exp\left\{\frac{i}{\hbar} \left(\tilde{S}_0[x(t')] - \tilde{S}_0[y(t')]\right)\right\} \times \mathcal{F}[x(t'), y(t')], \tag{3.33}$$

where $\tilde{S}_0$ is the combined action of the isolated system S_0 and the counter-term S_{CT}, and

$$\mathcal{F}[x(t'), y(t')] = \int d\mathbf{R}' \, d\mathbf{Q}' \, d\mathbf{R} \, \rho_R(\mathbf{R}', \mathbf{Q}', 0) \int_{\mathbf{R}'}^{\mathbf{R}} \int_{\mathbf{Q}'}^{\mathbf{R}} \mathcal{D}\mathbf{R}(t') \mathcal{D}\mathbf{R}(t')$$

$$\times \exp\left\{ \frac{i}{\hbar} \Big(S_I[x(t'), \mathbf{R}(t')] - S_I[y(t'), \mathbf{Q}(t')] + S_R[\mathbf{R}(t')] - S_R[\mathbf{Q}(t')] \Big) \right\}, \quad (3.34)$$

is the influence functional. It is the average of the product of two time evolutions over the initial state of the environment. For the case of the Caldeira-Leggett model, in which the reservoir consists of harmonic oscillators, we can explicitly calculate the influence functional.

Influence Functional for Caldeira-Leggett Model

To calculate the influence functional $\mathcal{F}[x, y]$, we recognize that Equation (3.34) is actually a set of integrals of the density matrix of the environment, $\rho_R(\mathbf{R}', \mathbf{Q}', 0)$, multiplied by the propagator of the forced harmonic oscillator and its time-reversed counterpart, with respect to the coordinates of the environment, $\mathbf{R}'$, $\mathbf{Q}'$ and $\mathbf{R}$. The expression for the kth environmental oscillator acted by a force $C_k x(t)$ is

$$K_{RI}^{(k)} = \sqrt{\frac{m_k \omega_k}{2\pi i \hbar \sin \omega_k(t)}} \exp\left[\frac{i}{\hbar} S[x_{cl}(t)] \right], \quad (3.35)$$

with

$$S[x_{cl}(t)] = \frac{m_k \omega_k}{2 \sin \omega_k T} \times \left\{ (R_k^2 + R_k'^2) \cos \omega_k T - 2 R_k R_k' \right.$$

$$+ 2 \int_0^t dr \frac{f(r)}{m_k \omega_k} \left[R_k' \sin \omega_k(t - r) + R_k \sin \omega_k r \right]$$

$$\left. - 2 \int_0^t \int_0^r dr \, ds \frac{f(r) f(s)}{m_k^2 \omega_k^2} \sin \omega_k(t - r) \sin \omega_k s \right\}. \quad (3.36)$$

The normalized density operator reads

$$\rho_R(R_k', Q_k', 0) = \sqrt{\frac{m_k \omega_k (\cosh \hbar \beta \omega_k - 1)}{\pi \hbar \sinh \hbar \beta \omega_k}} \exp\left\{ -\frac{m_k \omega_k}{2\hbar \sinh \hbar \beta \omega_k} \left[(R_k'^2 + Q_k'^2) \cosh \hbar \beta \omega_k - 2 R_K' Q_k' \right] \right\}.$$
$$(3.37)$$

The explicit calculations for the expressions of the action and normalized density operator are given in Appendix B and C, respectively.

We can therefore rewrite the influence functional, so that we get

$$\mathcal{F}[x, y] = \prod_k \mathcal{F}^{(k)}[x, y], \quad (3.38)$$

with

$$\mathcal{F}^{(k)}[x, y] = \int dR_k' \, dQ_k' \, dR_k \, \rho_R(R_k', Q_k', 0) \times K_{RI}^{(k)}(R_k, t, R_k', 0) \times K_{RI}^{(k)*}(R_k, t, Q_k', 0). \quad (3.39)$$

Using the expressions for the density matrix Equation (3.36) and the propagator Equation (3.35), the influence functional becomes

$$
\mathcal{F}^{(k)}[x, y] = \int dR'_k \, dQ'_k \, dR_k \; ACC^* \exp\left\{ -\frac{1}{\hbar} B \left[(R'^2_k - Q'^2_k) \cosh \hbar\beta\omega_k - 2R'_k Q'_k \right] \right\}
$$

$$
\times \exp\left\{ \frac{i}{\hbar} D \left[(R'^2_k - Q'^2_k) \cos\omega_k t + 2R_k Q'_k - 2R_k R'_k \right.\right.
$$

$$
+ 2R_k E \int_0^t dr \left[x(r) - y(r) \right] \sin\omega_k r
$$

$$
+ 2R'_k E \int_0^t dr \, x(r) \sin\omega_k (t - r)
$$

$$
- 2Q'_k E \int_0^t dr \, y(r) \sin\omega_k (t - r)
$$

$$
\left.\left. - E^2 \int_0^t \int_0^r dr \, ds \, y(r)y(s) \sin\omega_k(t - r) \sin\omega_k s \right] \right\},
$$

$$
(3.40)
$$

with constants

$$
A = \sqrt{\frac{m_k\omega_k(\cosh \hbar\beta\omega - 1)}{\pi\hbar \sinh \hbar\beta\omega}}, \quad B = \frac{m_k\omega_k}{2\sinh \frac{\hbar\omega_k}{k_B T}}, \quad C = \sqrt{\frac{m_k\omega_k}{2\pi i\hbar \sin \omega_k T}},
$$

$$
D = \frac{m_k\omega_k}{2\sin\omega_k T}, \quad E = \frac{C_k}{m_k\omega_k}.
$$

$$
(3.41)
$$

In order to solve Equation (3.40), we must perform three integrations. We will use the method of "completing the square" for each variable, to create a simple Gaussian integral

that can readily be integrated. We arrive at the following expression

$$
\mathcal{F}^{(k)}[x,y] = \sqrt{\frac{\pi^3 \hbar^3}{\kappa \lambda \mu}}\, ACC^* \exp \Bigg\{ -\frac{1}{\hbar} \Bigg[2iDE^2 \int_0^t \int_0^r \mathrm{d}r\, \mathrm{d}s\, \sin \omega_k(t-r) \sin \omega_k s [x(r)x(s) - y(r)y(s)]
$$

$$
+ \frac{D^2 E^2}{\kappa} \int_0^t \int_0^t \mathrm{d}r\, \mathrm{d}s\, \sin \omega_k(t-r) \sin \omega_k(t-s)[y(r)y(s)]
$$

$$
+ \frac{D^2 E^2}{\lambda} \int_0^t \int_0^t \mathrm{d}r\, \mathrm{d}s\, \sin \omega_k(t-r) \sin \omega_k(t-s) \left[x(r) - \frac{B}{\kappa} y(r) \right] \left[x(s) - \frac{B}{\kappa} y(s) \right]
$$

$$
+ \frac{D^4 E^2}{\lambda^2 \mu} \int_0^t \int_0^t \mathrm{d}r\, \mathrm{d}s\, \sin \omega_k(t-r) \sin \omega_k(t-s)[y(r)y(s)]
$$

$$
+ \frac{D^4 E^2}{\lambda^2 \mu} \left(\frac{B}{\kappa} - 1 \right)^2 \int_0^t \int_0^t \mathrm{d}r\, \mathrm{d}s\, \sin \omega_k(t-r) \sin \omega_k(t-s) \left[x(r) - \frac{B}{\kappa} y(r) \right] \left[x(s) - \frac{B}{l} y(s) \right]
$$

$$
+ \frac{D^4 E^2}{\kappa \lambda \mu} \left(\frac{B}{\kappa} - 1 \right) \int_0^t \int_0^t \mathrm{d}r\, \mathrm{d}s\, \sin \omega_k(t-r) \sin \omega_k(t-s)
$$

$$
\times \left(y(r) \left[x(s) - \frac{B}{\kappa} y(s) \right] + \left[x(r) - \frac{B}{\kappa} y(r) \right] y(s) \right)
$$

$$
+ \frac{D^2 E^2}{\mu} \int_0^t \int_0^t \mathrm{d}r\, \mathrm{d}s\, \sin \omega_k r \sin \omega_k s [x(r) - y(r)][x(s) - y(s)]
$$

$$
- i \frac{D^3 E^2}{\kappa \mu} \int_0^t \int_0^t \mathrm{d}r\, \mathrm{d}s \Bigg(\sin \omega_k r \sin \omega_k(t-s)[x(r) - y(r)]y(s)
$$

$$
+ \sin \omega_k(t-r) \sin \omega_k s\, y(r)[x(s) - y(s)] \Bigg)
$$

$$
+ i \frac{D^3 E^2}{\lambda \mu} \left(\frac{B}{\kappa} - 1 \right) \int_0^t \int_0^t \mathrm{d}r\, \mathrm{d}s \Bigg(\sin \omega_k r \sin \omega_k(t-s) \left[x(r) - y(r) \right] \left[x(s) - \frac{B}{\kappa} y(s) \right]
$$

$$
+ \sin \omega_k(t-r) \sin \omega_k s \left[x(r) - \frac{B}{\kappa} y(r) \right] [x(s) - y(s)] \Bigg) \Bigg] \Bigg\},
$$

$$
(3.42)
$$

where the constants resulting from the Gaussian integration are given by

$$
\kappa = B \cosh \hbar \beta \omega_k + iD \cos \omega_k t, \qquad \lambda = B \cosh \hbar \beta \omega_k - iD \cos \omega_k t - \frac{B^2}{\kappa}, \qquad \mu = D^2 \left(\frac{1}{\kappa} + \frac{1}{\lambda}(\frac{B}{\kappa} - 1)^2 \right).
$$

$$
(3.43)
$$

This long and seemingly complicated expression can be reduced to a real and an imaginary part. Using the fact that $\kappa \lambda \mu = 2BD^2(\cosh \hbar \beta \omega_k - 1)$, we find that the prefactors all cancel and we are left with

$$
\mathcal{F}[x,y] = \exp \left\{ -\frac{i}{\hbar} \int_0^t \int_0^r \mathrm{d}r\, \mathrm{d}s [x(r) - y(r)] \alpha_I [x(s) + y(s)] \right\}
$$

$$
\times \exp \left\{ -\frac{1}{\hbar} \int_0^t \int_0^r \mathrm{d}r\, \mathrm{d}s [x(r) - y(r)] \alpha_R [x(s) - y(s)] \right\}, \qquad (3.44)
$$

where

$$\alpha_I = -\sum_k \frac{C_k^2}{2m_k\omega_k} \sin\omega_k(r-s) \tag{3.45}$$

$$\alpha_R = \sum_k \frac{C_k^2}{2m_k\omega_k} \coth\frac{\hbar\beta\omega_k}{2} \cos\omega_k(r-s). \tag{3.46}$$

We can rewrite the expressions for α_I and α_R using the spectral function (3.18). This gives

$$\alpha_I = \eta\frac{\mathrm{d}}{\mathrm{d}(r-s)}\delta(r-s) \tag{3.47}$$

$$\alpha_R = \frac{\eta}{\pi}\int_0^\Omega \mathrm{d}\omega\,\omega\coth\frac{\hbar\omega}{2k_BT}\cos\omega(r-s). \tag{3.48}$$

We can now further evaluate the imaginary part of the influence functional (3.44), using partial integration

$$\int_0^t\int_0^r \mathrm{d}r\,\mathrm{d}s[x(r)-y(r)]\eta\frac{\mathrm{d}}{\mathrm{d}(r-s)}\delta(r-s)[x(s)+y(s)] =$$
$$-\eta\int_0^t \mathrm{d}r[x^2(r)-y^2(r)]\delta(0) + \frac{\eta}{2}\int_0^t \mathrm{d}r[x(r)\dot{x}(r)+x(r)\dot{y}(r)-y(r)\dot{x}(r)-y(r)\dot{y}(r)]. \tag{3.49}$$

We can approximate $\delta(0)$ by Ω/π, for which we do not have to take the limit $\Omega \to \infty$ [14], and define the relaxation constant

$$\gamma \equiv \frac{\eta}{2M} \tag{3.50}$$

and the frequency shift

$$(\Delta\omega)^2 \equiv \frac{4\gamma\omega}{\pi}. \tag{3.51}$$

Using these definitions, we finally find an expression for the superpropagator (3.33)

$$J(x,y,t;x',y',0) = \int_{x'}^x\int_{y'}^y \mathcal{D}x(t')\,\mathcal{D}y(t')\exp\frac{i}{\hbar}\Big\{S_0[x(t')]-S_0[y(t')]$$
$$-M\gamma\int_0^t \mathrm{d}r[x(r)\dot{x}(r)+x(r)\dot{y}(r)-y(r)\dot{x}(r)-y(r)\dot{y}(r)]\Big\}$$
$$\times\exp\Big\{-\frac{2M\gamma}{\pi\hbar}\int_0^\Omega \mathrm{d}\omega\,\omega\coth\frac{\hbar\omega}{2k_BT}\int_0^t\int_0^r \mathrm{d}r\,\mathrm{d}s[x(r)-y(r)]\cos\omega(r-s)[x(s)-y(s)]\Big\}, \tag{3.52}$$

where the extra harmonic term deriving from the integration by parts cancels against the counter-term in the combined action $\tilde{S}_0$. We can substitute this equation back into Equation (3.29) to find the full expression for the dynamical reduced density operator $\hat{\rho}$. This density operator then allows us to calculate the average value of any quantum mechanical observable, using $\langle A\rangle = \mathrm{Tr}[\hat{\rho}A]$.

So, to summarise, the development of SQUIDs created a need for a quantum mechanical description of systems described by the Langevin equation for Brownian motion. Due to the dissipative term, this system cannot be canonically quantized. However, by coupling the open system of interest to a reservoir, the quantum mechanical dynamics of the full composite system can be determined. Finally, the dynamics of the reservoir can be integrated out, resulting in the dynamical reduced density operator that describes the system of interest. The Caldeira-Leggett model uses this method and couples a system to a bath of harmonic oscillators to allow for a fully analytical solution.

4 Two-Level Systems

The Caldeira-Leggett model can be used to describe the quantum mechanical behaviour of open systems. This method couples the system of interest to a thermal bath to create a closed composite system. Subsequently extracting the behaviour of the heat bath will give you the quantum mechanical behaviour of the system of interest. Once the thermal bath is coupled, each particle in it will be perturbed by the system of interest. However, this is also where we find some disadvantages to the Caldeira-Leggett model. Because the system couples to all the harmonic oscillators, we cannot fine-tune the interactions between the system and the bath.

This is where "two-level systems" (TLSs) come into play [19]. Whereas the quantum harmonic oscillator has an infinite number of energy levels, the TLS only has two. It can therefore also be seen as a "truncated harmonic oscillator", as it displays the same behaviour in the very low temperature limit $(T \rightarrow 0)$. In this limit, we recover the Caldeira-Leggett model. However, at intermediate temperatures they are very different, which is precisely why they are so useful. We will see that in this model, where we couple the system to a bath of TLSs, we can use the temperature as a variable to select which frequencies of the bath are relevant.

4.1 Model

The model of a particle coupled to a bath of TLSs is established in two papers by A. Villares Ferrer *et al*. In the first paper, the system is used to compute the optimal conductivity and the direct current resistivity induced by the reservoir [20]. The second paper looks at the dynamical equations of the coupled particle [1]. It is this particular work that forms the basis for this thesis. The results published in the article show that a particle coupled to a reservoir of TLSs becomes "dynamically localised". This means that at low temperatures and in the sub-ohmic regime, the position of the particle oscillates as a function of time. Using the framework of time crystals, we can now revisit this model and question whether this composite system is a time crystal.

Following the calculations outlined in Ref. [20] and [1] we now derive the theoretical model for a particle coupled to a bath of TLSs. In order to describe it, we will once again calculate the reduced density operator and the spectral function. We shall start by writing down the Hamiltonian for this closed system

$$H = H_0 + H_R + H_I, \tag{4.1}$$

where

$$H_0 = \frac{\hat{p}^2}{2M} + exE, \tag{4.2}$$

$$H_R = \sum_{k=1}^{N} \frac{\hbar \omega_k}{2} \sigma_k^z, \qquad \text{and} \tag{4.3}$$

$$H_I = -\sum_{k=1}^{N} x J_k \sigma_k^x, \tag{4.4}$$

are the Hamiltonians of the particle in an external electric field, the thermal reservoir of TLSs, and the interaction between the two, respectively. Here, we denote with σ_k^j the Pauli matrices in k-space. The interaction strength is determined by the coupling constant J_k.

Influence Functional for TLS

To calculate the reduced density operator, we need to perform the trace over the reservoir degrees of freedom

$$\begin{aligned} \rho(x, y, t) &= \text{Tr}_R[\langle x|\rho(t)|y\rangle] \\ &= \text{Tr}_R[\langle x|e^{-iHt/\hbar}\rho(0)e^{iHt/\hbar}|y\rangle]. \end{aligned} \tag{4.5}$$

As before, we can assume that the heat bath and the system are initially not in contact with each other, and therefore we can write $\rho(0) = \rho_S(0) \times \rho_R(0)$. This gives us the following expression for the reduced density operator

$$\rho(x, y, t) = \iint \mathrm{d}x'\mathrm{d}y' \rho_S(x', y', 0) J(x, y, t, x', y', 0), \tag{4.6}$$

where the superpropagator $J(x, y, t, x', y', 0)$ is given by

$$J(x, y, t, x', y', 0) = \int_{x'}^{x} \mathcal{D}x(t') \int_{y'}^{y} \mathcal{D}y(t') \exp\left\{\frac{i}{\hbar}(S_0[x] - S_0[y])\right\} \times \mathcal{F}[x, y], \tag{4.7}$$

with

$$S_0[z] = \int_0^t L\,\mathrm{d}t = \int_0^t \left[\frac{1}{2}M\dot{z}^2(t') + ez(t')E(t')\right]\mathrm{d}t', \tag{4.8}$$

and $\mathcal{F}[x, y]$ is the influence functional.

For this model, the interaction Hamiltonian H_I is time-dependent, which means that we must pay special attention to its time evolution. We can rewrite the influence functional in terms of the unitary time evolution operator $U[x]$ and its conjugate $U^\dagger[y]$. The time evolution is taken over the interval $t \in [0, t]$. We find

$$\mathcal{F}[x, y] = \text{Tr}_R\left[\rho_R(0)U^\dagger[y]U[x]\right]. \tag{4.9}$$

The time evolution operator can be separated into the evolution operators for the interaction Hamiltonian and the reservoir Hamiltonian, such that

$$\begin{aligned} U[x] &= U_R[x]\,U_I[x] \\ &= e^{-iH_rt/\hbar}\,\overleftarrow{T}\exp\left\{-\frac{i}{\hbar}\int_0^t \tilde{H}_I(x(\tau))\,\mathrm{d}\tau\right\}, \end{aligned} \tag{4.10}$$

where $\overleftarrow{T}$ is the chronological time ordering operator and
$\tilde{H}_I(x(t)) = \exp\{iH_Rt/\hbar\}H_I(x(t))\exp\{-iH_Rt/\hbar\}$ is the interaction Hamiltonian in the interaction picture. The expression for $U^\dagger[y]$ is constructed in a similar way

$$\begin{aligned} U^\dagger[y] &= U_I^\dagger[y]\,U_R^\dagger[y] \\ &= \overrightarrow{T}\exp\left\{+\frac{i}{\hbar}\int_0^t \tilde{H}_I(y(\tau))\,\mathrm{d}\tau\right\}e^{+iH_rt/\hbar}, \end{aligned} \tag{4.11}$$

although here we find the anti-chronological time ordering operator $\overleftarrow{T}$.

Substituting this result into Equation (4.9), we find

$$\mathcal{F}[x,y] = \mathrm{Tr}_R\left[\rho_R(0)\left(\overrightarrow{T}\exp\left\{\frac{i}{\hbar}\int_0^t \tilde{H}_I(y_\tau)\,\mathrm{d}\tau\right\}\right)\left(\overleftarrow{T}\exp\left\{-\frac{i}{\hbar}\int_0^t \tilde{H}_I(x_\tau)\,\mathrm{d}\tau\right\}\right)\right] \quad (4.12)$$

$$= \mathrm{Tr}_R[\rho_R(0)\,A_{y'y}(0,t)\,A_{xx'}(t,0)]. \quad (4.13)$$

where we write $x_\tau \equiv x(\tau)$ and $y_\tau \equiv y(\tau)$ for the sake of brevity. Using the expansion of the exponential $e^x = \sum_{n=0}^{\infty}\frac{x^n}{n!} = 1 + \sum_{n=0}^{\infty}\frac{x^n}{n!}$, we can expand the terms $A_{xx'}$ and $A_{y'y}$ up to second order in the interaction strength J_k

$$A_{y'y}(0,t) = \mathbb{1} + \sum_{n=1}^{\infty}\frac{1}{n!}\left(\frac{i}{\hbar}\right)^n\int_0^t \mathrm{d}t_1\int_0^t \mathrm{d}t_2\ldots\int_0^t \mathrm{d}t_n\,\overrightarrow{T}[\tilde{H}_I(y(t_1))\tilde{H}_I(y(t_2))\cdots\tilde{H}_I(y(t_n))]$$

$$\approx \mathbb{1} + \frac{i}{\hbar}\int_0^t \mathrm{d}\tau\,\tilde{H}_I(y_\tau) - \frac{1}{\hbar^2}\int_0^t \mathrm{d}\tau\int_0^\tau \mathrm{d}\sigma\,\tilde{H}_I(y_\sigma)\tilde{H}_I(y_\tau),\,\text{and similarly} \quad (4.14)$$

$$A_{xx'}(t,0) \approx \mathbb{1} - \frac{i}{\hbar}\int_0^t \mathrm{d}\tau\,\tilde{H}_I(x_\tau) - \frac{1}{\hbar^2}\int_0^t \mathrm{d}\tau\int_0^\tau \mathrm{d}\sigma\,\tilde{H}_I(x_\tau)\tilde{H}_I(x_\sigma). \quad (4.15)$$

The product of these expressions is given by

$$A_{y'y}A_{xx'} \approx 1 + \frac{i}{\hbar}\left[\int_0^t \mathrm{d}\tau\,\tilde{H}_I(y_\tau) - \int_0^t \mathrm{d}\tau\,\tilde{H}_I(x_\tau)\right]$$

$$- \frac{1}{\hbar^2}\int_0^t \mathrm{d}\tau\int_0^\tau \mathrm{d}\sigma\left[\tilde{H}_I(y_\sigma)\tilde{H}_I(y_\tau) + \tilde{H}_I(x_\tau)\tilde{H}_I(x_\sigma) - \tilde{H}_I(y_\tau)\tilde{H}_I(x_\sigma) - \tilde{H}_I(y_\sigma)\tilde{H}_I(x_\tau)\right],$$

$$(4.16)$$

where the linear terms will vanish once we take the trace over the reservoir parameters, because H_I is proportional to the Pauli matrix σ^x which has no diagonal elements.

Substituting this into the influence functional, we find

$$\mathcal{F}[x,y] = 1 - \frac{1}{\hbar^2}\int_0^t \mathrm{d}\tau\int_0^\tau \mathrm{d}\sigma\left[\langle\tilde{H}_I(y_\sigma)\tilde{H}_I(y_\tau)\rangle + \langle\tilde{H}_I(x_\tau)\tilde{H}_I(x_\sigma)\rangle\right.$$

$$\left. -\langle\tilde{H}_I(y_\tau)\tilde{H}_I(x_\sigma)\rangle - \langle\tilde{H}_I(y_\sigma)\tilde{H}_I(x_\tau)\rangle\right], \quad (4.17)$$

where we define the average $\langle A\rangle = \mathrm{Tr}[\rho_R(0)A] = \mathrm{Tr}[(1/Z)\exp\{-\beta H_R\}\,A]$. The partition function is given by

$$Z = \mathrm{Tr}[e^{-\beta H_R}] = \prod_{k=1}^{N} 2\cosh\left(\frac{\hbar\omega_k}{2k_BT}\right). \quad (4.18)$$

For our purposes, we will decompose this average using the commutative properties of the

Pauli matrices to write

$$
\begin{aligned}
\langle A \rangle &= \mathrm{Tr}\left[\frac{1}{Z_1}e^{-\frac{\hbar\omega_1}{2kT}\sigma_1^z} \otimes \ldots \otimes \frac{1}{Z_k}e^{-\frac{\hbar\omega_k}{2kT}\sigma_k^z}A_k \otimes \ldots \otimes \frac{N}{Z_N}e^{-\frac{\hbar\omega_N}{2kT}\sigma_N^z}\right] \\
&= \mathrm{Tr}\left[\frac{1}{Z_1}e^{-\frac{\hbar\omega_1}{2kT}\sigma_1^z}\right]\cdot\ldots\cdot\mathrm{Tr}\left[\frac{1}{Z_k}e^{-\frac{\hbar\omega_k}{2kT}\sigma_k^z}A_k\right]\cdot\ldots\cdot\mathrm{Tr}\left[\frac{1}{Z_N}e^{-\frac{\hbar\omega_N}{2kT}\sigma_N^z}\right] \\
&= \mathrm{Tr}\left[\frac{1}{Z_k}e^{-\frac{\hbar\omega_k}{2kT}\sigma_k^z}A_k\right].
\end{aligned}
\tag{4.19}
$$

Each average in the influence functional, such as $\langle \tilde{H}_I(x_\tau)\tilde{H}_I(x_\sigma)\rangle$, is proportional to the product of two Pauli matrices σ_k^x and σ_q^x. However, for all $k \neq q$ the trace vanishes, so we only need to consider the case where $k = q$. To illustrate how these averages are calculated, we will explicitly consider the term

$$
\langle \tilde{H}_I(x_\tau)\tilde{H}_I(x_\sigma)\rangle = \mathrm{Tr}\left[\frac{1}{Z_k}e^{-\frac{\hbar\omega_k}{2kT}\sigma_k^z}\tilde{H}_I(x_\tau)\tilde{H}_I(x_\sigma)\right],
\tag{4.20}
$$

with

$$
\begin{aligned}
\tilde{H}_I(x_\tau) &= \exp\left\{\frac{i}{\hbar}H_R\tau\right\}H_I\exp\left\{-\frac{i}{\hbar}H_R\tau\right\} \\
&= \exp\left\{i\sum_q \frac{\omega_q}{2}\tau\sigma_q^z\right\}\left(-\sum_k x_\tau J_k\sigma_k^x\right)\exp\left\{-i\sum_{q'}\frac{\omega_{q'}}{2}\tau\sigma_{q'}^z\right\} \\
&= \sum_k \exp\left\{i\frac{\omega_k}{2}\tau\sigma_k^z\right\}(-x_\tau J_k\sigma_k^x)\exp\left\{-i\frac{\omega_k}{2}\tau\sigma_k^z\right\}.
\end{aligned}
\tag{4.21}
$$

Using the expansion $\exp\{\pm i\sigma^j\theta/2\} = \mathbb{1}\cos(\theta/2)\pm i\sigma^j\sin(\theta/2)$, we find

$$
\tilde{H}_I(x_\tau) = -\sum_k x_\tau J_k\left(\sigma_k^x\cos\omega_k\tau - \sigma_k^y\sin\omega_k\tau\right)
\tag{4.22}
$$

and similarly

$$
\tilde{H}_I(x_\sigma) = -\sum_k x_\sigma J_k\left(\sigma_k^x\cos\omega_k\sigma - \sigma_k^y\sin\omega_k\sigma\right).
\tag{4.23}
$$

Substituting these expressions into Equation (4.20), and using

$$
\frac{1}{Z_k}\exp\{-\beta H_R\} = \frac{1}{2}\left[\mathbb{1} - \sigma_k^z\tanh\left(\frac{\hbar\omega_k}{2k_BT}\right)\right],
$$

we find

$$
\begin{aligned}
\langle \tilde{H}_I(x_\tau)\tilde{H}_I(x_\sigma)\rangle = \mathrm{Tr}\left\{\frac{1}{2}\left[\mathbb{1} - \sigma_k^z\tanh\left(\frac{\hbar\omega_k}{2k_BT}\right)\right]\sum_k x_\tau x_\sigma J_k^2\left[\mathbb{1}\cos\omega_k(\tau - \sigma)\right.\right. \\
\left.\left. + i\sigma_k^z\sin\omega_k(\tau - \sigma)\right]\right\}.
\end{aligned}
\tag{4.24}
$$

Now, we can evaluate the trace, using that $\text{Tr}[\sigma^j] = 0$, $\text{Tr}[\mathbb{1}] = 2$, and $\text{Tr}[\sigma^i \sigma^j] = 2\delta^{ij}$ with $i, j = x, y, z$. This results in

$$\langle \tilde{H}_I(x_\tau) \tilde{H}_I(x_\sigma) \rangle = \sum_k x_\tau x_\sigma J_k^2 \left\{ \cos \omega_k (\tau - \sigma) - i \tanh \left(\frac{\hbar \omega_k}{2 k_B T} \right) \sin \omega_k (\tau - \sigma) \right\}. \quad (4.25)$$

Repeating these calculations for the other averages, we find that the influence functional is given by

$$\mathcal{F}[x, y] = 1 - \frac{1}{\hbar^2} \int_0^t d\tau \int_0^\tau d\sigma \sum_k J_k^2 \left\{ f(x, y) \cos \omega_k (\tau - \sigma) - i g(x, y) \tanh \left(\frac{\hbar \omega_k}{2 k_B T} \right) \sin \omega_k (\tau - \sigma) \right\},$$
$$(4.26)$$

with

$$f(x, y) = x_\tau x_\sigma - y_\sigma x_\tau - y_\tau x_\sigma + y_\sigma y_\tau \quad (4.27)$$
$$g(x, y) = x_\tau x_\sigma + y_\sigma x_\tau - y_\tau x_\sigma - y_\sigma y_\tau. \quad (4.28)$$

This equation deviates from Ref. [20], which has opposite signs for the second and third terms in Equation (4.28).

We can rewrite Equations (4.27) and (4.28) in terms of the particle center of mass q and the relative coordinate ξ, using $x = q + \xi/2$ and $y = q - \xi/2$. Therefore, $f(x, y) = \xi(\tau)\xi(\sigma)$ and $g(x, y) = 2q(\sigma)\xi(\tau)$ and the influence functional becomes

$$\mathcal{F}[q, \xi] = 1 - \frac{1}{\hbar^2} \int_0^t d\tau \int_0^\tau d\sigma \sum_k J_k^2 \Big\{ \xi(\tau)\xi(\sigma) \cos \omega_k (\tau - \sigma)$$
$$- 2i q(\sigma)\xi(\tau) \tanh \left(\frac{\hbar \omega_k}{2 k_B T} \right) \sin \omega_k (\tau - \sigma) \Big\}. \quad (4.29)$$

Due to the sign difference in the equation for $g(x, y)$, we find a similar sign difference from Ref. [20] in Equation (4.29).

Spectral function

In order to evaluate the influence functional, we must have enough knowledge of the system to perform the summation over k. This is usually not the case. However, we can calculate the spectral density function using the definition given in Equation (3.18). The force of the particle on the bath of two-level systems is given by $F(t) = \sum_k J_k \sigma_k^x(t)$. We will start by

calculating the commutation relation

$$
[F(t), F(t')] = \left[\sum_k J_k \sigma_k^x(t), \sum_q J_q \sigma_q^x(t') \right]
$$

$$
= \left[\sum_k J_k\, e^{i\frac{\omega_k}{2}\sigma_k^z t}\, \sigma_k^x\, e^{-i\frac{\omega_k}{2}\sigma_k^z t}, \sum_q J_q\, e^{i\frac{\omega_q}{2}\sigma_q^z t'}\, \sigma_q^x\, e^{-i\frac{\omega_q}{2}\sigma_q^z t'} \right],
$$

$$
= \sum_{k,q} J_k J_q \Big\{ \left[\sigma_k^x, \sigma_q^x\right] \cos(\omega_k t)\cos(\omega_q t') + \left[\sigma_k^y, \sigma_q^y\right] \sin(\omega_k t)\sin(\omega_q t')
$$

$$
- \left[\sigma_k^x, \sigma_q^y\right] \cos(\omega_k t)\sin(\omega_q t') - \left[\sigma_k^y, \sigma_q^x\right] \sin(\omega_k t)\cos(\omega_q t') \Big\}. \quad (4.30)
$$

Similar to the calculation of the influence functional, when we will take the trace over this expression all terms with $k \neq q$ will vanish. This leaves only the case $k = q$, for which we can calculate the average, taking the trace over the parameters of the bath

$$
\langle [F(t), F(t')] \rangle = \mathrm{Tr}\left[\frac{1}{Z_k} e^{-\frac{\hbar\omega_k}{2k_B T}} \sum_k 2i J_k^2 \sigma_k^z \sin\omega_k(t - t') \right]
$$

$$
= \sum_k 2i J_k^2 \tanh\left(\frac{\hbar\omega_k}{2k_B T} \right) \sin\omega_k(t - t'). \quad (4.31)
$$

Inserting this into the spectral density function (3.18), we can write

$$
J(\omega, T) = \mathrm{Im}\left\{ -\int_\infty^\infty dt\, e^{-i\omega t}\theta(t - t') \sum_k 2 J_k^2 \tanh\left(\frac{\hbar\omega_k}{2k_B T} \right) \sin\left[\omega_k(t - t')\right] \right\}. \quad (4.32)
$$

We can use the convolution theorem to calculate the Fourier transform

$$
f(t)g(t) = \frac{1}{2\pi}(\hat{f} * \hat{g})(\omega) \quad (4.33)
$$

with

$$
f(t) = \theta(t) \qquad\qquad \hat{f}(\omega) = \pi\left(\frac{1}{i\pi\omega} + \delta(\omega) \right) \quad (4.34)
$$

$$
g(t) = \sin\omega_k t \qquad\qquad \hat{g}(\omega) = -i\pi\big(\delta(\omega - \omega_k) - \delta(\omega + \omega_k) \big). \quad (4.35)
$$

This gives

$$
\int_\infty^\infty dt\, e^{-i\omega t}\theta(t - t') \sin\omega_k(t - t') = \frac{1}{2}\left(\frac{1}{\omega + \omega_k} - \frac{1}{\omega - \omega_k} \right) + i\frac{\pi}{2}\left[\delta(\omega + \omega_k) - \delta(\omega - \omega_k) \right]. \quad (4.36)
$$

Taking only positive frequencies into account and using the imaginary part of the Fourier transform, we find the final expression for the spectral density function

$$
J(\omega, T) = \sum_k \pi J_k^2 \tanh\left(\frac{\hbar\omega_k}{2k_B T} \right) \delta(\omega - \omega_k). \quad (4.37)
$$

This is an important result as we can now see the temperature dependence of our system. The hyperbolic tangent has two limits: for a small argument, it will vanish ($\lim_{x \to 0} \tanh(x) \to 0$); for a large argument, its value will approach 1 ($\lim_{x \to \infty} \tanh(x) \to 1$). Therefore, we can see that depending on the argument of the hyperbolic tangent, different frequencies will be selected. If $\hbar \omega_k << k_B T$, the hyperbolic tangent vanishes and all TLSs with these frequencies will not be selected. However, for $\hbar \omega_k >> k_B T$, the frequencies are relevant and we recover the Caldeira-Leggett model. The temperature can now act as a tuning parameter allowing us to control which bath frequencies to include. This is where the TLS has a clear advantage over the Caldeira-Leggett model.

We can now rewrite the influence functional, by substituting Equation (4.37) into Equation (4.29) and re-exponentiating the expression

$$
\mathcal{F}[q, \xi] = 1 - \frac{1}{\hbar^2} \int_0^t d\tau \int_0^\tau d\sigma \int_0^\infty d\omega \frac{J(\omega)}{\pi} \left[\coth\left(\frac{\hbar\omega}{2k_B T}\right) \xi(\tau)\xi(\sigma) \cos\omega(\tau - \sigma) \right.
$$
$$
\left. - 2iq(\sigma)\xi(\tau) \sin\omega(\tau - \sigma) \right]
$$
$$
\approx \exp\left\{ -\frac{1}{\hbar^2} \int_0^t d\tau \int_0^\tau d\sigma \int_0^\infty d\omega \frac{J(\omega)}{\pi} \left[\coth\left(\frac{\hbar\omega}{2k_B T}\right) \xi(\tau)\xi(\sigma) \cos\omega(\tau - \sigma) \right. \right.
$$
$$
\left. \left. - 2iq(\sigma)\xi(\tau) \sin\omega(\tau - \sigma) \right] \right\}.
$$
$$
(4.38)
$$

This allows us to find an expression for the superpropagator in terms of the particle center of mass coordinate q and the relative coordinate ξ. First, we will substitute Equation (4.38) into Equation (4.7) and perform the same change of variables as we did for the influence functional

$$
J = \int \mathcal{D}q(t') \int \mathcal{D}\xi(t') \exp\left\{ \frac{i}{\hbar}(S_0[q + \xi/2] - S_0[q - \xi/2]) \right\} \times \mathcal{F}[q, \xi]
$$
$$
= \int \mathcal{D}q(t') \int \mathcal{D}\xi(t') \exp\left\{ \frac{i}{\hbar} S_{eff}[q, \xi] \right\} \exp\left\{ -\frac{1}{\hbar}\phi[\xi] \right\}.
$$
$$
(4.39)
$$

The effective action in the imaginary part of the exponent is given by

$$
S_{eff} = \int_0^t d\tau \left[M\dot{q}(\tau)\dot{\xi}(\tau) + eE(\tau)\xi(\tau) + \int_0^\tau d\sigma \Lambda_1(\tau - \sigma)q(\sigma)\xi(\tau) \right]
\tag{4.40}
$$

with

$$
\Lambda_1(\tau - \sigma) = \frac{2}{\pi\hbar} \int_0^\infty d\omega \, J(\omega, T) \sin\omega(\tau - \sigma).
$$

In the real part, the functional ϕ has the form

$$
\phi[\xi] = \int_0^t d\tau \int_0^\tau d\sigma \Phi(\tau - \sigma)\xi(\tau)\xi(\sigma),
\tag{4.41}
$$

with

$$\Phi(\tau - \sigma) = \frac{1}{\pi \hbar} \int_0^\infty \mathrm{d}\omega \, J(\omega, T) \coth\left(\frac{\hbar \omega}{2 k_b T}\right) \cos \omega(\tau - \sigma).$$

Equations of motion

From the effective action we can derive the equations of motion for q and ξ. Varying the action gives us the equations of motion

$$\frac{\delta S_{eff}}{\delta \xi(\alpha)} = \int_0^t \mathrm{d}\tau \left[-M\ddot{q}(\tau) + eE(\tau) + \int_0^\tau \mathrm{d}\sigma \Lambda_1(\tau - \sigma)q(\sigma) \right] \delta(\tau - \alpha)$$

$$= -M\ddot{q}(\alpha) + eE(\alpha) + \int_0^\alpha \mathrm{d}\sigma \Lambda_1(\alpha - \sigma)q(\sigma), \tag{4.42}$$

and

$$\frac{\delta S_{eff}}{\delta q(\alpha)} = \int_0^t \mathrm{d}\tau \left[-M\ddot{\xi}(\tau)\delta(\tau - \alpha) + \int_0^\tau \mathrm{d}\sigma \Lambda_1(\tau - \sigma)\delta(\sigma - \alpha)\xi(\tau) \right]$$

$$= -M\ddot{\xi}(\alpha) + \int_0^t \mathrm{d}\tau \Lambda_1(\tau - \alpha)\xi(\tau). \tag{4.43}$$

Setting $\frac{\delta S_{eff}}{\delta \xi(\alpha)} = 0$ and $\frac{\delta S_{eff}}{\delta q(\alpha)} = 0$, integrating the last term by parts and changing the variables $\alpha \to t$ and $\sigma \to \tau$, we find

$$M\ddot{q}(t) + \int_0^t \mathrm{d}\tau \Lambda(t - \tau)\dot{q}(\tau) = eE(t), \tag{4.44}$$

$$M\ddot{\xi}(t) - \int_0^t \mathrm{d}\tau \Lambda(t - \tau)\dot{\xi}(\tau) = 0, \tag{4.45}$$

where we assume that boundary terms vanish and Λ is the primitive of Λ_1 with respect to σ,

$$\Lambda(t - \tau) = \frac{2}{\pi \hbar} \int_0^\infty \mathrm{d}\omega \, \frac{J(\omega, T)}{\omega} \cos \omega(t - \tau). \tag{4.46}$$

The spectral density function $J(\omega, T)$ is given in terms of microscopic quantities by Equation (4.37). However, we need to rewrite this function in terms of macroscopic quantities to be able to study the behaviour of the system in experiments. An assumption for the spectral function that keeps the temperature dependent behaviour intact, is proposed in [1]. Here we have added a factor $\hbar\pi/2$ for consistency.

$$J(\omega, T) = \frac{\hbar \eta}{2} \left(\frac{\omega}{\omega_c}\right)^s \tanh\left(\frac{\hbar \omega}{2 k_B T}\right) \theta(\Omega - \omega), \tag{4.47}$$

where η is the coupling strength between the particle and the bath, ω_c is a characteristic frequency that allows for a dimensionless coupling strength, s determines the long-time damping properties of the bath, and Ω is a cut-off value for the frequencies. Substituting this spectral density into the equations of motion, we find

$$\ddot{q}(t) + \frac{2\gamma}{\pi} \int_0^t d\tau \Gamma(t-\tau)\dot{q}(\tau) = \frac{eE(t)}{M}, \tag{4.48}$$

$$\ddot{\xi}(t) - \frac{2\gamma}{\pi} \int_0^t d\tau \Gamma(t-\tau)\dot{\xi}(\tau) = 0, \tag{4.49}$$

where $\gamma = \eta/2M$ is the damping constant, and

$$\Gamma(t) = \int_0^\Omega d\omega \frac{\omega^{s-1}}{\omega_c^s} \tanh\left(\frac{\hbar\omega}{2k_BT}\right)\cos(\omega t). \tag{4.50}$$

To solve these equations, we can perform a Laplace transformation, which gives

$$\bar{q}(z) = \frac{q(0)[z + \frac{2\gamma}{\pi}\Gamma(z)] + \dot{q}(0) + \frac{e}{M}E(z)}{z^2 + \frac{2\gamma}{\pi}z\Gamma(z)} \tag{4.51}$$

$$\bar{\xi}(z) = \frac{\xi(0)[z - \frac{2\gamma}{\pi}\Gamma(z)] + \dot{\xi}(0)}{z^2 - \frac{2\gamma}{\pi}z\Gamma(z)}. \tag{4.52}$$

From here on, we assume that the external electric field $E(t)$ is set to zero, for ease of calculations. Assuming $q(0) = 0$ and $\dot{q}(0) = v_0$, we have

$$\bar{q}(z) = \frac{v_0}{z^2 + \frac{2\gamma}{\pi}z\Gamma(z)} \tag{4.53}$$

$$\bar{\xi}(z) = \frac{\xi(0)[z - \frac{2\gamma}{\pi}\Gamma(z)] + \dot{\xi}(0)}{z^2 - \frac{2\gamma}{\pi}z\Gamma(z)}, \tag{4.54}$$

where $\Gamma(z)$ is the Laplace transform of $\Gamma(t)$. In order to calculate this function we use that $\tanh\left(\frac{\pi x}{2}\right) = \frac{4x}{\pi}\sum_{n=1}^\infty \frac{1}{(2n-1)^2+x^2}$ and $\mathcal{L}\{\cos(\omega t)\} = \frac{z}{z^2+\omega^2}$. This gives

$$\Gamma(z) = \frac{4k_BTz}{\hbar}\sum_{n=1}^\infty \underbrace{\int_0^\Omega d\omega \frac{(\omega/\omega_c)^s}{(\lambda_n^2+\omega^2)(z^2+\omega^2)}}_{\mathbb{I}(n,\Omega)}, \tag{4.55}$$

where $\lambda_n = (2n-1)\pi k_BT/\hbar$. The integral $\mathbb{I}(n,\Omega)$ can be rewritten by separating the fraction and using the integral expression $\int_0^\Omega d\omega \frac{\omega^{s-2}}{\omega^2+\alpha^2} = \frac{\Omega^{s-1}}{\alpha^2}\sum_{m=0}^\infty \frac{(-1)^m}{2m+s-1}\left(\frac{\Omega}{\alpha}\right)^{2m}$. This gives

$$\mathbb{I}(n,\Omega) = \frac{1}{z^2+\lambda_n^2}\left[z^2\int_0^\Omega d\omega \frac{\omega^{s-2}}{z^2+\omega^2} - \lambda_n^2\int_0^\Omega d\omega \frac{\omega^{s-2}}{\lambda_n^2+\omega^2}\right]$$

$$= \frac{\Omega^{s+1}}{\lambda_n^2-z^2}\sum_{m=1}^\infty \frac{(-1)^{m-1}}{2m+s-1}\left[\frac{1}{z^2}\left(\frac{\Omega}{z}\right)^{2m-2} - \frac{1}{\lambda_n^2}\left(\frac{\Omega}{\lambda_n}\right)^{2m-2}\right] \tag{4.56}$$

We can now use the hypergeometric function to find a more compact notation of this function. Inserting

$$_2F_1(a; b; c; x) = \sum_{n=0}^{\infty} \frac{(a)^n (b)^n}{(c)^n} \frac{x^n}{n!} \tag{4.57}$$

$$F(s, -\frac{\Omega^2}{\alpha^2}) \equiv {}_2F_1(1, \frac{1+s}{2}, \frac{3+s}{2}, -\frac{\Omega^2}{\alpha^2}) = \sum_{n=1}^{\infty} \frac{s+1}{2n+s-1}(-1)^{n-1}\left(\frac{\Omega}{\alpha}\right)^{2n-2} \tag{4.58}$$

into our expression for $\mathbb{I}(n, \Omega)$, we find that the Laplace transform $\Gamma(z)$ can be written as

$$\Gamma(z) = \frac{4k_B T z}{\hbar \omega_c^s (s+1)} \sum_{n=1}^{\infty} \frac{\Omega^{s+1}}{\lambda_n^2 - z^2} \left[\frac{1}{z^2} F(s, -\frac{\Omega^2}{z^2}) - \frac{1}{\lambda_n^2} F(s, -\frac{\Omega^2}{\lambda_n^2}) \right]. \tag{4.59}$$

4.2 Sub-Ohmic regime

High-T limit

Now we can study the dynamics of the particle centre of mass coordinate q. We first look at the sub-ohmic regime ($s < 1$) in the high-temperature limit. We find that for $s = 0$, the Laplace transform of the damping function reads

$$\Gamma(z) = \sum_{n=1}^{\infty} \frac{4k_B T z}{\hbar(\lambda_n^2 - z^2)} \left[\frac{1}{z} \arctan\left(\frac{\Omega}{z}\right) - \frac{1}{\lambda_n} \arctan\left(\frac{\Omega}{\lambda_n}\right) \right]. \tag{4.60}$$

Then, taking the cut-off frequency $\Omega \to \infty$, we know that $\lim_{\Omega \to \infty} \frac{1}{\alpha} \arctan\left(\frac{\Omega}{\alpha}\right) - \frac{1}{\beta} \arctan\left(\frac{\Omega}{\beta}\right) = \frac{\pi}{2}\left[\sqrt{\frac{1}{\alpha^2}} - \sqrt{\frac{1}{\beta^2}}\right]$. Then, for $T \to \infty$, we find that the high-temperature limit of the damping function is given by

$$\lim_{T \to \infty} \sum_{n=1}^{\infty} \frac{4k_B T z}{\hbar(\lambda_n^2 - z^2)} \frac{\pi}{2} \left[\sqrt{\frac{1}{z^2}} - \sqrt{\frac{1}{\lambda_n^2}} \right] = \frac{2\hbar z \sqrt{\frac{1}{z^2}}}{\pi T k_B} \sum_{n=1}^{\infty} \frac{1}{(2n-1)^2} + \mathcal{O}(\frac{1}{T})^2$$

$$\approx \frac{\pi \hbar}{4k_B T}. \tag{4.61}$$

We can then use this expression to easily solve the inverse Laplace transform to find

$$q(t) = \frac{v_0}{\hbar \gamma / 2k_B T}(1 - e^{-\hbar \gamma t / 2k_B T}). \tag{4.62}$$

We notice that the position of the particle is now explicitly dependent on T, as it is usually the case in classical systems. We essentially recover the Caldeira-Leggett model for a harmonic oscillator bath, though with an ohmic ($s = 1$) temperature dependent damping constant. We

can investigate this further by looking at the damping function $\Gamma(t)$ for the case that $s = 0$ and $\hbar\omega \ll k_B T$,

$$
\begin{aligned}
\Gamma(t - \tau) &= \int_0^\infty \left(\frac{\omega}{\omega_c}\right)^s \frac{\hbar}{2k_B T} \cos\omega(t - \tau) \\
&= \frac{\hbar\pi}{2k_B T}\delta(t - \tau).
\end{aligned}
\tag{4.63}
$$

This instantaneous function shows that the dissipation process is Markovian, i.e. the future of the system does not depend on its past, as is also the case for Brownian motion. Physically, the high-T limit corresponds to a weak interaction between the particle and the bath. Because most of the TLSs are occupied, the bath behaves like harmonic oscillators causing no or little damping on the particle.

Low-T limit

In the low temperature limit, on the other hand, it is not possible to create a Markovian damping function. In this limit, $\lim_{x \to \infty} \tanh(x) = 1$, the damping function $\Gamma(t)$ becomes

$$
\Gamma(t - \tau) = \int_o^\infty d\omega \frac{1}{\omega} \cos\omega(t - \tau).
\tag{4.64}
$$

Looking at our equations of motion, we can say that the damping function acts as a kind of friction force on the particle. For a bath of TLSs, we have already seen that this force is temperature dependent, but in the low-T limit, it also becomes dependent on the previous velocities of the particle, each with different weights given by the damping function.

From Equation (4.64), we can see that the cosine oscillates rapidly, except when $\omega \ll (t-\tau)^{-1}$. In that case, the cosine becomes 1 and the damping function is independent of time.

In order to study the dynamics of the particle, we can perform numerical calculations to approximate the results. For the case where $s = 0$, the solution to Equation (4.59) can be calculated analytically. However, for other values of s, this calculation proves to be more involved and requires a numerical approach in which we terminate the infinite sum. In the next part, we will give the numerical results of the equation of motion $q(t)$.

PART II

NUMERICAL RESULTS

5   Time Crystalline Behaviour

In this section, we will calculate and analyse our results of the equation of motion for the particle $q(t)$. Based on the previous research by Ref [1], we expect to find oscillations in $q(t)$ under certain conditions. If we can find a characteristic frequency that is not related to any driving of the system, then this implies that the continuous time-translation symmetry is reduced to a discrete time-translation symmetry. Therefore, these oscillations point to the possibility of a time crystal. By quantifying the regime in which these oscillations occur, we can establish the conditions under which a time crystal in a particle-TLS bath system is formed. In our analysis, we focus on the influence of three parameters on this function: the damping constant γ, the temperature T and the number s which determines the long time damping properties of the bath. In this section, we will provide a qualitative look at the time crystalline regime. The results are obtained numerically. In Section 6, we will analyse the poles of the inverse Laplace transform (Equation (5.6)) for a more quantified understanding of the behaviour.

5.1   Dimensionless parameters

We start by redefining some of our parameters to make them dimensionless. Currently, the dimensions of our parameters are as follows:

$$[z] = s^{-1}, \ [\Omega] = s^{-1}, \ [\lambda_n] = \left[(2n-1)\pi\frac{k_B T}{\hbar}\right] = s^{-1}, \ [\eta] = kgs^{-2}, \ [\gamma] = \left[\frac{\eta}{2M}\right] = s^{-2}, \ [v_0] = ms^{-1}.$$
$$(5.1)$$

We can make these parameters dimensionless using powers of the cut-off frequency Ω, which allows us to write

$$\tilde{z} = \frac{z}{\Omega}, \qquad \tilde{T} = \frac{k_B}{\hbar\Omega}T, \qquad \tilde{\lambda_n} = \frac{\lambda_n}{\Omega}, \qquad \tilde{\gamma} = \frac{\gamma}{\Omega^2}, \qquad \tilde{v}_0 = \frac{v_0}{\Omega L_s}. \qquad (5.2)$$

From these parameters, we can also define a time scale, t_s [1], and a length scale, L_s. From dimensional analysis, we can derive the following scales up to a constant coefficient,

$$t_s \propto \frac{1}{\sqrt{\gamma}} \qquad (5.3)$$

$$L_s \propto \sqrt{\frac{\hbar\Omega}{\eta}} = \sqrt{\frac{\hbar\Omega}{2M\gamma}}. \qquad (5.4)$$

We now set $\hbar = 1$, $M = 1$, and $\Omega = 1$, such that both our units of length and time are defined in terms of $1/\sqrt{\gamma}$.

---

[1]For the time scale, Verstraten *et al.* [21] also suggests $t_s = 1/\sqrt{2\gamma}$. Although their time scale is derived through a fractional derivative approach to the Langevin equation and hence depends on s, it provided a good basis.

5.2 Results for $q(t)$

In this section, we show our results for the dynamics of the particle, $q(t)$. For convenience, we will restate here the dimensionless versions of the equations which need to be solved. From the equation of motion,

$$\ddot{q}(t) + \frac{2\tilde{\gamma}}{\pi} \int_0^t \mathrm{d}\tau \Gamma(t - \tau)\dot{q}(\tau) = 0, \tag{5.5}$$

we start with a Laplace transformation

$$\bar{q}(\tilde{z}) = \frac{\tilde{v}_0}{\left[\tilde{z}^2 + \frac{2\tilde{\gamma}}{\pi}\tilde{z}\Gamma(\tilde{z})\right]}, \tag{5.6}$$

where

$$\Gamma(\tilde{z}) = \frac{4\tilde{T}\tilde{z}}{\omega_c^s(s + 1)} \sum_{n=1}^{\infty} \frac{1}{\tilde{\lambda}_n^2 - \tilde{z}^2} \left[\frac{1}{\tilde{z}^2} F\left(s, -\frac{1}{\tilde{z}^2}\right) - \frac{1}{\tilde{\lambda}_n^2} F\left(s, -\frac{1}{\tilde{\lambda}_n^2}\right) \right]. \tag{5.7}$$

The sum over the hypergeometric functions in Equation (5.7) is solved numerically. The dynamics of the particle as a function of time, $q(t)$, are found by simply performing the inverse Laplace transformation of Equation (5.6).

Checks

We start by performing several checks on the system. Because the hypergeometric functions for the case $s = 0$ are quite simple, we can use this case to test some of the aspects of our calculation. A typical result is shown in Figure 5.1. This figure is obtained at $s = 0$, $\tilde{\gamma} = 0.3$ and varying temperatures. We can observe the same oscillatory behaviour as Villares Ferrer *et al.* did in Ref. [1]. At low temperatures, we see that the oscillations persist for a relatively long time, whereas for high temperatures, i.e. $\tilde{T} = 0.01$ and above, this behaviour is damped more quickly.
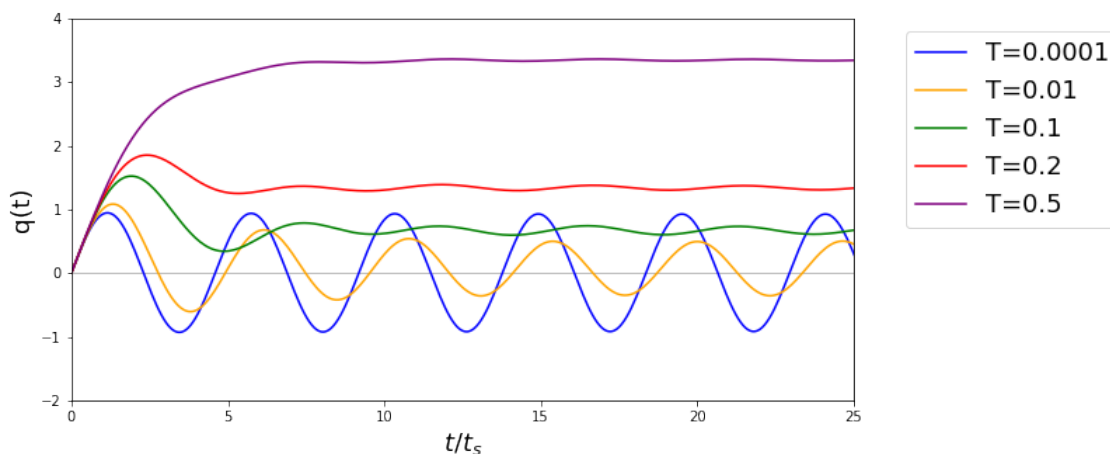
Figure 5.1: The dynamical behaviour of the particle with center of mass coordinate q as a function of time for the case $s = 0$. The other parameters are set as $\tilde{\gamma} = 0.3$, $\tilde{v}_0 = 1$, $n = 100$. The temperature is varied in the range $\tilde{T} = 10^{-4}$, 10^{-2}, 0.1, 0.2, 0.5. The time has been rescaled.

The most important factor to determine before we do an analysis of our results, is the effect of terminating the infinite sum in Equation (5.7) after a certain number of terms n. Figures 5.2(a) and 5.2(b) show the influence of this parameter on the behaviour of the dynamical function $q(t)$. We can numerically determine the amplitude and period using the first maximum and minimum of the function. Although this is only a rough approximation of the amplitude and period, it gives an indication of how they are affected by the number of terms n. We notice that both the amplitude and the period of the oscillations become smaller as we increase the number of terms included in the sum. However, this decrease does seem to stabilise. Unfortunately, as is the nature of most numerical calculations, the more terms included in the calculation, the longer the computation time becomes. For the calculations of the dynamical function $q(t)$, we have chosen $n = 100$ as an appropriate cut-off value for the number of terms included in the sum in order to limit the computation time. For calculations regarding the poles of Equation (5.6), we have taken $n = 500$ as a cut-off value for better precision as the computation time is much lower (see Section 6). Notice that the period and amplitude, shown in Figure 5.2(b), does not change much for $n > 300$.

(a)   (b)
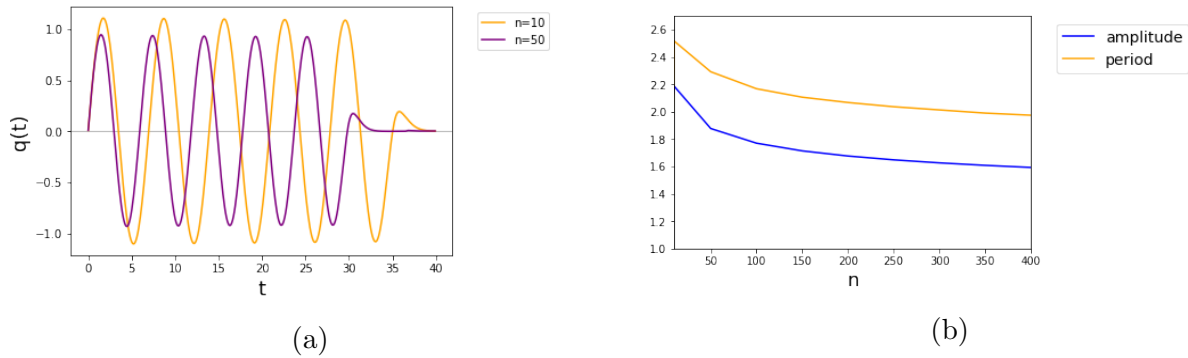
Figure 5.2: The dependence of the simulation results on the number of terms included in the sum. (a) Position as a function of time for $\tilde{\gamma} = 0.3$, $\tilde{v}_0 = 1$ and $\tilde{T} = 10^{-4}$. The number of terms in the sum is varied, with $n = 10$ (orange) and $n = 50$ (purple). (b) The amplitude (blue) and the period (yellow) of the graph as a function of the number of terms n.

Another check that we can perform on our calculations is to check whether our suggestion for the characteristic time scale t_s is correct. This check is shown in Figure 5.3. After performing the calculations for various values of the damping constant γ, we find that this parameter influences both the amplitude and period of the oscillations. However, rescaling the time by a factor of $t_s = 1/\sqrt{2\gamma}$ gives a perfectly aligned period for each curve.

(a)   (b)
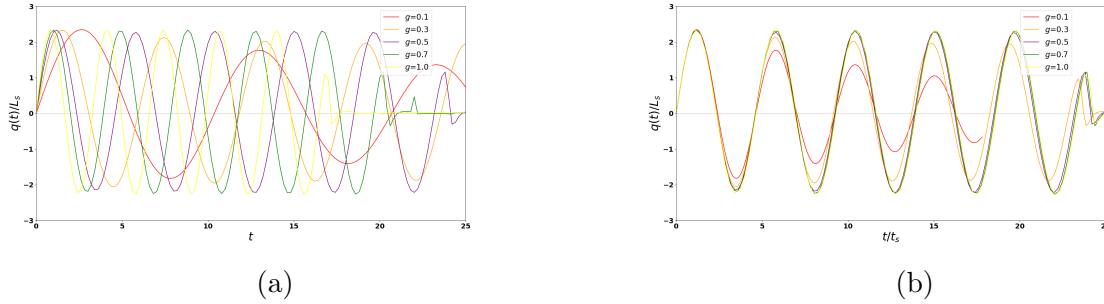
Figure 5.3: (a) The position of the particle as a function of time for $\tilde{v}_0 = 1$ and $\tilde{T} = 10^{-4}$. The parameter $\tilde{\gamma}$ is varied for $\tilde{\gamma} = 0.1, 0.3, 0.5$, and 0.7. (b) The same graph, but for a rescaling of the time such that $t \to t/t_s = t\sqrt{2\gamma}$.

Results

Below, we show the results for $q(t)$ for several combinations of parameters $\tilde{T}$ and s. We keep one of these parameters constant, while varying the other over a range of values in order to provide a qualitative idea of the dependence. The damping constant $\tilde{\gamma}$ has a more subtle effect on the oscillations and will therefore be analysed in further depth in Section 6.

We start by fixing the temperature and varying s. The results are shown in Figures 5.4 – 5.8. We find that the position of the particle is oscillating in time, at least for some values of s. If we focus on the low temperature behaviour in Figure 5.4, we see oscillations in $q(t)$ for nearly all values of s, except $s = 1$. We also notice that the period and amplitude of the oscillations decreases with s. Furthermore, by increasing s, the oscillations are more damped. We see that for $s = 0$ (blue curve), there is a strong periodic structure over a long time. However, for $s = 0.5$ (purple curve), the amplitude after a single period has already significantly decreased. If we then increase the temperature, we find that this damping effect is exacerbated. Whereas for $s = 0$ (blue curve) the oscillations are present for temperatures in the range $\tilde{T} = 10^{-4}$–10^{-2} (see Figures 5.4– 5.6), they quickly dampen for $s = 0.1$ (red curve) and $s = 0.2$ (yellow curve) when the temperature is increased to $\tilde{T} = 10^{-3}$ (Figure 5.5). The more we increase the temperature, the further we have to look in the sub-ohmic regime to find oscillations. At $\tilde{T} = 10^1$, none of the curves exhibit any oscillatory behaviour at all (see Figure 5.8).

We also notice that for high values of s and intermediate T, the curve shows an increase and then freezes, as is common in glass phases. This can be seen for example in Figures 5.6 and 5.7.
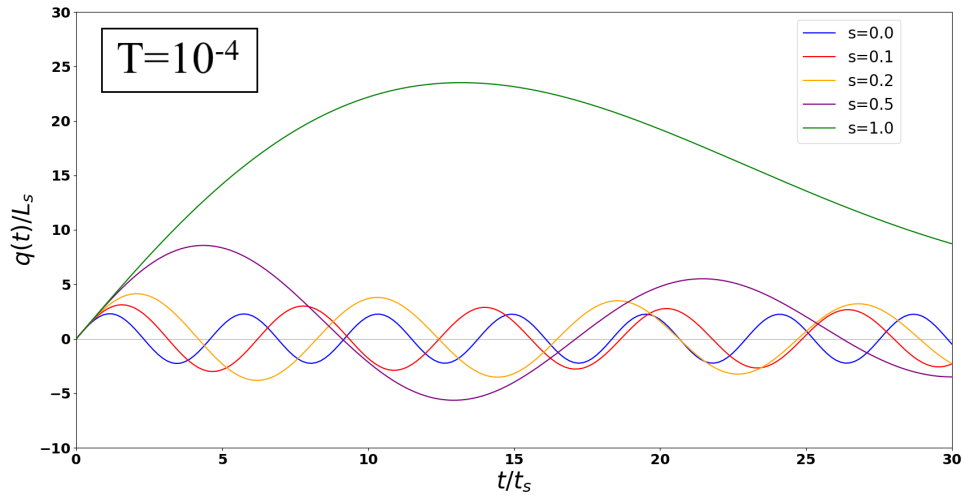
Figure 5.4: The position of the particle as a function of the rescaled time with parameters $\tilde{T} = 10^{-4}$, $\tilde{\gamma} = 0.3$ and $\tilde{v}_0 = 1.0$. The value of s is varied for each curve: $s = 0.0, 0.1, 0.2, 0.5$ and 1.0.
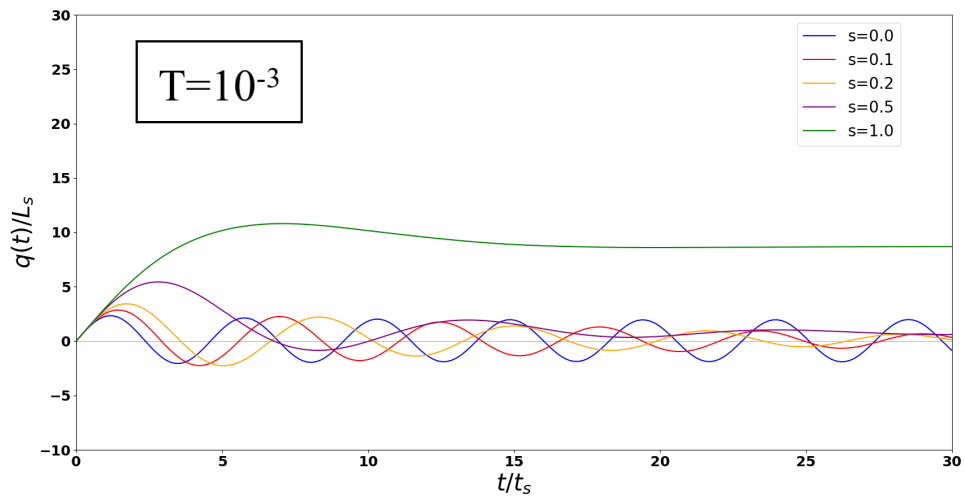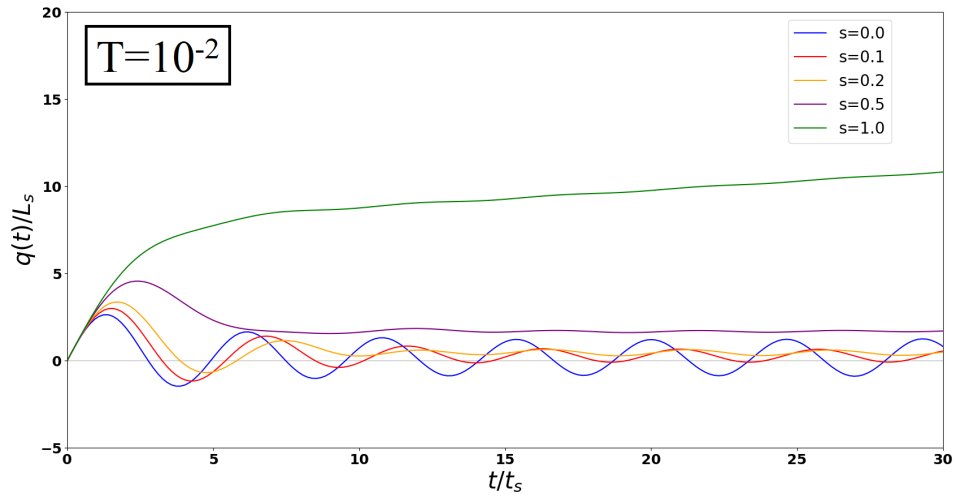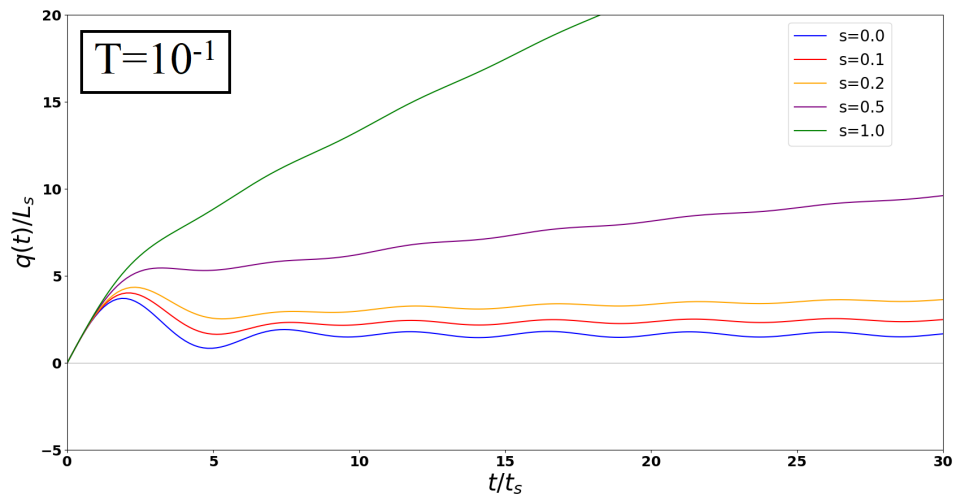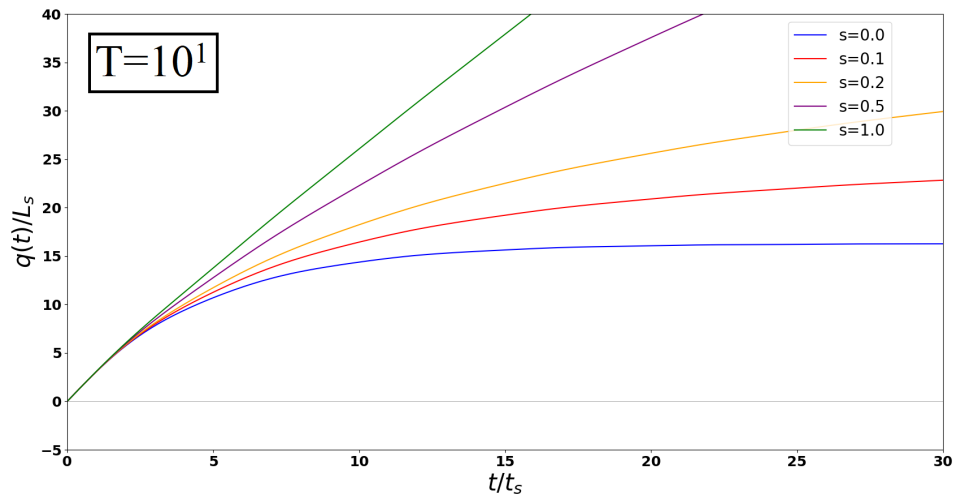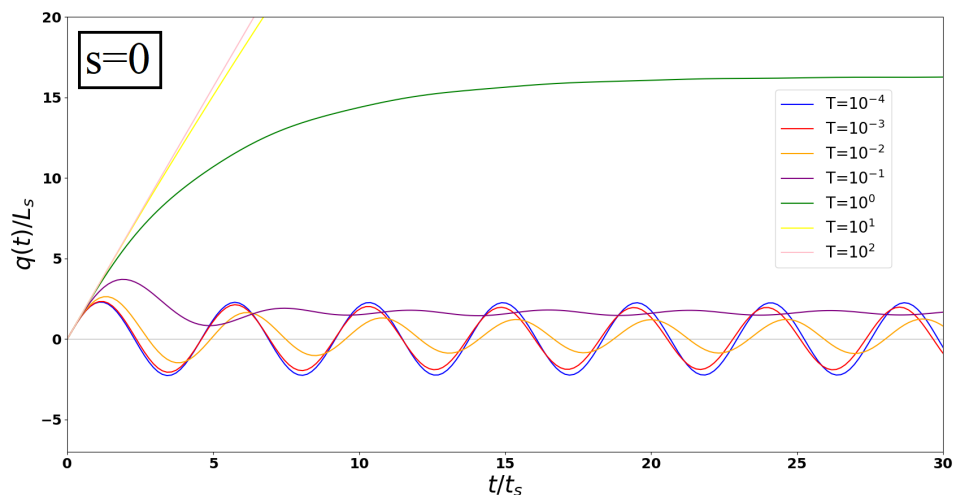

Figure 5.5: The position of the particle as a function of the rescaled time with parameters $\tilde{T} = 10^{-3}$, $\tilde{\gamma} = 0.3$ and $\tilde{v}_0 = 1.0$. The value of s is varied for each curve: $s = 0.0, 0.1, 0.2, 0.5$ and 1.0.
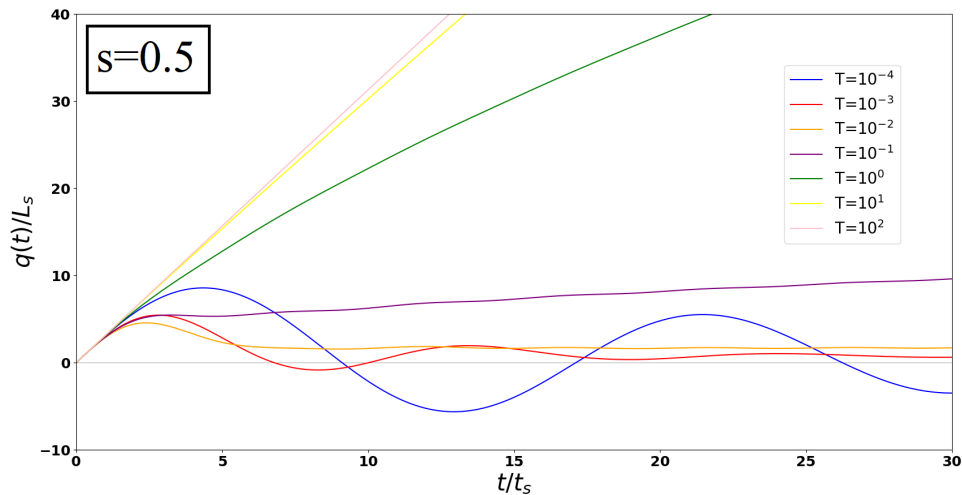
Figure 5.6: The position of the particle as a function of the rescaled time with parameters $\tilde{T} = 10^{-2}$, $\tilde{\gamma} = 0.3$ and $\tilde{v}_0 = 1.0$. The value of s is varied for each curve: $s = 0.0, 0.1, 0.2, 0.5$ and 1.0.

Figure 5.7: The position of the particle as a function of the rescaled time with parameters $\tilde{T} = 10^{-1}$, $\tilde{\gamma} = 0.3$ and $\tilde{v}_0 = 1.0$. The value of s is varied for each curve: $s = 0.0, 0.1, 0.2, 0.5$ and 1.0.

Figure 5.8: The position of the particle as a function of the rescaled time with parameters $\tilde{T} = 10^1$, $\tilde{\gamma} = 0.3$ and $\tilde{v}_0 = 1.0$. The value of s is varied for each curve: $s = 0.0, 0.1, 0.2, 0.5$ and 1.0.

We can also vary the temperature, while keeping s fixed. The results for $s = 0$ and $s = 0.5$ are shown in Figures 5.9 and 5.10, respectively. We see that for $s = 0$, the oscillations are fairly robust for low temperatures $\tilde{T} = 10^{-4}$ and 10^{-3}. If the temperature is increased further, the oscillations are damped until they are no longer visible. For $s = 0.5$, we see that the oscillations are damped for every value of $\tilde{T}$.

Figure 5.9: The position of the particle as a function of the rescaled time with parameters $s = 0$, $\tilde{\gamma} = 0.3$ and $\tilde{v}_0 = 1.0$. The temperature is varied for each curve in the range: $\tilde{T} = 10^{-4}$–10^2.

Figure 5.10: The position of the particle as a function of the rescaled time with parameters $s = 0.5$, $\tilde{\gamma} = 0.3$ and $\tilde{v}_0 = 1.0$. The temperature is varied for each curve in the range: $\tilde{T} = 10^{-4}$–10^2.

To summarise our results, we found that there are oscillations on $q(t)$. For small $\tilde{T}$ and s, these are persistent oscillations with a period determined by $\tilde{\gamma}$ that is proportional to the coupling of the particle to the reservoir. This characteristic period is not related to any timescale of the coupling, showing that there is a spontaneous symmetry breaking of continuous time-translation invariance. Therefore, the particle presents a time crystal phase. For high $\tilde{T}$ and s, the oscillations are damped and the particle is localised for long times. This seems to indicate that there are phase transitions associated to $\tilde{T}$ and s. In the following Chapter we address this issue considering the pole structure of $\tilde{q}$ as function of $\tilde{T}$ and s.

6   Investigating the Poles

In order to understand the oscillatory behaviour exhibited by the equation of motion for the particle center of mass $q(t)$ (Equation (5.5)), we study the behaviour of the poles of its Laplace transform $\bar{q}(\tilde{z})$ (Equation (5.6)). Essentially, we analyse the function in the frequency domain, with $\tilde{z}$ representing the Laplace transformed time variable. The poles of $\bar{q}(\tilde{z})$ correspond to peaks in frequency. We find that there are in general two major peaks that we can distinguish on the imaginary axis, a peak at $\tilde{z} = 0$, i.e. the "zero peak", and a peak that travels along the axis, i.e. the "non-zero peak" (see Figure 6.1).[2] As in the presence of the peak, $q(t)$ can be approximated by $\exp{(\tilde{z}_p t)}$. The peak for a finite imaginary value is related to oscillations with frequency $\tilde{z}_p$, while the zero peak characterises non-oscillatory/localised behaviour. Therefore, a stronger non-zero peaks indicates that the (continuous) time translation symmetry is broken and that the system is in a time crystalline phase. Analysing the behaviour of the peaks as a function of the parameters of our system allows us to quantify the time crystal regime.
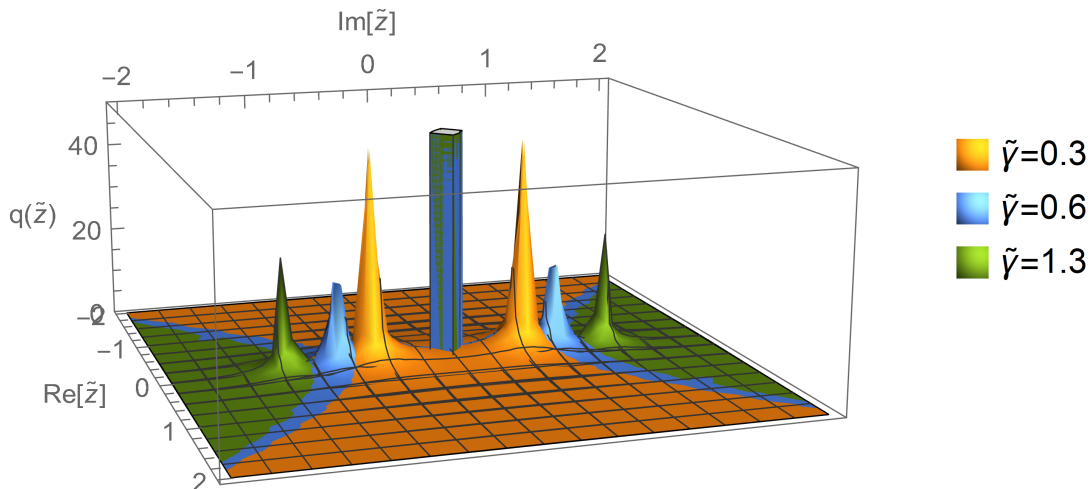
Figure 6.1: An example of the two peaks on the imaginary axis in the frequency domain. For each value of $\tilde{\gamma} = 0.3, 0.6, 1.3$, there exists a central peak at $\tilde{z} = 0$ and a second peak at $\tilde{z} \neq 0$. This second, non-zero peak, is mirrored on both sides of the central peak and its position, amplitude, and width are dependent on the value of $\tilde{\gamma}$. Here, $\tilde{T} = 10^{-4}$ and $s = 0.1$ are fixed.

In this section, we will first discuss the results for the zero peak, followed by the results for the non-zero peak. We analyse the peaks as a function of the three dimensionless parameters: the damping constant $\tilde{\gamma}$, the temperature $\tilde{T}$, and s. For all figures, we have used that $\tilde{v}_0 = 1$, $\Omega = 1$, and $n = 500$.

---

[2]A third peak can be found just after $\tilde{z} = 1$, (at $\tilde{z} = 1$, the inverse Laplace function is always zero), but this peak is usually very small, unless the position of the non-zero peak coincides with it. Due to its often negligible size, it proved difficult to study mathematically and because it might be just a numerical instability we have chosen not to further investigate this peak.

6.1   Zero peak

In most cases, the zero peak is a very high and narrow, almost delta-like, peak centred at $\tilde{z} = 0$. Therefore, it was not possible to accurately determine the width of this peak, but only its amplitude. The amplitude was calculated at a value of $\tilde{z}$ close to $\tilde{z} = 0$, as the function is not clearly defined at $\tilde{z} = 0$. The amplitude of the zero peak represents the statics of the system, i.e. it gives us the general qualitative behaviour of its dependence on our chosen parameters.

The results for the amplitude of the zero peak, $A_{z=0}$, are shown in Figure 6.2. We find that the amplitude is inversely proportional to the damping constant $\tilde{\gamma}$ (see Figure 6.2(a)). This figure also shows that $A_{z=0}$ increases as $\tilde{T}$ and s increase. From Figure 6.2(b), we find that $A_{z=0}$ is directly proportional to $\tilde{T}$, although for high values of s and low values of $\tilde{\gamma}$ (i.e. $s = 0.5$ and $\tilde{\gamma} = 0.01$) the amplitude seems to reach a stationary value. Finally, from Figure 6.2(c) we find that there is a clear phase transition signalled by a change of $A_{z=0}$ around $s = 1$. In the sub-ohmic regime ($s < 1$), the amplitude is qualitatively similar for all parameters, except for a slight variation depending on $\tilde{T}$ and s. However, as we switch to a super-ohmic regime ($s > 1$), the graphs converge to a maximum value and the behaviour becomes universal for all parameters.
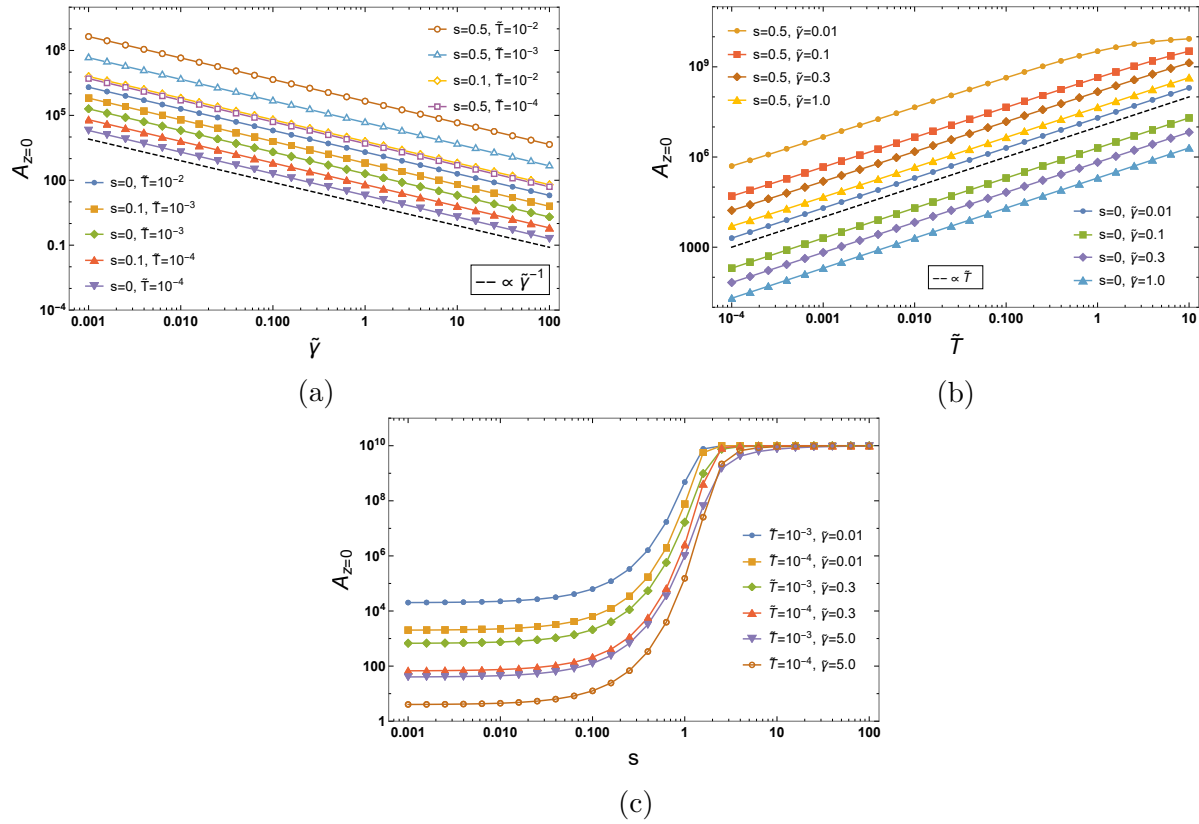
(a)

(b)

(c)

Figure 6.2: The amplitude of the zero peak as a function of (a) the damping constant $\tilde{\gamma}$ for $\tilde{T} = 10^{-4}, 10^{-3}, 10^{-2}$ and $s = 0, 0.1, 0.5$, (b) the temperature $\tilde{T}$ for $\tilde{\gamma} = 0.01, 0.1, 0.3, 1.0$ and $s = 0, 0.5$, and (c) s for $\tilde{\gamma} = 0.01, 0.3, 5.0$ and $\tilde{T} = 10^{-4}, 10^{-3}$. The amplitude of the zero peak is inversely proportional to $\tilde{\gamma}$ and proportional to $\tilde{T}$. There is a phase transition for $s = 1$.

6.2   Non-zero peak

The study of the non-zero peak includes more aspects than that of the zero peak. We look not only at the amplitude of this peak, but also at its width and its position. To do so, we fit the data to a Lorentzian of the form

$$f_L = A_{nzp}/[(z - z_{nzp})^2 + \sigma_{nzp}^2], \tag{6.1}$$

where A_{nzp} is the amplitude, σ_{nzp} the width, and z_{nzp} the position of the non-zero peak. In addition, the ratio of the amplitude to the width is also calculated.

Each of these aspects gives us information about the behaviour of the system and the time crystalline phase. Firstly, the position of the non-zero peak corresponds to the period of the oscillations that we see in the solutions for $q(t)$. If there is no secondary peak, then there are no oscillations. The amplitude then gives us an idea of the intensity of this effect, while the width corresponds to the losses of the system. A small, broad peak signifies a less stable regime than a high, narrow one. Combining them, the ratio of the amplitude and width represents the robustness of this phase.

Although this method does provide us with a general idea of the behaviour of the non-zero peak, it does not allow for a direct comparison with the zero peak due to the different calculation methods. Therefore, we have also calculated the absolute amplitude at the position of the non-zero peak and calculated the ratio of this to the amplitude of the zero peak. This should also give us an indication of the robustness of the time crystalline regime. If the non-zero peak is much smaller than the zero peak, the system may not be robust enough to realise.

We start by discussing the results for the influence of the damping constant $\tilde{\gamma}$ on the behaviour of the non-zero peak.

Dependence on $\tilde{\gamma}$

Figure 6.3 shows the position of the non-zero peak as a function of the damping constant, $\tilde{\gamma}$. We examine it at three values of $s = 0, 0.1$ and 0.5. We should note, however, that for $s = 0.5$, the fit used to identify the non-zero peak did not give consistent results for high temperatures, i.e. $\tilde{T} = 10^{-3} - 10^{-2}$. In these cases, the non-zero peak would sometimes be confused with the zero peak due to their close proximity. Therefore, the results for these values should be taken with a grain of salt. We nevertheless wish to include them here to provide a perspective of the behaviour at the boundaries of our time crystalline regime.

We find that in general, the position behaves according to a power law: $z_{nzp} \propto \tilde{\gamma}^\alpha$. However, we see that in some cases there is a 'kink' in the curve at a critical value $\tilde{\gamma}_c$. This 'kink' becomes more pronounced as $\tilde{T}$ or s is increased, as can be seen in Figure 6.3(b). For $s = 0.5$, it is even visible at $\tilde{T} = 10^{-4}$ (see Figure 6.4(d)). Furthermore, we find that its position is dependent on the value of s. Whereas it lies around $\tilde{\gamma}_c = 0.2$ for $s = 0$, it moves to $\tilde{\gamma}_c = 0.3$ for $s = 0.1$, and $\tilde{\gamma}_c = 1$ for $s = 0.5$.

In Figure 6.4, we analyse the values of the power law exponent before and after this transition. We find that for $\tilde{\gamma} > \tilde{\gamma}_c$ the exponent is equal to $\alpha \approx 0.5$, regardless of the value of s or T,

consistent with the results found in Chapter 5. When no 'kink' is visible, the curve seems to follow this power law exponent for all values of $\tilde{\gamma}$. However, if there is a 'kink', we find that for $\tilde{\gamma} < \tilde{\gamma}_c$ the value of α is larger than 0.5. The change in slope depends on both $\tilde{T}$ and s.
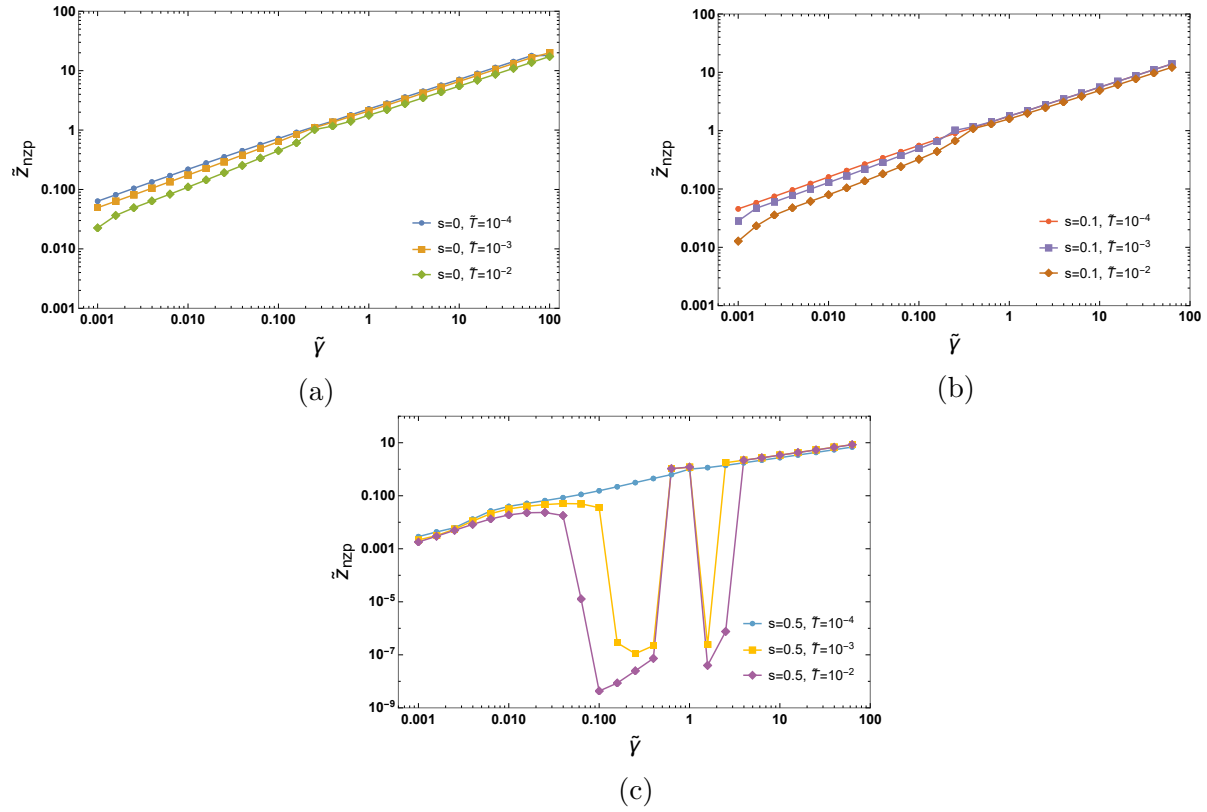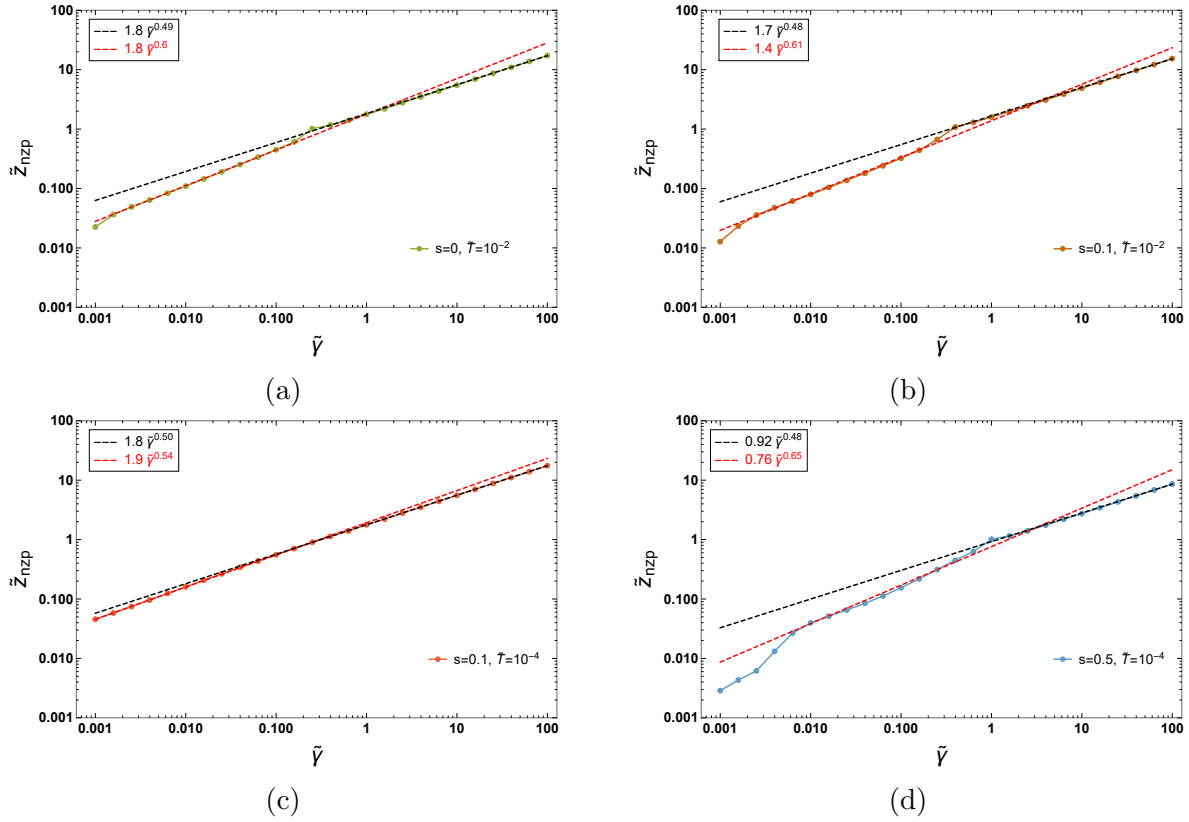

Figure 6.3: The position of the non-zero peak as a function of the damping constant $\tilde{\gamma}$, for (a) $s = 0$, (b) $s = 0.1$ and (c) $s = 0.5$. The temperature is varied over a range of $\tilde{T} = 10^{-4} - 10^{-2}$. For $s = 0.5$, the results for the non-zero peak are less reliable at $\tilde{T} = 10^{-3}$ and 10^{-2}.

Figure 6.4: The position of the non-zero peak as a function of the damping constant $\tilde{\gamma}$ for (a) $s = 0$ and $\tilde{T} = 10^{-2}$, (b) $s = 0.1$ and $\tilde{T} = 10^{-2}$, (c) $s = 0.1$ and $\tilde{T} = 10^{-4}$, and (d) $s = 0.5$ and $\tilde{T} = 10^{-4}$. Each line is fitted around the break with two fits. Where the fit for values of $\tilde{\gamma} > \tilde{\gamma}_c$ is given by $\propto \tilde{\gamma}^{0.5}$ (black line), the fit for $\tilde{\gamma} < \tilde{\gamma}_c$ is of varying proportionality (red line).
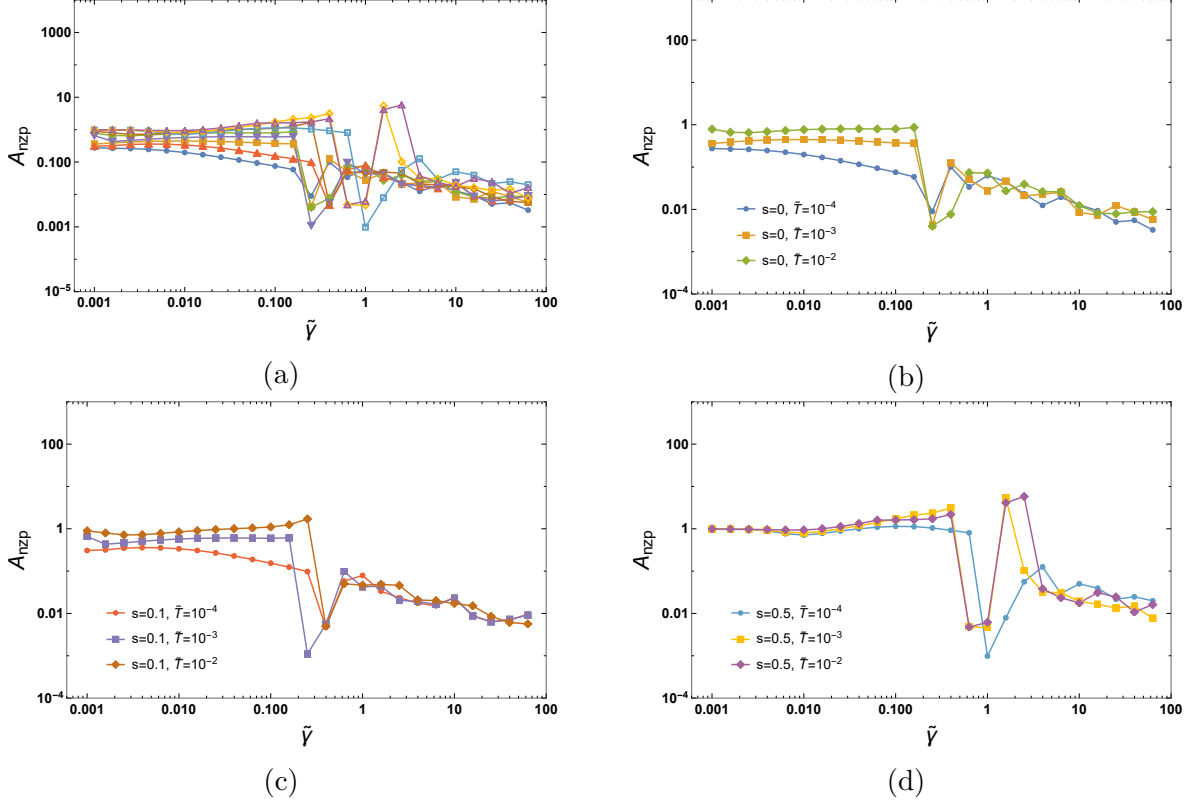
Figure 6.5: The amplitude of the non-zero peak as a function of the damping constant $\tilde{\gamma}$. In (a) all graphs are shown together for better understanding of the overall behaviour. The results are also shown separately for (b) $s = 0$, (c) $s = 0.1$, and (d) $s = 0.5$. For each s, the temperature is varied over $\tilde{T} = 10^{-4}$, 10^{-3}, 10^{-2}. The results show that there exists a critical value of $\tilde{\gamma}$, around which the amplitude has a discontinuity. This $\tilde{\gamma}_c$ depends strongly on s and slightly on $\tilde{T}$. For $s = 0, 0.1, 0.5$, we find that $\tilde{\gamma}_c = 0.2$, $\tilde{\gamma}_c = 0.3$, and $\tilde{\gamma}_c = 1.0$, respectively.

The amplitude of the non-zero peak will determine whether the oscillations are more important in the behaviour of the particle than the localisation, which is associated to the zero peak amplitude. Therefore, it acts as a natural order parameter for the time crystalline phase in analogy to the spectral function in charge-density waves [22]. The results for the amplitude of the non-zero peak are shown in Figure 6.5. We find that in general, after the phase transition, the amplitude as a function of $\tilde{\gamma}$ is decreasing as $\tilde{\gamma}$ increases (see Figure 6.5(a)). However, analysing the results separately for each value of s, we can see more clearly that the behaviour can be divided into two regimes. This transition occurs at the same values of $\tilde{\gamma}$ as before, i.e. $\tilde{\gamma}_c = 0.2$, $\tilde{\gamma}_c = 0.3$, and $\tilde{\gamma}_c = 1.0$ for $s = 0$, 0.1 and, 0.5, respectively. The height of the amplitude before this transition is determined by the temperature. For high $\tilde{T}$, we can see that the amplitude is increasing with $\tilde{\gamma}$, whereas for low $\tilde{T}$, it decreases. At the critical point, A_{nzp} shows a sudden decrease. After this abrupt drop, the amplitude increases slightly and all curves converge on a decreasing line. Notice that the stability of the curve also changes. Before the drop, A_{nzp} changes smoothly with $\tilde{\gamma}$, while after it oscillates. This could be indicative of a change from a ballistic to a diffusive regime.
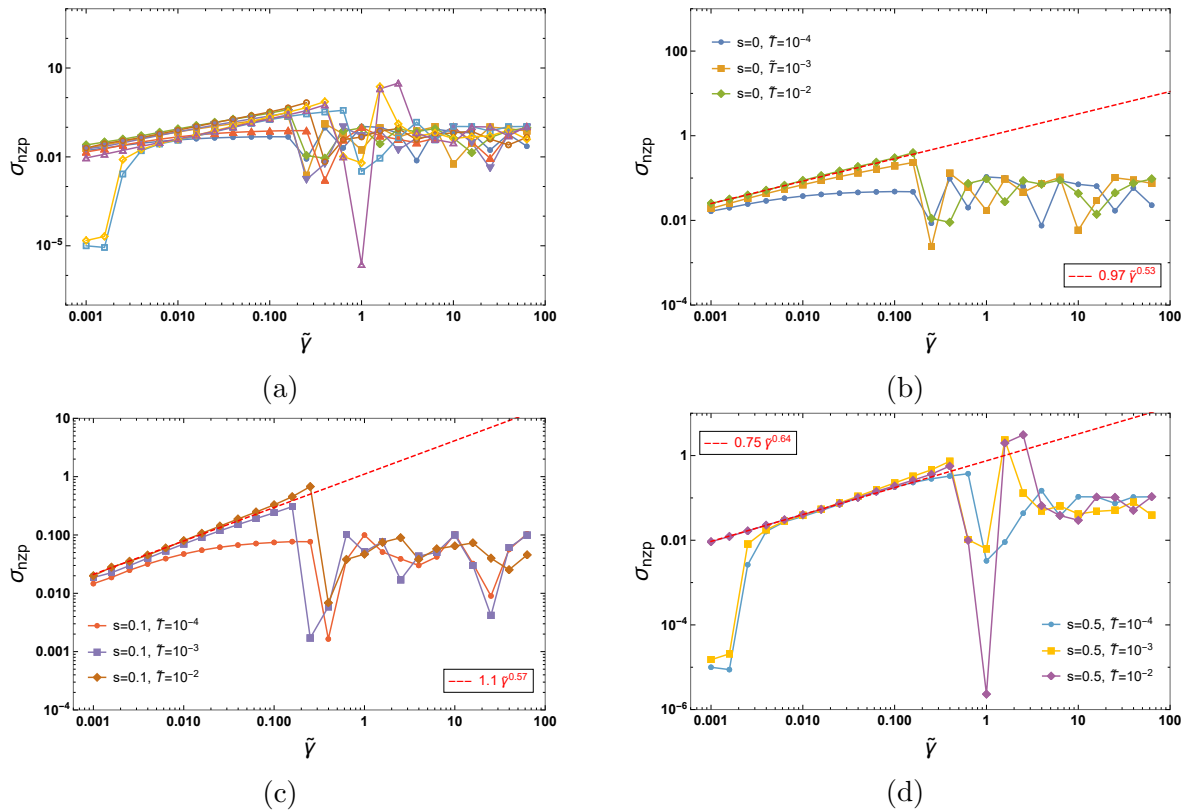
Figure 6.6: The width of the non-zero peak as a function of the damping constant $\tilde{\gamma}$. In (a) all graphs are shown together for better understanding of the overall behaviour. The results are also shown separately for (b) $s = 0$, (c) $s = 0.1$, and (d) $s = 0.5$. For each s, the temperature is varied over $\tilde{T} = 10^{-4}, 10^{-3}, 10^{-2}$. The plots indicate a similar discontinuity as for the amplitude of the non-zero peak. Similarly, the critical value is found for $s = 0, 0.1, 0.5$, at $\tilde{\gamma}_c = 0.2$, $\tilde{\gamma}_c = 0.3$, and $\tilde{\gamma}_c = 1.0$, respectively. Before the critical point, the width behaves according to a power law, which depends strongly on s and weakly on $\tilde{T}$.

The width of the non-zero peak, σ_{nzp} supports our previous findings, as a similar shift in behaviour is visible around $\tilde{\gamma}_c$ (see Figure 6.6). Before the phase transition, the width increases according to a power law $\propto \tilde{\gamma}^\beta$, where β depends strongly on the value of s. We also find that for low temperatures, $\tilde{T} = 10^{-4}$, the width does not follow this power law, but instead has a less pronounced increase. At the phase transition, the width of the non-zero peak becomes narrower, after which it slowly stabilises for all curves.
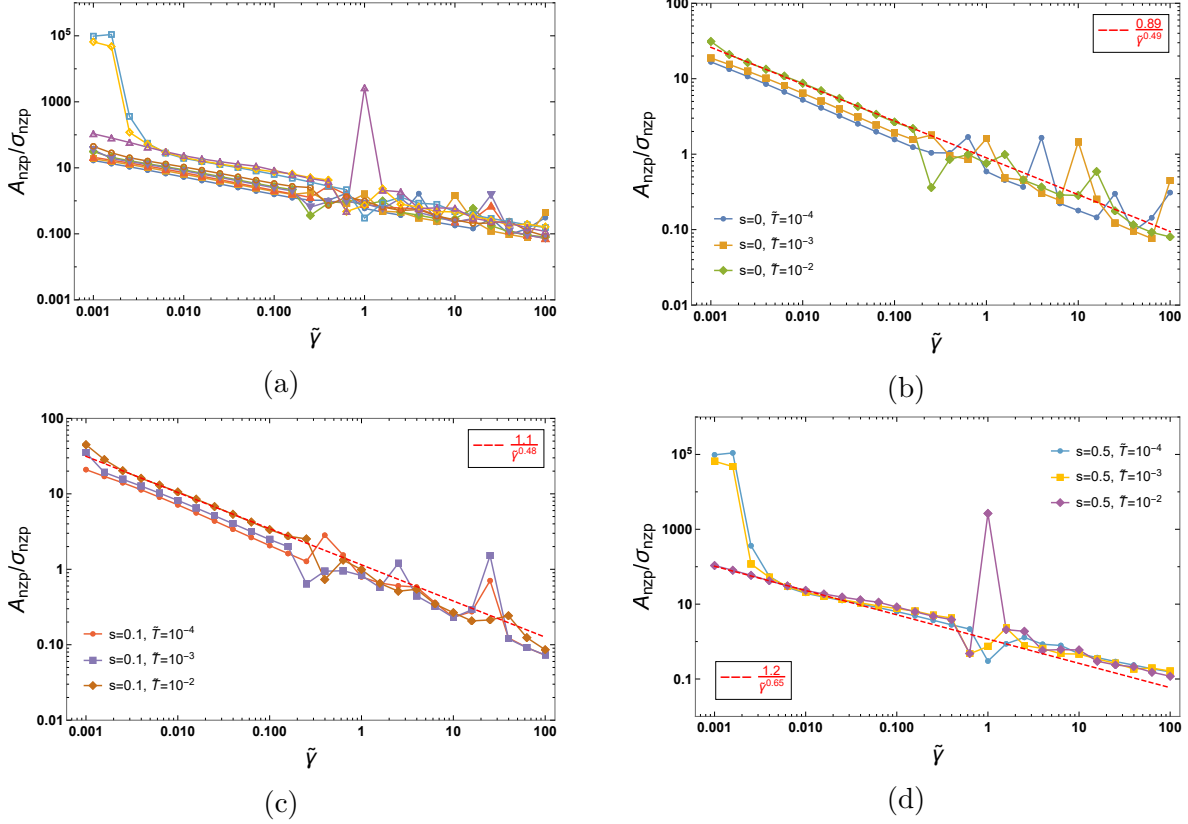
Figure 6.7: The ratio of the amplitude and width of the non-zero peak as a function of $\tilde{\gamma}$. In (a) all graphs are shown together for better understanding of the overall behaviour. The results are also shown separately for (b) $s = 0$, (c) $s = 0.1$, and (d) $s = 0.5$. For each s, the temperature is varied over $\tilde{T} = 10^{-4}$, 10^{-3}, 10^{-2}. Although a similar discontinuity is visible around the critical value of $\tilde{\gamma}_c = 0.2$, $\tilde{\gamma}_c = 0.3$, and $\tilde{\gamma}_c = 1.0$, for $s = 0, 0.1, 0.5$ respectively, the overall behaviour of the ratio goes according to a power law that depends strongly on s and weakly on $\tilde{T}$.

Due to the nature of the Lorentzian fit used in the calculations, we also look at the ratio between A_{nzp} and σ_{nzp} (see Figure 6.7). This quantity is basically the figure of merit that quantifies the ratio between oscillations and damping in oscillatory systems. Generally speaking, this ratio is high for sharp peaks, and low for broad peaks. The ratio of the amplitude to the width of the non-zero peaks is shown in Figure 6.7. The ratio follows a power law $\propto \tilde{\gamma}^{\delta}$, with $\delta = 0.49, 0.48$, and, 0.65 for $s = 0, 0.1,$ and 0.5, respectively. We notice that before the critical point the curves are separated by temperature, whereas after the critical point they oscillate, although they still follow a similar trajectory. This can be explained again by the fact that $\tilde{\gamma} < \tilde{\gamma}_c$ is the ballistic regime, and $\tilde{\gamma} > \tilde{\gamma}_c$ is the diffusive regime.
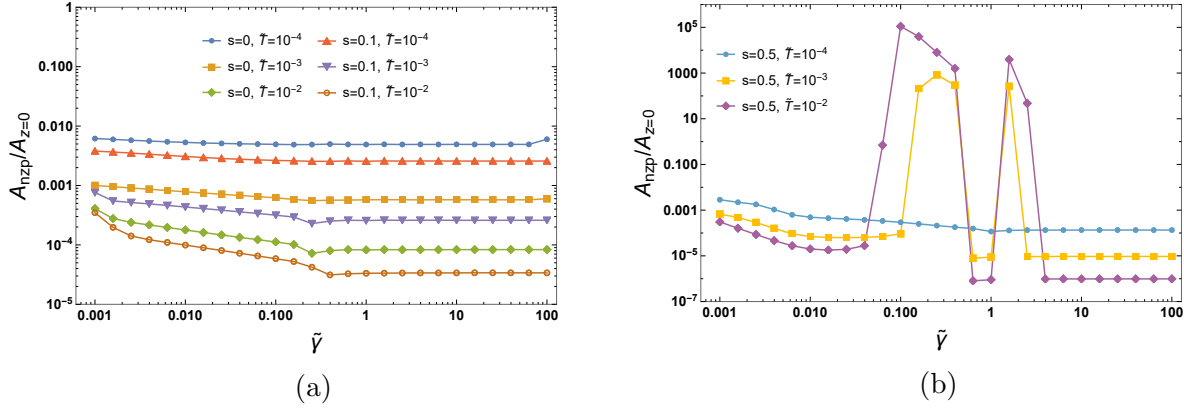
Figure 6.8: The ratio of the amplitude of the non-zero peak to the amplitude of the zero peak as a function of $\tilde{\gamma}$ for (a) $s = 0$ and $s = 0.1$ and for (b) $s = 0.5$.

The ratio of the absolute amplitudes of the non-zero peak to the zero peak is shown in Figure 6.8. The ratio seems to be constant, except for small dips that occur at the same critical values. For example, looking at the curves obtained for $\tilde{T} = 10^{-2}$, we see a dip at $\tilde{\gamma}_c = 0.2$, 0.3 and 1.0 for $s = 0$, 0.1 and 0.5, respectively. In general, the amplitude of the zero peak is larger than that of the non-zero peak, regardless of the value of $\tilde{\gamma}$.

Dependence on $\tilde{T}$

Let us now look more closely at the temperature dependence of the behaviour of the peaks. We will start by examining the position of the non-zero peak, $\tilde{z}_{nzp}$, as a function of temperature (see Figure 6.10).

We find that generally $\tilde{z}_{nzp}$ is larger for smaller values of s and for larger values of $\tilde{\gamma}$. It slowly decreases with temperature, until a certain critical temperature, $\tilde{T}_c$, is reached, after which $\tilde{z}_{nzp}$ goes to zero. Due to the nature of our calculations, once the non-zero peak has become so small, or has vanished completely, the Lorentzian fit used to calculate its characteristics instead picks up the characteristics of the zero peak.

$\tilde{T}_c$ depends on both s and $\tilde{\gamma}$. For $s = 0$, this point lies around $\tilde{T}_c = 0.05$, and a larger value of $\tilde{\gamma}$ increases the critical temperature slightly. However, for $s = 0.5$ it occurs at a much lower temperature in the region $\tilde{T} = 10^{-3} - 10^{-2}$, and a larger value of $\tilde{\gamma}$ decreases the critical temperature.

It is important to remember in the discussion of the amplitude, width, and their ratio, that the behaviour of the curves after this critical point is most likely only due to the presence of the zero peak, as the non-zero peak is no longer visible after this point.
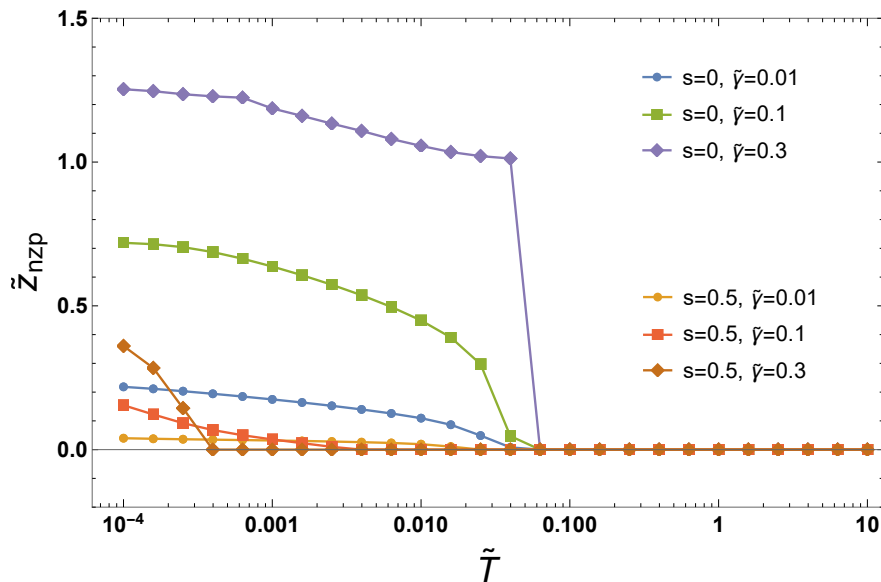

Figure 6.9

Figure 6.10: The position of the non-zero peak as a function of $\tilde{T}$, shown in a log-linear scale for $s = 0$ and $s = 0.5$, and $\tilde{\gamma} = 0.01, 0.1$, and 0.3. The position of the non-zero peak depends strongly on both $\tilde{\gamma}$ and s. For $s = 0$, the non-zero peak vanishes at temperatures above $\tilde{T} > 10^{-1}$, whereas for $s = 0.5$ it vanishes at temperatures above $\tilde{T} = 10^{-2}$.
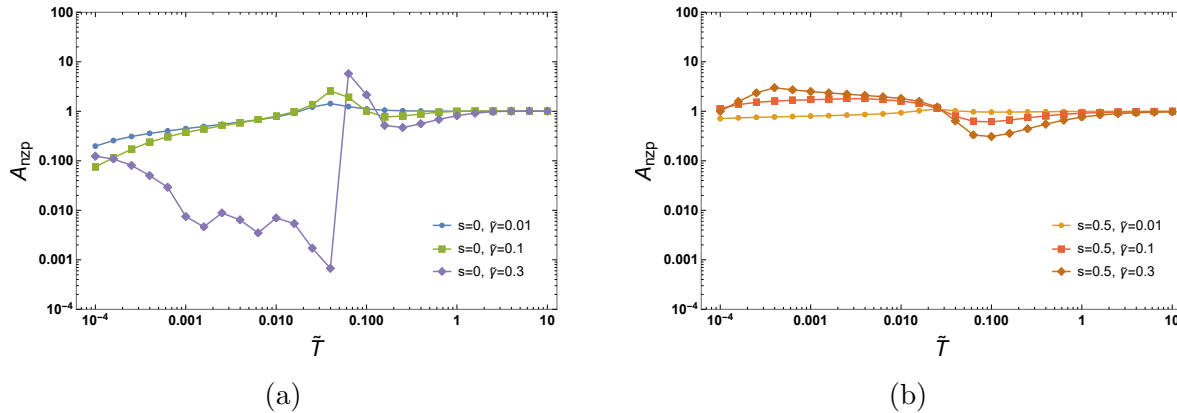
Figure 6.11: The amplitude of the non-zero peak as a function of $\tilde{T}$ for (a) $s = 0$, and (b) $s = 0.5$. $\tilde{\gamma} = 0.01, 0.1$, and 0.3. It should be noted that the results show only the behaviour of the non-zero peak for temperatures below $\tilde{T} = 10^{-1}$ and $\tilde{T} = 10^{-2}$ for $s = 0$ and $s = 0.5$, respectively.

Figure 6.11 shows the amplitude of the non-zero peak, A_{nzp} as a function of $\tilde{T}$ as determined by the Lorentzian fit. For $s = 0$ (see Figure 6.11(a)), we find that the amplitude increases for low values of $\tilde{\gamma}$ with $\tilde{T}$, up until $\tilde{T}_c$. However, for $\tilde{\gamma} = 0.3$ the amplitude shows a very different type of behaviour, it decreases with temperature. From our analysis of the $\tilde{\gamma}$-dependence of the non-zero peak, we may remember that there is a phase transition at $\tilde{\gamma}_c = 0.2$ and for $s = 0$. Here, we see that for values $\tilde{\gamma} < \tilde{\gamma}_c$, the amplitude increases with $\tilde{T}$, but for values $\tilde{\gamma} > \tilde{\gamma}_c$, it decreases. As the critical temperature is reached, the amplitude reaches a maximum, and starts to decrease. After this point, there is an inflection point at $\tilde{T} \approx 2 \cdot 10^{-1}$ as the non-zero peak is no longer present.

Figure 6.11(b) shows the amplitudes for $s = 0.5$. The behaviour is the same as for low values of s, but now the critical value $\tilde{\gamma}_c$ is equal to 1, and thus the curve at $\tilde{\gamma} = 0.3$ is also in line with the others. However, the inflection point (at which the non-zero peak disappears) occurs earlier, around $\tilde{T} = 3 \cdot 10^{-2}$.
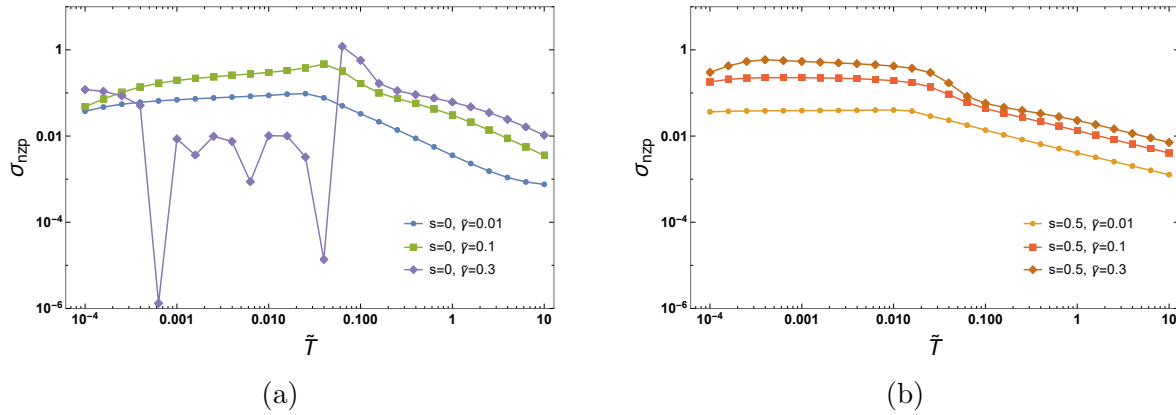
Figure 6.12: The width of the non-zero peak as a function of $\tilde{T}$ for (a) $s = 0$, and (b) $s = 0.5$. It should be noted that the results show only the behaviour of the non-zero peak for temperatures below $\tilde{T} = 10^{-1}$ and $\tilde{T} = 10^{-2}$ for $s = 0$ and $s = 0.5$, respectively.

The width of the non-zero peak shows a similar temperature dependence as the amplitude (see Figure 6.12). For $s = 0$ and $\tilde{\gamma} < \tilde{\gamma}_c = 0.2$, the width of the non-zero peak slowly increases until the critical temperature is reached. For values above the critical damping constant $\tilde{\gamma} > \tilde{\gamma}_c$, the width of the peak fluctuates around a much smaller value. After the critical temperature is reached all curves converge on a decreasing path of equal slope. For $s = 0.5$, the values of $\tilde{\gamma}$ used in the plots are smaller than the critical damping constant and the width of the non-zero peak only shows a slight increase with temperature until the critical temperature is reached.
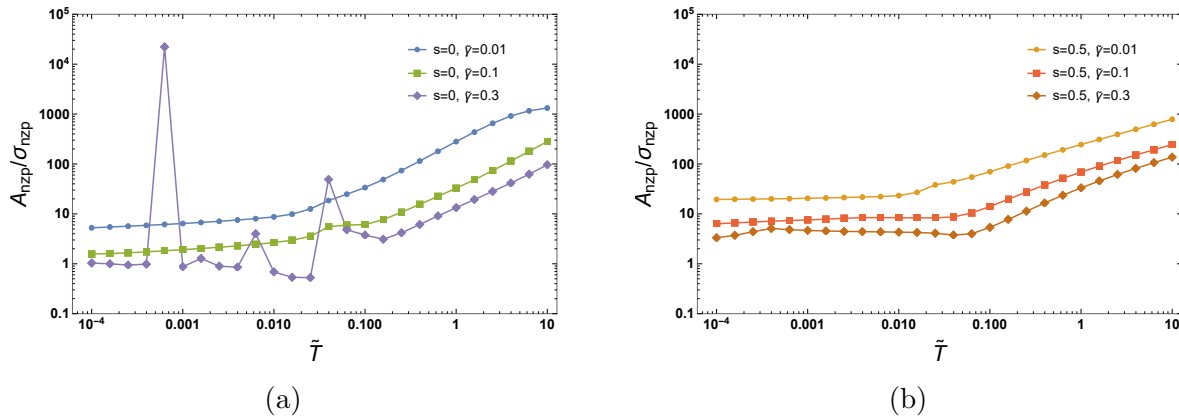
(a)   (b)

Figure 6.13: The ratio of the amplitude and the width of the non-zero peak as a function of $\tilde{T}$ for (a) $s = 0$, and (b) $s = 0.5$. It should be noted that the results show only the behaviour of the non-zero peak for temperatures below $\tilde{T} = 10^{-1}$ and $\tilde{T} = 10^{-2}$ for $s = 0$ and $s = 0.5$, respectively. Before this point, the ratio shows a slight, but stable increase.

Figure 6.13 shows the ratio of the amplitude to the width of the non-zero peak as a function of temperature. For both $s = 0$ and $s = 0.5$, the curves show a gradual positive slope, which becomes steeper after the critical temperature. As we have noted before, the amplitude and width of the curve at $\tilde{\gamma} > \tilde{\gamma}_c$ fluctuate much more, resulting in a rather odd curve for the ratio of $s = 0$ and $\tilde{\gamma} = 0.3$. However, it generally follows the same curve as the other two values for $s = 0$ (see Figure 6.13(a)).
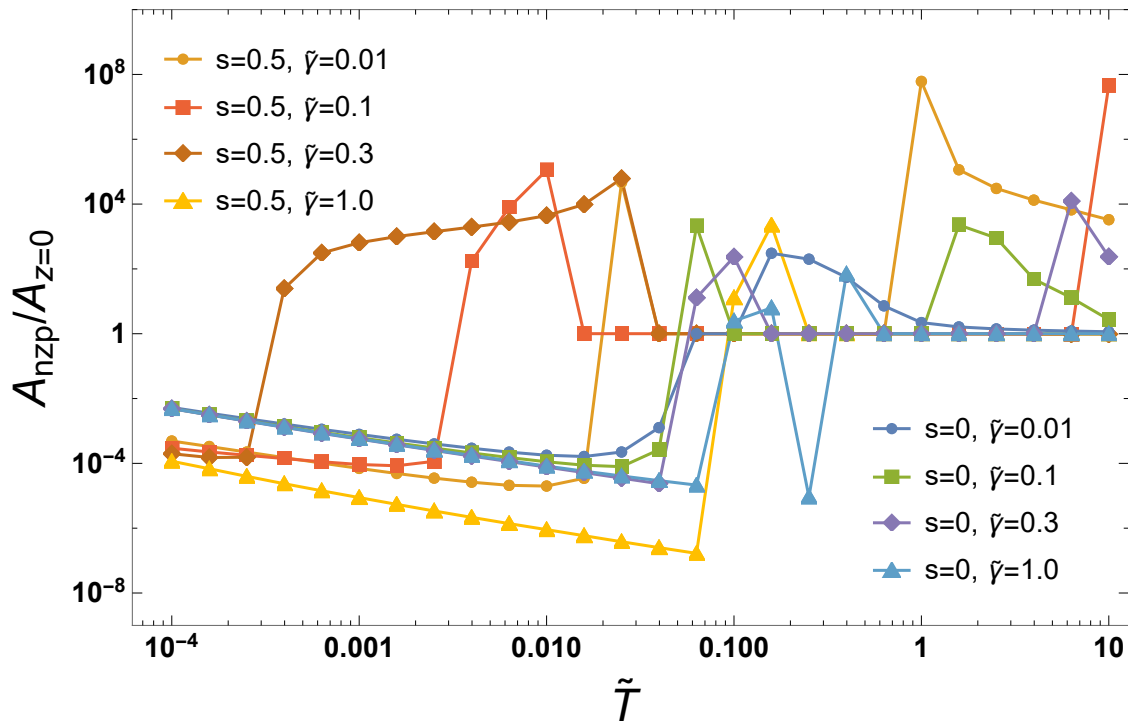
Figure 6.14: The ratio of the amplitude of the non-zero peak to the amplitude of the zero peak as a function of $\tilde{T}$.

The ratio of the absolute amplitudes of the non-zero to the zero peak (see Figure 6.14) also reveals a critical temperature. Before the phase transition, the ratio of the amplitudes decreases (i.e. the zero peak becomes larger than the non-zero peak as the temperature increases) until it hits the critical temperature. We know that the non-zero peak after this point does not exist, and the fit picks up the behaviour of the zero peak. This is reflected by the fact that the ratio of the two amplitudes calculated goes to 1. These features explain why the oscillations that we observed in the previous chapter exist for small temperatures and the effect of temperature is to destroy them. This is analogous to the "melting" of the time crystalline phase reported in Ref. [23].
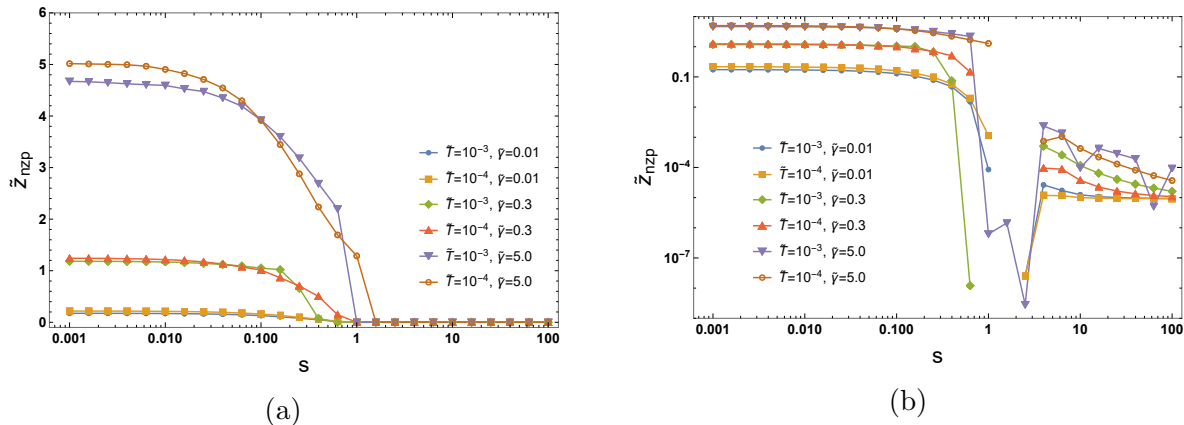
Dependence on s

(a)   (b)

Figure 6.15: The position of the non-zero peak as a function of s, shown in both a (a) linear scale and a (b) logarithmic scale, for $\tilde{T} = 10^{-4}$, 10^{-3} and 10^{-2}, and $\tilde{\gamma} = 0.01$, 0.3, and 5.0. The position of the non-zero peak depends strongly on $\tilde{\gamma}$ and slightly on $\tilde{T}$. (a) and (b) show that the non-zero peak vanishes at $s = 1$ for all chosen values of $\tilde{\gamma}$ and $\tilde{T}$, after which only the behaviour of the zero peak is picked up.

Finally, we look at the s-dependence of the behaviour of the non-zero peak. As before, we start by examining its position as a function of s (see Figure 6.15). We see that the position of the non-zero peak is higher for larger values of the damping constant $\tilde{\gamma}$, as also previously established. Increasing the temperature by a factor of 10 only has a small effect on the position of the peak, in comparison to the lower temperature. We also note that there appears to be a phase transition around $s_c = 1$. At this point, the position goes to zero, i.e. the Lorentzian fit used in the calculation identifies only the zero peak. In the log-log plot (see Figure 6.15(b)), it can be clearly seen that this phase transition occurs for all parameters at roughly the same point, where there is a steep drop-off from the original curve.
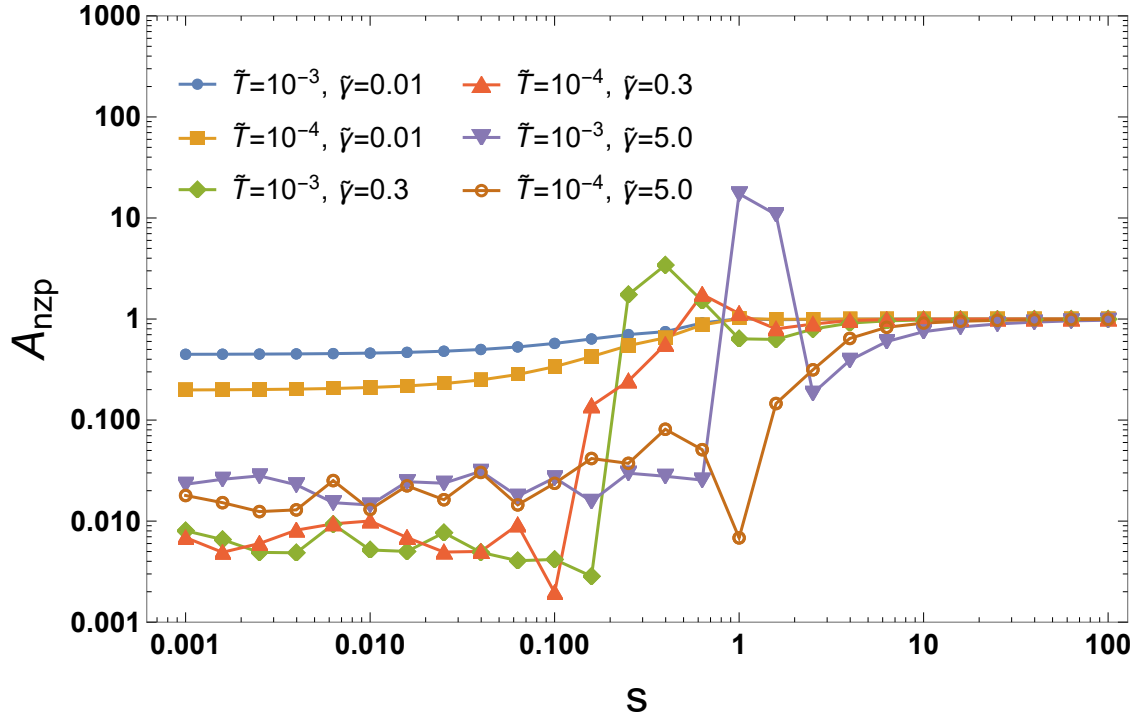
Figure 6.16: The amplitude of the non-zero peak as a function of s, for $\tilde{T} = 10^{-4}$, and 10^{-3}, and $\tilde{\gamma} = 0.01$, 0.3, and 5.0. The amplitude for $\tilde{\gamma} = 0.3$ is much smaller than for $\tilde{\gamma} = 0.01$ and $\tilde{\gamma} = 5.0$. After $s = 1$, the results show the behaviour of the zero peak as the non-zero peak has vanished.

The amplitude of the non-zero peak (see Figure 6.16) increases slightly with s, until the phase transition occurs at $s = 1$. After this point, the non-zero peak is no longer visible as we concluded from Figure 6.15. The results at $s > 1$ are, in fact, showing the behaviour of the zero peak, which indeed reaches a constant amplitude, similar to what we saw in Figure 6.2(c). The difference in absolute value of the amplitudes in both figures can be explained by the different calculation methods used for the zero and the non-zero peak. Interesting to note is that before the critical $s_c = 1$, the amplitude of the non-zero peak is lower for the curves at $\tilde{\gamma} = 0.3$ (red and green) than for $\tilde{\gamma} = 5.0$ (purple and brown) for the values $s < 0.2$. Remembering that there is a critical damping constant $\tilde{\gamma}_c$ that shifts from $\tilde{\gamma}_c = 0.2$ to $\tilde{\gamma}_c = 1$ as s increases, we can conclude that the curves at $\tilde{\gamma} = 0.3$ fall precisely at this phase transition. We saw in Figure 6.5 that at this transition the amplitude of the non-zero peak has a sharp decrease. As $s > 0.2$, the critical damping constant increases, such that the red and green curves now have $\tilde{\gamma} > \tilde{\gamma}_c$. As we saw in Chapter 4, the parameter s controls the dependence of the spectral function in frequency and marks the different regimes of diffusion. For $s < 1$, there is a sub-ohmic regime, $s = 1$ is ohmic, and $s > 1$ is super-ohmic. Therefore, the universality of the phase transition in s seems to indicate that this change of regime drastically affects the time crystalline behaviour.
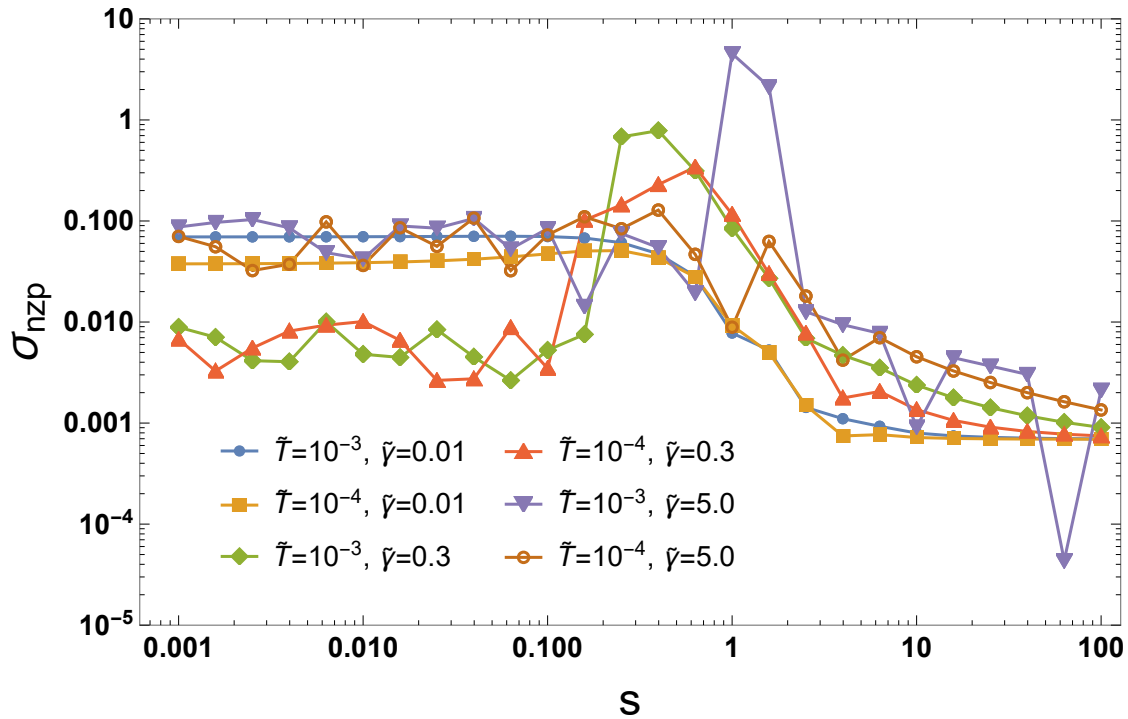
Figure 6.17: The width of the non-zero peak as a function of s, for $\tilde{T} = 10^{-4}$, and 10^{-3}, and $\tilde{\gamma} = 0.01$, 0.3, and 5.0. The width for $\tilde{\gamma} = 0.3$ is much smaller than for $\tilde{\gamma} = 0.01$ and $\tilde{\gamma} = 5.0$. After $s = 1$, the results show the behaviour of the zero peak, as the non-zero peak has vanished.

The results for the width of the non-zero peak as a function of s are shown in Figure 6.17. The width is fairly constant until the phase transition, after which it shows a gradual decrease to a lower constant. Although the curves for different damping constants were separated by damping constant before the transition, they come together after it. In addition, the curves at $\tilde{\gamma} = 0.3$ (red and green) are again affected by the critical region of the damping constant, as they are lower than the curves at $\tilde{\gamma} = 5.0$ (brown and purple).
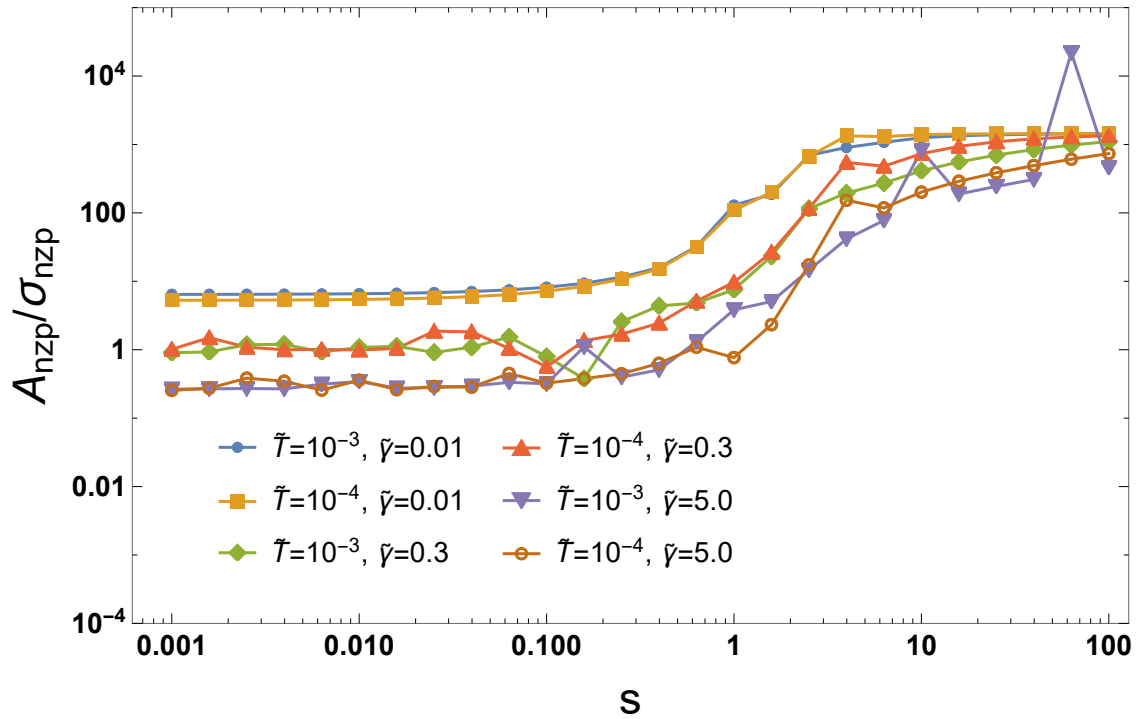
Figure 6.18: The ratio of the amplitude and the width of the non-zero peak as a function of s, for $\tilde{T} = 10^{-4}$ and 10^{-3}, and $\tilde{\gamma} = 0.01$, 0.3, and 5.0. The ratio quantitatively depends on $\tilde{\gamma}$, but the qualitative behaviour is generic. After $s = 1$, the results show the behaviour of the zero peak, as the non-zero peak has vanished.

Using these results, we can compute the ratio of the amplitude and width (see Figure 6.18). We see that this ratio is constant before the phase transition, and increases afterwards to a higher constant value. The curves are clustered by the value of damping constant before $s_c = 1$, but converge to a universal curve once this critical point is reached.
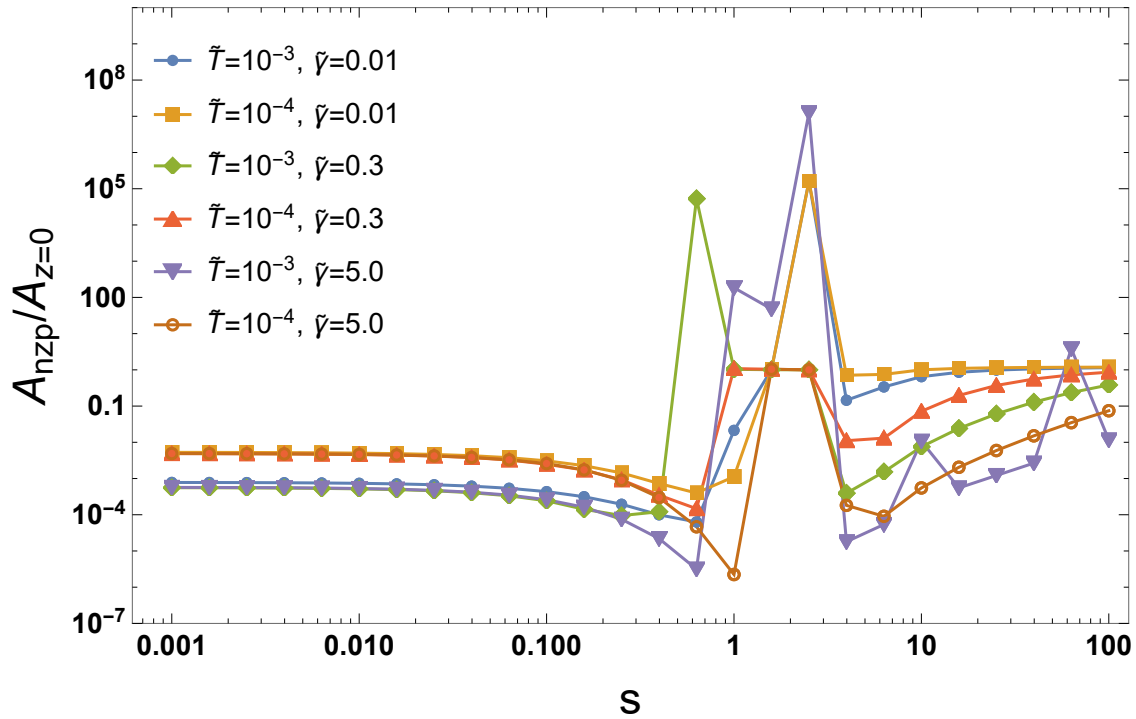
Figure 6.19: The ratio of the amplitudes of the non-zero peak and the zero peak as a function of s.

The ratio of the absolute amplitudes of the non-zero to the zero peak is shown in Figure 6.19. In the sub-ohmic regime ($s < 1$), the curves are clustered by the value of $\tilde{T}$ regardless of $\tilde{\gamma}$. The erratic behaviour at $s = 1$ signals the phase transition. At this point, the non-zero peak disappears and the Lorentzian fit has trouble identifying the correct amplitude. As we go further into the super-ohmic regime ($s > 1$), the ratios converge to the same curve, which behaves exactly as the zero peak.

7   Conclusion

In this thesis, we have looked at a particle-bath system from a time crystalline perspective. In analogy to the Caldeira-Leggett model, explained in Section 4, we have taken a particle and coupled it to a thermal reservoir. However, instead of harmonic oscillators, we used a bath consisting of two-level systems, which only have two energy levels available. As a result of this change, we have seen that the spectral function, which controls the influence of the reservoir in the system, now depends on temperature, such that the dynamical behaviour of the system is more sensitive to it.

We have calculated the equations of motion for the particle and solved them numerically to determine its behaviour. As expected from the literature [1], the particle exhibits oscillatory motion in the sub-ohmic regime. Ref. [1] showed that this system exhibits persistent oscillatory motion in the sub-ohmic regime that resembles time crystalline behaviour. The main goal of this thesis has been to determine which parameters govern the limits of this time crystalline regime. We have analysed the position of the particle center of mass, $q(t)$, in both the time and the frequency domain, focusing our attention on three parameters: the damping constant γ, the temperature T, and s, a real number determining the long time properties of the bath.

A qualitative analysis of the dynamical equation for the particle indicates that both temperature and s play a large role in determining the time crystal regime. At low temperatures ($\tilde{T} = 10^{-4}$), oscillations occur at all values of $s \leq 1$, although they are more damped for higher values of s. When T is increased by a factor 10, the oscillations become increasingly damped for all values of $s \leq 1$ except for $s = 0$, which appears more robust to temperature changes. However, if T is increased further, all oscillations eventually disappear and the particle position becomes constant, reminiscent of a glass phase. Moreover, by increasing s or T, the amplitude and period of the oscillations also increases.

We also investigated the behaviour of the poles of the Laplace transform $\bar{q}(z)$ in the frequency domain as a function of γ, T, and s. We found that the time crystalline regime is characterised by the appearance of a second "non-zero" peak in the frequency domain. The position of this peak on the imaginary axis corresponds directly to the period of the oscillations of the particle, i.e. the characteristic frequency. Its amplitude and width, on the other hand, inform us about the robustness of the oscillations.

We found that while s and T mainly determine whether the system forms a time crystal, the value of γ determines more strongly its characteristic frequency.

The parameter that poses the biggest restriction on the boundaries of the time crystal regime is s. For $0 \leq s \leq 1$, a time crystal can be formed, although it seems to be more robust at low temperatures and small values of γ. At $s = 1$, a phase transition occurs after which the non-zero peak, and thus the time crystal, disappears. T also plays a role in determining the boundaries of the time crystal regime. When s is small, e.g. $s = 0$, the critical temperature below which the system forms a time crystal is $\tilde{T}_c = 10^{-1}$. However, as s is increased, T_c decreases. For example, for $s = 0.5$ the critical temperature can be as low as 10^{-3}. While γ does not significantly influence the limits of the time crystal phase, it does play a large role

in the characteristic frequency of the oscillations of the particle. This frequency increases according to a power law γ^α. However, there seems to be a critical value γ_c, which depends on s and T, which indicates a transition between two phases with slightly different behaviour.

In conclusion, a time crystal can only form in the sub-ohmic regime. Moreover, the further we increase s, the more we have to lower the temperature to preserve the time crystal phase. Finally, the characteristic frequency of the oscillations is largely determined by γ.

Outlook

There are several options to continue this research. It may be interesting, for example, to further investigate the robustness of the time crystal regime. One could switch on an oscillating electric field and analyse how the system behaves accordingly. It is also possible to test the systems robustness to a change of initial conditions, out of the criteria to establish a time crystal phase.

Another possibility is to look at the equation of motion of the relative coordinate $\xi(t)$ to get a more complete picture of the behaviour of the system coupled to the bath.

Typical values of the constants can be estimated to see whether this model can be realised in a realistic experimental setup and the time crystalline phase observed. Further, the effects and interplay of an interacting reservoir can be interesting to investigate. A final extension would be to use an effective Hamiltonian language, dealing with non-Hermitian Hamiltonians [24], and see whether these results can be obtained in this language and how it connects with the imaginary time crystals observed in such systems [25].

Acknowledgements

APPENDICES

A   SQUIDs and Josephson Junctions

In superconductors, electrons can condense into a 'macroscopic quantum state', which can be described with a single wave function ψ, depending on the density of quasi-particles in the macroscopic state n_s and a common phase φ

$$\psi = \sqrt{n_s}e^{i\varphi}. \tag{A.1}$$

The electric current density $\mathbf{J}$ for particles in a vector potential $\mathbf{A}$ can be calculated using

$$\mathbf{J} = \frac{e^*\hbar}{2im^*}[\psi^*\nabla\psi - \psi\nabla\psi^*] - \frac{e^{*2}\mathbf{A}}{m^*c}\psi^*\psi$$
$$\stackrel{\text{Eq. (A.1)}}{=} \frac{n_s e^*}{m^*}\left(\hbar\nabla\varphi - \frac{e^*}{c}\mathbf{A}\right), \tag{A.2}$$

where e^* is the electric charge and m^* is the mass of the condensate. Another formula for the current density is $\mathbf{J} = n_s e^*\mathbf{v}$, which in combination with Eq. (A.2) gives us $\hbar\nabla\varphi = m^*\mathbf{v} + e^*/c\mathbf{A}$. We can integrate this expression over the endpoints 1 and 2 of the system to find

$$\int_1^2 \left(m^*\mathbf{v} + \frac{e^*}{c}\mathbf{A}\right) \cdot \mathrm{d}\mathbf{r} = \int_1^2 \hbar\nabla\varphi \cdot \mathrm{d}\mathbf{r} = \hbar(\varphi_2 - \varphi_1). \tag{A.3}$$

By setting $\psi_1 = \psi_2$, we effectively create a superconducting ring. The phase difference between the wave functions of the endpoints must therefore become an integer multiple of 2π. We can rewrite Eq. (A.3) to find an expression for the total magnetic flux through a superconducting ring

$$\oint \left(m^*\mathbf{v} + \frac{e^*}{c}\mathbf{A}\right) \cdot \mathrm{d}\mathbf{r} = \frac{e^*}{c}\oint (\Lambda\mathbf{J} + \mathbf{A}) \cdot \mathrm{d}\mathbf{r} = 2\pi\hbar n, \tag{A.4}$$

with $\Lambda = m^*c/e^{*2}n_s$ and n an integer. For $e^* = 2e$, we find

$$\oint (\Lambda\mathbf{J} + \mathbf{A}) \cdot \mathrm{d}\mathbf{r} = \frac{2\pi\hbar c}{2e}n \equiv n\phi_0, \tag{A.5}$$

where $\phi_0 = hc/2e$. For a simply connected ring $\mathbf{J}$ and $\mathbf{A}$ are continuous, which means that the integral on the left hand side of Eq. (A.5) will be zero. However, this is not the case for thick rings. When we choose an integration path in the centre of the ring, where the current $\mathbf{J}$ is zero, we find that the magnetic flux through the ring is quantized in units of $\phi_0 = hc/2e$. So the total magnetic flux through a ring is given by

$$\phi = n\phi_0, \tag{A.6}$$

where n is an integer number.

Instead of using a normal superconducting ring, one can also create a SQUID (Superconduction QUantum Interference Device) ring, which is closed by a Josephson junction. This junction consists of two superconductors separated by a non-superconducting material of thickness d. When d is small enough for the superconducting wave functions to overlap, the

Schrödinger equations become coupled. This is the defining feature of the Josephson junction. Due to this coupling, the current through the junction becomes dependent on the phase difference between the superconductors. As a result, a constant current, up to a critical value j_0, can develop without generating a voltage. In other words, electrons can tunnel through the junction without any resistance. This is called the Josephson effect.

The quantisation of the magnetic flux through a SQUID ring is also dependent on this phase difference $\bar{\varphi}$. To show this, we calculate the current density of the ring as before, but we change the boundaries of our integral to explicitly include the Josephson junction. We start by rewriting the integral over the current density from Eq. (A.2), using $c = e^* \phi_0 / 2\pi\hbar$

$$\int_1^2 \mathbf{J} \cdot d\mathbf{r} = \int_1^2 \frac{n_s e^*}{m^*} \left(\hbar \nabla \varphi - \frac{e^*}{c} \mathbf{A} \right) \cdot d\mathbf{r}$$
$$= \frac{n_s e^* \hbar}{m^*} \int_1^2 \nabla \varphi \cdot d\mathbf{r} - \frac{n_s e^* \hbar}{m^*} \frac{2\pi}{\phi_0} \int_1^2 \mathbf{A} \cdot d\mathbf{r}. \tag{A.7}$$

The left hand side of this equation is zero for a path that lies deep within the ring. The integral in the second term on the right hand side is the total magnetic flux, ϕ, through the ring, when we integrate over a closed loop $(2 = 1)$. This approximation is valid for a continuous vector potential $\mathbf{A}$. For the first term on the right hand side we can rewrite the integral over the path through the ring to an integral over a closed ring minus the integral over the junction. This gives

$$\int_1^2 \nabla \varphi \cdot d\mathbf{r} = \oint \nabla \varphi \cdot d\mathbf{r} - \int_2^1 \nabla \varphi \cdot d\mathbf{r}$$
$$= 2\pi n - (\varphi_1 - \varphi_2)$$
$$= 2\pi n - \bar{\varphi}, \tag{A.8}$$

where we define the phase difference $\bar{\varphi} \equiv \varphi_1 - \varphi_2$.

Combining these results, we can now write down the quantization for SQUID rings

$$\phi + \frac{\phi_0}{2\pi} \bar{\varphi} = n\phi_0. \tag{A.9}$$

B   Solving the Forced Harmonic Oscillator Path Integral

We have a harmonic oscillator driven by a time-dependent force $f(t)$. The action describing this system is given by

$$S[x(t)] = \int L(x(t), \dot{x}(t))\, \mathrm{d}t = \int \frac{m}{2}\dot{x}^2(t) - \frac{m\omega^2}{2}x(t)^2 + f(t)x(t)\, \mathrm{d}t. \tag{B.1}$$

Varying the action with respect to $x(t)$ gives us the equation of motion

$$m\ddot{x} + m\omega^2 x = f(t). \tag{B.2}$$

We want to find an expression for the action in terms of the beginning and end points of the system. We will start with an integration by parts of Eq. (B.1)

$$S = \frac{m}{2}x\dot{x}\Big|_{t_a}^{t_b} - \int_{t_a}^{t_b} \frac{x}{2}[\underbrace{m\ddot{x} + m\omega^2 x}_{=f(t),\text{ using Eq. (B.2)}} -2f(t)]\, \mathrm{d}t$$

$$= \frac{m}{2}\left(x\dot{x}\Big|_{t_a}^{t_b} + \int_{t_a}^{t_b} \frac{f(t)}{m}x\, \mathrm{d}t\right). \tag{B.3}$$

For the harmonic oscillator, we assume that $x(t)$ is of the form

$$x(t) = A(t)e^{i\omega t} + B(t)e^{-i\omega t}. \tag{B.4}$$

Calculating the derivatives $\dot{x}(t)$ and $\ddot{x}(t)$, and using the equation of motion, we can write down expressions for $A(t)$ and $B(t)$.

$$A(t) = \frac{A_a + A_b}{2} + \frac{1}{2}\int_{t_a}^{t} \frac{f(s)}{2im\omega}e^{-i\omega s}\, \mathrm{d}s - \frac{1}{2}\int_{t}^{t_b} \frac{f(s)}{2im\omega}e^{-i\omega s}\, \mathrm{d}s \tag{B.5}$$

$$B(t) = \frac{B_a + B_b}{2} - \frac{1}{2}\int_{t_a}^{t} \frac{f(s)}{2im\omega}e^{-i\omega s}\, \mathrm{d}s + \frac{1}{2}\int_{t}^{t_b} \frac{f(s)}{2im\omega}e^{-i\omega s}\, \mathrm{d}s, \tag{B.6}$$

where $A_a = A(t_a)$ and $A_b = A(t_b)$ (and similarly for B_a and B_b) are expressed at the boundaries. From now on, we will also drop the explicit time dependency for clarity, i.e. $A(t) = A$ and $B(t) = B$. Using these expressions, we can rewrite the terms in Eq. (B.3)

$$x\dot{x}\Big|_{t_a}^{t_b} = i\omega\left(A_b^2 e^{2i\omega t_b} - B_b^2 e^{-2i\omega t_b} - A_a^2 e^{2i\omega t_a} + B_a^2 e^{2i\omega t_a}\right) \tag{B.7}$$

$$\int_{t_a}^{t_b} \frac{f(t)}{m}x\, \mathrm{d}t = \int_{t_a}^{t_b} \frac{f(t)}{2m}\left(A_a e^{i\omega t} + A_b e^{i\omega t} + B_a e^{-i\omega t} + B_b e^{-i\omega t}\right)\, \mathrm{d}t$$

$$+ \int_{t_a}^{t_b}\int_{t_a}^{t} \frac{f(t)f(s)}{2m^2\omega}\sin\omega(t-s)\, \mathrm{d}s\, \mathrm{d}t - \int_{t_a}^{t_b}\int_{t}^{t_b} \frac{f(t)f(s)}{2m^2\omega}\sin\omega(t-s)\, \mathrm{d}s\, \mathrm{d}t. \tag{B.8}$$

Multiplying both terms by $1 = \frac{\sin \omega(t_b - t_a)}{\sin \omega T}$, the action becomes

$$S[x] = \frac{m\omega}{2\sin\omega T} \times \left\{ \frac{1}{2} \left[A_b^2 \left(e^{i\omega(3t_b - t_a)} - e^{i\omega(t_b + t_a)} \right) + A_a^2 \left(e^{-i\omega(t_b - 3t_a)} - e^{i\omega(t_b + t_a)} \right) \right. \right.$$

$$\left. + B_b^2 \left(e^{-i\omega(3t_b - t_a)} - e^{-i\omega(t_b + t_a)} \right) + B_a^2 \left(e^{i\omega(t_b - 3t_a)} - e^{-i\omega(t_b + t_a)} \right) \right] \quad \text{(B.9)}$$

$$+ \int_{t_a}^{t_b} \frac{f(t)}{4im\omega} \left[(A_a + A_b) \left(e^{i\omega(t_b - t_a + t)} - e^{-i\omega(t_b - t_a - t)} \right) \right.$$

$$\left. + (B_a + B_b) \left(e^{i\omega(t_b - t_a - t)} - e^{-i\omega(t_b - t_a + t)} \right) \right] dt \quad \text{(B.10)}$$

$$+ \int_{t_a}^{t_b} \int_{t_a}^{t} \frac{f(t)f(s)}{2m^2\omega^2} \sin\omega(t - s) \sin\omega(t_b - t_a) \, ds \, dt$$

$$\left. - \int_{t_a}^{t_b} \int_{t}^{t_b} \frac{f(t)f(s)}{2m^2\omega^2} \sin\omega(t - s) \sin\omega(t_b - t_a) \, ds \, dt \right\}. \quad \text{(B.11)}$$

This expression looks very complex, but it can be rewritten into a simpler form using some useful trigonomic identities. We start by rewriting Eq. (B.10), using

$$\left(e^{i\omega(t_b - t_a + t)} - e^{-i\omega(t_b - t_a - t)} \right) = 2i \left(e^{i\omega t_a} \sin\omega(t_b - t) + e^{i\omega t_b} \sin\omega(t - t_a) \right),$$

$$\left(e^{i\omega(t_b - t_a - t)} - e^{-i\omega(t_b - t_a + t)} \right) = 2i \left(e^{-i\omega t_a} \sin\omega(t_b - t) + e^{-i\omega t_b} \sin\omega(t - t_a) \right).$$

Furthermore, we can use the expressions for $x_a = x(t_a)$ and $x_b = x(t_b)$ calculated from Eq. (B.4) in combination with Eq. (B.5) and Eq. (B.6) to find

$$A_b e^{i\omega t_a} + B_b e^{-i\omega t_a} = x_a - \int_{t_a}^{t_b} \frac{f(t)}{m\omega} \sin\omega(t - t_a) \, dt$$

$$A_a e^{i\omega t_b} + B_a e^{-i\omega t_b} = x_b - \int_{t_a}^{t_b} \frac{f(t)}{m\omega} \sin\omega(t_b - t) \, dt.$$

Substituting these expressions back into Eq. (B.10) gives

$$Eq.(\text{B.10}) = \int_{t_a}^{t_b} \frac{f(t)}{2m\omega} \left[2x_a \sin\omega(t_b - t) + 2x_b \sin\omega(t - t_a) \right] dt$$

$$- \int_{t_a}^{t_b} \int_{t_a}^{t_b} \frac{f(t)f(s)}{2m^2\omega^2} \left[\sin\omega(t_b - t) \sin\omega(s - t_a) + \sin\omega(t_b - s) \sin\omega(t - t_a) \right] dt.$$

$$\text{(B.12)}$$

In order to rewrite Eq. (B.11), we will need the following trigonomic identity

$$\sin(a - b)\sin(c - d) = \sin(a - c)\sin(b - d) - \sin(a - d)\sin(b - c). \quad \text{(B.13)}$$

Using this relation, we get

$$Eq.(\text{B.11}) = \int_{t_a}^{t_b} \int_{t_a}^{t} \frac{f(t)f(s)}{2m^2\omega^2} \left[\sin\omega(t - t_a) \sin\omega(t_b - s) - \sin\omega(t_b - t) \sin\omega(s - t_a) \right] ds \, dt$$

$$- \int_{t_a}^{t_b} \int_{t}^{t_b} \frac{f(t)f(s)}{2m^2\omega^2} \left[\sin\omega(t - t_a) \sin\omega(t_b - s) - \sin\omega(t_b - t) \sin\omega(s - t_a) \right] ds \, dt.$$

$$\text{(B.14)}$$

All the double integrals in Eq. (B.12) and Eq. (B.14) can be combined using simple substitution methods until we arrive at the following expression

$$- 2 \int_{t_a}^{t_b} \int_t^{t_b} \frac{f(t)f(s)}{m^2\omega^2} \sin\omega(t_b - t) \sin\omega(s - t_a) \, \mathrm{d}s \, \mathrm{d}t. \tag{B.15}$$

All that remains is to rewrite Eq. (B.9). It can be checked that it is equal to

$$Eq.(B.9) = (x_b^2 + x_a^2) \cos\omega T - 2x_b x_a + \int_{t_a}^{t_b} \frac{f(t)}{m\omega} \left[x_a \sin\omega(t_b - t) + x_b \sin\omega(t - t_a) \right] \, \mathrm{d}t. \tag{B.16}$$

Therefore, we can write down the final expression for the action of a forced harmonic oscillator

$$S[x] = \frac{m\omega}{2\sin\omega T} \times \left\{ (x_b^2 + x_a^2) \cos\omega T - 2x_b x_a \right.$$
$$+ 2 \int_{t_a}^{t_b} \frac{f(t)}{m\omega} \left[x_a \sin\omega(t_b - t) + x_b \sin\omega(t - t_a) \right] \, \mathrm{d}t$$
$$\left. - 2 \int_{t_a}^{t_b} \int_t^{t_b} \frac{f(t)f(s)}{m^2\omega^2} \sin\omega(t_b - t) \sin\omega(s - t_a) \, \mathrm{d}s \, \mathrm{d}t \right\}. \tag{B.17}$$

The propagator, or kernel, of the forced harmonic oscillator is given by the path integral

$$K = \mathcal{N} \int_{x_a}^{x_b} \mathcal{D}x(t) \exp\left\{ \frac{i}{\hbar} S[x_{cl}(t)] \right\}, \tag{B.18}$$

where $x_a = x(t_a)$ and $x_b = x(t_b)$, and $\mathcal{N}$ a normalisation constant. To calculate the kernel for the quantum mechanical forced harmonic oscillator, we can perform a perturbative expansion around the classical path, $x_{cl}(t)$. We take

$$x(t) = x_{cl}(t) + \xi(t), \qquad \text{with } \xi(t_a) = \xi(t_b) = 0. \tag{B.19}$$

The kernel then becomes

$$K = \mathcal{N} \exp\left\{ \frac{i}{\hbar} S[x_{cl}(t)] \right\} \int_{\xi_a=0}^{\xi_b=0} \mathcal{D}\xi(t) \exp\left\{ \frac{i}{\hbar} S[\xi(t)] \right\}, \tag{B.20}$$

with $S[\xi(t)] = m/2 \int [\dot{\xi}^2 - \omega^2\xi^2] \, \mathrm{d}t = m/2 \int \xi[-\partial_t^2 - \omega^2\xi] \, \mathrm{d}t$, the action of an unforced harmonic oscillator.

We would like to calculate the path integral over the quantum fluctuations, so therefore we must calculate the action for the harmonic oscillator. We assume the usual wave function for the harmonic oscillator, and make a Fourier expansion.

$$\xi(t) = \sum_{k=1}^{\infty} a_k \phi_k(t) \tag{B.21}$$

$$\phi_k(t) = \sqrt{\frac{2}{(t_b - t_a)}} \sin\left(\frac{k\pi(t - t_a)}{t_b - t_a} \right), \tag{B.22}$$

where $\phi(t_a) = \phi(t_b) = 0$. This assumption allows us to write down the eigenstates, λ_k, for the harmonic oscillator

$$L(t)\phi_k(t) = \lambda_k \phi_k(t), \qquad \text{with} \qquad \lambda_k = \left(\frac{k\pi}{t_b - t_a}\right)^2 - \omega^2. \tag{B.23}$$

Substituting Eq. (B.21) into the action, we find that $S[\xi] = m/2 \sum_k \lambda_k a_k^2$, which reduces the path integral Eq. (B.20) to a product of Gaussian integrals, which can easily be evaluated

$$\begin{aligned}
K &= \mathcal{N} \exp\left\{\frac{i}{\hbar} S[x_{cl}(t)]\right\} \int_{\xi_a=0}^{\xi_b=0} \mathcal{D}[a_k, \phi_k] \exp\left\{\frac{im}{2\hbar} \sum_k \lambda_k a_k^2\right\} \\
&= \mathcal{N}^* \exp\left\{\frac{i}{\hbar} S[x_{cl}(t)]\right\} \left(\Pi_k \frac{m}{2\pi i\hbar} \lambda_k\right)^{-1} \\
&= \frac{\mathcal{N}^*}{\sqrt{\mathcal{M}}} \sqrt{\frac{\omega(t_b - t_a)}{\sin \omega(t_b - t_a)}} \exp\left\{\frac{i}{\hbar} S[x_{cl}(t)]\right\},
\end{aligned} \tag{B.24}$$

where $\mathcal{N}^*$ has absorbed the normalisation constant from the path integral and where we have made use of the Fourier series for sine functions, $\Pi_k \left(1 - \left(\frac{x}{k\pi}\right)^2\right) = \frac{\sin x}{x}$, in the last line. All that is left for us to do is to find the prefactor $\mathcal{N}^*/\sqrt{\mathcal{M}}$, which can be found by calculating the propagator for the free particle. Using the Hamiltonian for a free particle, $H = p^2/2m$, we find the following propagator

$$\begin{aligned}
K_f &= \langle x_b | e^{\frac{i}{\hbar} H(t_b - t_a)} | x_a \rangle \\
&= \sqrt{\frac{m}{2\pi i\hbar(t_b - t_a)}} \exp\left\{\frac{i}{\hbar} \frac{m(x_b - x_a)^2}{2(t_b - t_a)}\right\}.
\end{aligned} \tag{B.25}$$

From this, we infer that $\mathcal{N}^*/\sqrt{\mathcal{M}} = \sqrt{\frac{m}{2\pi i\hbar(t_b - t_a)}}$, which gives us our final expression for the propagator of the forced harmonic oscillator

$$K = \sqrt{\frac{m\omega}{2\pi i\hbar \sin \omega(t_b - t_a)}} \exp\left\{\frac{i}{\hbar} S[x_{cl}(t)]\right\}. \tag{B.26}$$

C   Density Operator

We will also need to calculate the expression for the density operator of the environment, $\rho(x, x')$. For thermodynamic systems, the density matrix can be calculated using the partition function, Z. It is given by

$$\rho(x, x') = \frac{1}{Z}\langle x|\exp(-\beta H)|x'\rangle, \qquad \text{with} \qquad Z = \int dx \langle x|exp(-\beta H)|x\rangle. \qquad (C.1)$$

Because the heat bath in the Caldeira-Leggett model consists of harmonic oscillators, we use the following Hamiltonian

$$H = \frac{p^2}{2m} + \frac{m\omega^2}{2}x^2. \qquad (C.2)$$

Using the Wick rotation $\beta = 1/k_B T = \tau/\hbar$, we can now recognize Eq. (C.1) as the Euclidean propagator of the harmonic oscillator, which we can easily write down

$$\langle x|\exp\left(-\frac{1}{\hbar}H\tau\right)|x'\rangle = \sqrt{\frac{m\omega}{2\pi\hbar\sinh\omega\tau}}\exp\left\{-\frac{1}{\hbar}\frac{m\omega}{2\sinh\omega\tau}\left[(x^2 + x'^2)\cosh\omega\tau - 2xx'\right]\right\}.$$
$$(C.3)$$

The partition function reduces to $Z = (2\cosh\hbar\beta\omega - 2)^{-1/2}$, which leaves us with the following expression for the density operator

$$\rho(x, x') = \sqrt{\frac{m\omega(\cosh\hbar\beta\omega - 1)}{\pi\hbar\sinh\hbar\beta\omega}}\exp\left\{-\frac{m\omega}{2\hbar\sinh\hbar\beta\omega}\left[(x^2 + x'^2)\cosh\hbar\beta\omega - 2xx'\right]\right\}. \qquad (C.4)$$

References

[1] A. V. Ferrer and C. M. Smith, *Dynamical localization of a particle coupled to a two-level system thermal reservoir*, Phys. Rev. B **76**, 214303 (2007).

[2] F. Wilczek, *Quantum time crystals*, Phys. Rev. Lett. **109**, 160401 (2012).

[3] P. Bruno, *Comment on "quantum time crystals"*, Phys. Rev. Lett. **110**, 118901 (2013).

[4] K. Sacha and J. Zakrzewski, *Time crystals: a review*, Rep. Prog. Phys. **81**, 016401 (2017).

[5] A. Syrwid, J. Zakrzewski, and K. Sacha, *Time crystal behavior of excited eigenstates*, Phys. Rev. Lett. **119**, 250602 (2017).

[6] K. Sacha, *Modeling spontaneous breaking of time-translation symmetry*, Phys. Rev. A **91**, 033617 (2015).

[7] K. Giergiel, A. Kosior, P. Hannaford, and K. Sacha, *Time crystals: Analysis of experimental conditions*, Phys. Rev. A **98**, 013613 (2018).

[8] K. Giergiel, T. Tran, A. Zaheer, A. Singh, A. Sidorov, K. Sacha, and P. Hannaford, *Creating big time crystals with ultracold atoms*, New Journal of Physics **22**, 085004 (2020).

[9] D. V. Else, B. Bauer, and C. Nayak, *Floquet time crystals*, Phys. Rev. Lett. **117**, 090402 (2016).

[10] V. Khemani, A. Lazarides, R. Moessner, and S. L. Sondhi, *Phase structure of driven quantum systems*, Phys. Rev. Lett. **116**, 250401 (2016).

[11] S. Choi, J. Choi, R. Landig, G. Kucsko, H. Zhou, J. Isoya, F. Jelezko, S. Onoda, H. Sumiya, V. Khemani, C. V. Keyserlingk, N. Y. Yao, E. Demler, and M. D. Lukin, *Observation of discrete time-crystalline order in a disordered dipolar many-body system*, Nature **543**, 221 (2017).

[12] J. Zhang, P. W. Hess, A. Kyprianidis, P. Becker, A. Lee, J. Smith, G. Pagano, I. D. Potirniche, A. C. Potter, A. Vishwanath, N. Y. Yao, and C. Monroe, *Observation of a discrete time crystal*, Nature **543**, 217 (2017).

[13] C. Booker, B. Buča, and D. Jaksch, *Non-stationarity and dissipative time crystals: spectral properties and finite-size effects*, New Journal of Physics **22**, 085007 (2020).

[14] A. Caldeira and A. Leggett, *Quantum tunnelling in a dissipative system*, Annals of Physics **149**, 374 (1983).

[15] F. Wilczek, *Crystals in time*, Scientific American **321**, 28 (2019).

[16] P. W. Anderson and J. M. Rowell, *Probable observation of the Josephson superconducting tunneling effect*, Phys. Rev. Lett. **10**, 230 (1963).

[17] R. C. Jaklevic, J. Lambe, A. H. Silver, and J. E. Mercereau, *Quantum interference effects in Josephson tunneling*, Phys. Rev. Lett. **12**, 159 (1964).

[18] R. P. Feynman, R. B. Leighton, and M. Sands, *The Feynman lectures on physics; New millennium ed.* (Basic Books, New York, NY, 2010). Originally published 1963-1965.

[19] A. O. Caldeira, A. H. Castro Neto, and T. Oliveira de Carvalho, *Dissipative quantum systems modeled by a two-level-reservoir coupling*, Phys. Rev. B **48**, 13974 (1993).

[20] A. Villares Ferrer, A. O. Caldeira, and C. M. Smith, *Optical conductivity of charge carriers interacting with a two-level systems reservoir*, Phys. Rev. B **74**, 184304 (2006).

[21] R. C. Verstraten, R. F. Ozela, and C. Morais Smith, *Time glass: A fractional calculus approach*, Phys. Rev. B **103**, L180301 (2021).

[22] G. Grüner, *The dynamics of charge-density waves*, Reviews of modern physics **60**, 1129 (1988).

[23] M. Yue, X. Yang, and Z. Cai, *Thermal melting of discrete time crystals: A dynamical phase transition induced by thermal fluctuations*, Phys. Rev. B **105**, L100303 (2022).

[24] E. J. Bergholtz, J. C. Budich, and F. K. Kunst, *Exceptional topology of non-hermitian systems*, Reviews of Modern Physics **93**, 015005 (2021).

[25] R. Arouca, E. Marino, and C. M. Smith, *Non-hermitian quantum gases: a platform for imaginary time crystals*, arXiv preprint arXiv:2108.01747 (2021).